

AD-757 677

STRUCTURE AND PROPERTY CONTROL THROUGH
RAPID QUENCHING OF LIQUID METALS

Nicholas J. Grant, et al

Massachusetts Institute of Technology

Prepared for:

Advanced Research Projects Agency

31 December 1972

DISTRIBUTED BY:

NTIS

National Technical Information Service
U. S. DEPARTMENT OF COMMERCE
5285 Port Royal Road, Springfield Va. 22151

**BEST
AVAILABLE COPY**

AD757677

TECHNICAL REPORT

Semi-Annual Technical Report No. 5

STRUCTURE AND PROPERTY CONTROL THROUGH
RAPID QUENCHING OF LIQUID METALS

Sponsored by
Advanced Research Projects Agency
Contract No.: DAHC15 70 C 0283

This document has been approved
for public release and sale; its
distribution is unlimited.

CENTER FOR
MATERIALS SCIENCE AND ENGINEERING

Reproduced by
NATIONAL TECHNICAL
INFORMATION SERVICE
U S Department of Commerce
Springfield VA 22151



Massachusetts Institute of Technology
Cambridge, Massachusetts 02139

R

For period - July 31, 1972 to December 31, 1972

Semi-Annual Technical Report No. 5

STRUCTURE AND PROPERTY CONTROL THROUGH
RAPID QUENCHING OF LIQUID METALS

Sponsored by
Advanced Research Projects Agency
Contract No.: DAHC15 70 C 0283

ARPA Order No.: 1608
Program Code No.: OD10

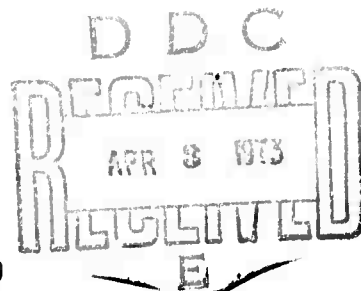
Contractor:

Massachusetts Institute of Technology
Cambridge, Massachusetts 02139

This document has been approved
for public release and sale; its
distribution is unlimited.

Principal Investigator:

N. J. Grant
(617) 253-5638
and Industrial Materials Technology
Woburn, Massachusetts 01801
(617) 933-1124



Effective date of Contract: June 22, 1970
Contract Expiration Date: June 21, 1973

Total Amount of Contract: \$470,300
ARPA Order No. 1608

The views and conclusions contained in this document are those of the authors and should not be interpreted as necessarily representing the official policies, either expressed or implied, of the Advanced Research Projects Agency or the U.S. Government.

I-a

DOCUMENT CONTROL DATA - R&D

(Security Classification of title, body of abstract and indexing annotation must be entered when the overall report is classified)

1. ORIGINATING ACTIVITY (Corporate author) Massachusetts Institute of Technology Cambridge, Massachusetts 02139		2a. REPORT SECURITY CLASSIFICATION unclassified	
		2b. GROUP	
3. REPORT TITLE Structure and Property Control Through Rapid Quenching of Liquid Metals			
4. DESCRIPTIVE NOTES (Type of report and inclusive dates)			
5. AUTHOR(S) (Last name, first name, initial) Grant, Nicholas J.; Pelloux, Regis M.; Flemings, Merton C.; Argon, Ali S.			
6. REPORT DATE December 31, 1972		7a. TOTAL NO. OF PAGES 115	7b. NO. OF REFS
8a. CONTRACT OR GRANT NO. DAHC 70 C 0283		8a. ORIGINATOR'S REPORT NUMBER(S)	
b. PROJECT NO. ARPA Order #1608			
c.		8b. OTHER REPORT NO(S) (Any other numbers that may be assigned this report)	
d. Program Code #0D10			
10. AVAILABILITY/LIMITATION NOTICES			
11. SUPPLEMENTARY NOTES Details of illustrations in this document may be better studied on microfiche.		12. SPONSORING MILITARY ACTIVITY Advanced Research Projects Agency 1400 Wilson Blvd. Arlington, Virginia 22209	
13. ABSTRACT This report presents the results and accomplishments of the fifth six-month period of a three year research program investigating the processing of billets from rapidly quenched liquid metals. Various powder metallurgy (P/M) and quench-casting techniques have been employed to generate extremely fine dendrite arm spacings and homogeneous structures. Iron, nickel and cobalt-base alloy powders, produced by steam atomization (coarse powders), argon atomization, vacuum atomization, and the rotating electrode process, have been consolidated into dense billets by hot isostatic pressing (HIP) and/or extrusion. The hot working properties of P/M billets and quench-cast bars have been evaluated by hot rolling, high strain rate tests, and creep (superplastic) testing. Two P/M superalloys, MAR-M-509 (cobalt-base) and IN-100 (nickel-base) after HIP and hot extrusion demonstrated excellent hot workability under high strain rate and creep forming conditions, respectively. Detailed analyses of microstructure, heat treatment, and mechanical properties are presented for all P/M alloys and compared to equivalent cast materials. Room temperature properties of P/M alloys continue to be far superior to their cast counterparts. Elevated temperature properties are significantly improved by proper heat treatments.			

DD FORM 1 JAN 64 1473

I-6

Security Classification

14.

KEY WORDS

Rapid Quenching
Structure and Segregation Control
Powder Metallurgy

LINK A

LINK B

LINK C

ROLE

WT

ROLE

WT

ROLE

WT

INSTRUCTIONS

1. **ORIGINATING ACTIVITY:** Enter the name and address of the contractor, subcontractor, grantee, Department of Defense activity or other organization (corporate author) issuing the report.

2a. **REPORT SECURITY CLASSIFICATION:** Enter the overall security classification of the report. Indicate whether "Restricted Data" is included. Marking is to be in accordance with appropriate security regulations.

2b. **GROUP:** Automatic downgrading is specified in DoD Directive 5200.10 and Armed Forces Industrial Manual. Enter the group number. Also, when applicable, show that optional markings have been used for Group 3 and Group 4 as authorized.

3. **REPORT TITLE:** Enter the complete report title in all capital letters. Titles in all cases should be unclassified. If a meaningful title cannot be selected without classification, show title classification in all capitals in parenthesis immediately following the title.

4. **DESCRIPTIVE NOTES:** If appropriate, enter the type of report, e.g., interim, progress, summary, annual, or final. Give the inclusive dates when a specific reporting period is covered.

5. **AUTHOR(S):** Enter the name(s) of author(s) as shown on or in the report. Enter last name, first name, middle initial. If military, show rank and branch of service. The name of the principal author is an absolute minimum requirement.

6. **REPORT DATE:** Enter the date of the report as day, month, year; or month, year. If more than one date appears on the report, use date of publication.

7a. **TOTAL NUMBER OF PAGES:** The total page count should follow normal pagination procedures, i.e., enter the number of pages containing information.

7b. **NUMBER OF REFERENCES:** Enter the total number of references cited in the report.

8a. **CONTRACT OR GRANT NUMBER:** If appropriate, enter the applicable number of the contract or grant under which the report was written.

8b, &, & 8d. **PROJECT NUMBER:** Enter the appropriate military department identification, such as project number, subproject number, system numbers, task number, etc.

9a. **ORIGINATOR'S REPORT NUMBER(S):** Enter the official report number by which the document will be identified and controlled by the originating activity. This number must be unique to this report.

9b. **OTHER REPORT NUMBER(S):** If the report has been assigned any other report numbers (either by the originator or by the sponsor), also enter this number(s).

10. **AVAILABILITY/LIMITATION NOTICES:** Enter any limitations on further dissemination of the report, other than those

imposed by security classification, using standard statements such as:

- (1) "Qualified requesters may obtain copies of this report from DDC."
- (2) "Foreign announcement and dissemination of this report by DDC is not authorized."
- (3) "U. S. Government agencies may obtain copies of this report directly from DDC. Other qualified DDC users shall request through _____."
- (4) "U. S. military agencies may obtain copies of this report directly from DDC. Other qualified users shall request through _____."
- (5) "All distribution of this report is controlled. Qualified DDC users shall request through _____."

If the report has been furnished to the Office of Technical Services, Department of Commerce, for sale to the public, indicate this fact and enter the price, if known.

11. **SUPPLEMENTARY NOTES:** Use for additional explanatory notes.

12. **SPONSORING MILITARY ACTIVITY:** Enter the name of the departmental project office or laboratory sponsoring (paying for) the research and development. Include address.

13. **ABSTRACT:** Enter an abstract giving a brief and factual summary of the document indicative of the report, even though it may also appear elsewhere in the body of the technical report. If additional space is required, a continuation sheet shall be attached.

It is highly desirable that the abstract of classified reports be unclassified. Each paragraph of the abstract shall end with an indication of the military security classification of the information in the paragraph, represented as (TS), (S), (C), or (U).

There is no limitation on the length of the abstract. However, the suggested length is from 150 to 225 words.

14. **KEY WORDS:** Key words are technically meaningful terms or short phrases that characterize a report and may be used as index entries for cataloging the report. Key words must be selected so that no security classification is required. Identifiers, such as equipment model designation, trade name, military project code name, geographic location, may be used as key words but will be followed by an indication of technical context. The assignment of links, rules, and weights is optional.

I-C

TABLE OF CONTENTS

	<u>Page Number</u>
TASK I PROCESSING OF ALLOYS	1
I. Introduction	1
II. Experimental Work	1
A. Melting and Atomization	1
B. Powder Consolidation	1
1. Hot Isostatic Pressing	1
2. Forging	2
3. Extrusions	3
4. Microstructures	4
C. Gas Studies	5
III. Conclusions	6
Tables	7
Figures	14
TASK II SOLIDIFICATION RESEARCH	18
I. Filomatization	19
II. Evaluation of Powder Particles Produced by Different Atomization Processes	22
Tables	26
Figures	27
TASKS III and IV THERMOMECHANICAL TREATMENT, MICROSTRUCTURE AND MECHANICAL PROPERTIES	31
I. Mechanical Properties of 300 Grade Maraging Steels	32
A. Introduction	32
B. Tensile and Fracture Toughness Properties	32

I-d

	<u>Page Number</u>
C. Fatigue of Maraging 300 Steel	35
Tables	37
Figures	39
II. Development of P/M Cobalt-Base Alloys Using Rapidly Quenched, Pre-Alloyed Powders	44
A. Powder Processing and Alloy Consolidation	44
B. High Temperature Treatments	48
C. Mechanical Properties	54
D. Summary	59
Tables	62
Figures	85
III. Processing of PM IN-100	92
A. Grain Growth Studies	92
B. Sintering	93
C. Hot Plasticity	93
D. Crack Propagation at Elevated Temperatures	94
E. Future Work	95
Tables	96
Figures	98
IV. Inclusion Separation in Ductile Matrices	109
A. Introduction	109
B. Inclusion Separation at Elevated Temperatures	109
C. Separation of Copper-Chromium Inclusions in Copper	111
D. Hole Nucleation from Plate-Like Inclusions	112
E. Evaluation of Inhomogeneous Strain Fields	112
Figures	114

LIST OF TABLES

<u>Table Number</u>		<u>Page Number</u>
<u>TASK I</u>		
I	Atomization Runs	7
II	Coarse Powder Chemistry	8
III	Hot Isostatic Pressing Runs	9
IV	Extrusion Runs	12
V	Gas Analysis	13
<u>TASK II</u>		
I	Powder Description	26
<u>TASKS III and IV</u>		
<u>Maraging Steels</u>		
I	Tensile Test Data 300 Grade Maraging Steel	37
II	Fracture Toughness of Several 300 Grade Maraging Steels	38
<u>Cobalt-Base Alloys</u>		
I	HIP Alloys and Some Impurity Analyses Before and After HIP	62
II	Density Changes during Annealing	63
III	X-Ray Powder Diffraction Patterns of Phases Electrolytically Extracted from HIP and HIP + Hot Rolled MAR-M-509 P/M Alloys	65
IV	X-Ray Powder Diffraction Patterns of Phases Electrolytically Extracted from HIP + Extruded MAR-M-509-Type Alloys	66
V	X-Ray Diffraction Data After Isochronal (1 Hour) Annealing Treatments	68
VI	Calculated Carbide Weight and Volume Fractions Based on Stoichiometric Phases	70
VII	Ageing Data on MAR-M-509 Type Alloys	72
VIII	Solutionizing and Ageing Data	74
IX	Examples of Grain Sizes in P/M Cobalt Base Alloys After Annealing at 2300°F (1260°C)	75
X	Room Temperature Tensile Properties of MAR-M-509 Type P/M Alloys	76
XI	Room Temperature Tensile Properties of Co-HfC P/M and Cast Alloys	78

<u>Table Number</u>		<u>Page Number</u>
XII	Stress for 10 and 100 Hour Rupture Life	80
XIII	Electrolytically Extracted Phases	83
	<u>P/M IN-100</u>	
I	The Hot Plasticity Data of IN-100 P/M Under Varied Hot Isostatic Pressing Conditions	96
II	The Hot Plasticity Data of IN-100 P/M Hot Isostatically Pressed at 2150°F, 15 + ksi for 5 Hours Under Varying Testing Temperatures	97

LIST OF FIGURES

<u>Figure Number</u>		<u>Page Number</u>
<u>TASK I</u>		
1	HIP billet IN-100 LC 8" diameter x 4" high ready for pressing. Can No. 2H21.	14
2	VM-300 sheet bar. Hot isostatically pressed and press forged. Transverse section. Can No. 2G10.	15
3	VM-300 sheet bar. HIP, press forged and hot rolled to 5/8" thickness. Can No. 2G10.	15
4	IN-100 LC. 33 lb. billet HIP'ed at 2150°F, 15 ksi, 5 hrs. and press forged to ≈12" diameter disc. Can No. 2H21.	16
5	IN-100 LC press forged HIP billets. Top: 2H21 HIP'ed at 2150°F, 15 Ksi, 5 hrs., Middle: 2H19 HIP'ed at 2200°F, 15 ksi, 5 hrs., Bottom: 2H20 HIP'ed at 2250°F, 15 ksi, 5 hrs.	16
6	Left half: IN-100 LC HIP'ed at 2235°F, 15 ksi, 2 hrs., Chemstrand 400μ powder. Can No. 2J34. Etched. 100X. Right half: IN-100 LC HIP'ed at 2235°F, 15 ksi, 2 hrs. plus extrusion at 2050°F, ≈24X R.A. Can No. 2J62. Internal tearing at prior particle boundary. Etched, 100X.	17
7	Left half: MAR-M-509 HIP'ed at 2235°F, 15 ksi, 2 hrs. Homogeneous Metals -80 mesh powder. Can No. 2142. Etched, 500X. Right half: MAR-M-509 HIP'ed at 2235°F, 15 ksi, 2 hrs. plus extrusion at 2050°F, ≈25X R.A. Can No. 2139. Etched, 500X.	17
<u>TASK II</u>		
1	Calculated radial fraction liquid and volume fraction solid versus free fall time and distance for different size powder particles of Maraging 300 steel alloy.	27
2	Secondary dendrite arm spacings versus powder particle diameter of Maraging 300 steel alloy obtained by different atomization processes.	28
3	SEM micrograph views of atomized powder particles of IN-100 alloy; (a) and (b) show spin atomized powders at 56X and 215X, respectively, (c) and (d) show vacuum atomized powders at 57X and 22.5X, respectively, (e) and (f) show inert gas atomized fine powders at 210X and 1050X, respectively.	29
4	Spin atomized powders of Maraging 300 steel alloy; (a) and (b) are SEM micrograph views at 19X and 240X, respectively, (c) is a photomicrograph of a polished and etched cross-section at 200X.	30

LIST OF FIGURES

<u>Figure Number</u>		<u>Page Number</u>
<u>TASKS III and IV</u>		
<u>Maraging Steels</u>		
1	Tension-Compression S-N curves for Vascomax 300 tested in dry argon.	39
2	Development of hysteresis loop tips of aged Vascomax 300 exposed to blocks of increasing and decreasing strain.	40
3	Monotonic and cyclic stress strain curves for aged and annealed Vascomax 300.	41
4	Cyclic workhardening exponent of aged and annealed Vascomax 300 as determined from the cyclic stress strain curve.	42
5	Plot of low and high cycle fatigue of annealed Vascomax 300. The values of the elastic plastic and total strain in low cycle are indicated.	43
<u>Cobalt-Base Alloys</u>		
1	Effect of tap temperature and chemistry on the morphology of steam atomized coarse cobalt powders.	85
2	Steam atomized Co-HfC powders showing: (a) Co-1 atom % HfC powder morphology with (right) and without (left) 0.8% Si additions, X1; (b) typical morphology of alloys with greater than about 3% Hf additions, X1.	86
3	P/M MAR-M-509 alloy after holding 2 hours at 1330°C (2426°F) and air cooled. (a) Etched. 150X. (b) Etched to reveal four major types of phases after partial melting. 750X.	87
4	Porosity in HIP + hot rolled P/M MAR-M-509 after annealing two hours at (a) 2265°F (1240°C); (b) 2300°F (1260°C); (c) 2330°F (1280°C), X150. Etched electro. chromic acid.	88
5	HIP + extruded P/M Cobalt-3 atom % HfC in (a) as-extruded condition; (b) after one hour anneal at 2440°F (1340°C). X1500. Etched electro. Oxalic-HCl acids.	89
6	Oxidation samples, loose scale and cross section photomicrographs after 100 hours at 2000°F (1093°C). (a) X1; (b) P/M Co-3 atom % HfC (CH6); (c) P/M MAR-M-509 alloy (C51), cross sections, X400. Carbides stained.	90

LIST OF FIGURES

<u>Figure Number</u>		<u>Page Number</u>
7	Photomicrographs of P/M cobalt alloys after 100 hour exposure in air at 2000°F (1093°C), X200. (a) HiZr-modified MAR-M-509 (CZ1); (b) Hi W + Cr modified MAR-M-509 (C52); (c) Co-1 atom % HfC (CH2); (d) Co-2 atom % HfC (CH7). Carbides stained.	91
<u>P/M 100</u>		
1	Effect of time at temperature on average grain size for as-extruded IN-100 (N.M.)	98
2	Logarithm of growth rate (slope of grain growth isotherms) vs. reciprocal of absolute temperature.	99
3	The formation of interparticle necks from sintering, at 2150°F, in vacuum, of IN 100 powder. 240X.	100
4	The surface of IN 100 powder particle after vacuum sintering at 2150°F for 2 hours, 775X.	100
5	The oxide formation on the surface of sintered IN 100. 78X.	101
6	A nodular and spore type oxide formed on the surface of sintered IN 100. 2420X.	101
7	A whisker type oxide formed on the surface of sintered IN 100. 800X.	102
8	High strain rate log stress vs. log rupture time at a test temperature of 2100°F.	103
9	High strain rate log stress vs. log deformation rate at test temperature of 2100°F.	104
10	High strain rate effect of deformation rate on percent elongation at 2100°F.	105
11	High strain rate effect of stress on rupture time at varying temperatures.	106
12	High strain rate effect of stress on deformation rate at varying test temperatures	107
13	High strain rate effect on deformation rate on percent elongation.	108
<u>Ductile Matrices</u>		
1	Cumulative density of inclusions of all sizes (1), density of separated inclusions near the fracture surface (2), density of separated inclusions along the axis a distance of three neck radii away (3), in specimen fractured at 630°C.	114

LIST OF FIGURES

<u>Figure Number</u>		<u>Page Number</u>
2	Cumulative density of inclusions of all sizes (1), density of separated inclusions near the fracture surface (2), density of separated inclusions along the axis a distance of three neck radii away (3), in specimen fractured at room temperature.	115

~~IX~~

TASK I

PROCESSING OF ALLOYS

P.E. Price

R. Widmer

TASK I

Processing of Alloys

I. INTRODUCTION

Task I work on structure and property control through rapid quenching of liquid metals has included the following major aspects during the present reporting period:

(1) steam atomization of Mar M509 to produce material for consolidation and property determination by Task III, (2) production of hot isostatically pressed forging billets, (3) forging and hot rolling of HIP billets, (4) production of IN-100 LC HIP bars for hot plasticity studies by Task III, and (5) gas analysis of powders before and after hot isostatic pressing.

II. EXPERIMENTAL WORK

A. Melting and Atomization

One experimental cobalt base alloy was steam atomized. Atomization conditions are given in Table I and analyzed composition in Table II. A -4/+30 fraction was chemically cleaned and canned for hot isostatic pressing and extrusion.

B. Powder Consolidation

1. Hot Isostatic Pressing

Hot isostatic pressing was carried out to produce forging billets, extrusion billets, and direct HIP material for high temperature plasticity studies. Forging billets were produced to demonstrate the feasibility of the use of HIP in the process route for manufacture of forged superalloy parts starting from powder. In the case of IN-100 LC, three HIP conditions were used to explore the effects of HIP parameters on subsequent forgeability. In parallel with this full scale forging study, direct HIP IN-100 LC material was prepared in the form of bars using the same process parameters as for the forging preforms. Additional parameters were also used.

The objective was to determine the usefulness of an independent plasticity study to determine optimum HIP conditions for subsequent forging. This work is currently in progress in Task III, using material prepared by Task I.

A summary of all hot isostatic pressing runs carried out by Task I in the present reporting period is given in Table III. It is to be noted that except for Run No. 2, all processing was carried out at ~15,000 psi. This step was taken so that property data obtained by Task III will be useful for future reference when commercial production of large HIP forging preforms will utilize larger presses with 15,000 psi operating limits. Furthermore, as discussed later in this report, enough gas analyses showing argon in consolidated material have been obtained so that it was considered prudent to reduce the driving force (process pressure) for argon leakage through the welding cans even though the mechanism (s) of argon penetration is not fully understood in the cases where it occurred.

For the particular IN-100 LC forging billets in the current program, Figure 1 illustrates a welded can (2 H21) 8" ϕ x 4" high ready for consolidation by hot isostatic pressing. Evacuation and seal-off have been completed. Bake-out temperatures used for all cans before sealing were 1200-1400°F. In Figure 1, a 1/2" - 13" hex nut has been welded to the top of the can to facilitate handling through use of an eye-bolt.

2. Forging

Forgings were obtained using HIP preforms produced by Task I. All work was done at the Wyman-Gordon, Grafton, Massachusetts plant. Details of the press-forging practice employed were not available because of Wyman-Gordon's proprietary interests.

Figure 2 shows a transverse section of a VM-300 sheet bar, press forged in the 3 3/4" direction after HIP (2G10, Run No. 1, Table III). The original corners of the VM-300 powder compact may be seen as "flutes" on the top and bottom.

To provide a VM-300 consolidated powder material wherein the original powder particle boundaries were substantially deformed by hot-work, the forged compact was cut in half. One-half was hot rolled by 5/8" thickness (Figure 3) and the other to 3/8" thickness. Rolled material was forwarded to Task III for study of fracture toughness.

Three 33 lb. IN-100 LC HIP forging billets (Can nos. 2H19, 2H20, 2H21, Table III) were forged to $\sim 12" \phi \times 1"$ thick discs at Wyman-Gordon Company. The three HIP billets represented three different process temperatures: 2H20 - 2250°F; 2H19 - 2200°F; and 2H21 - 2150°F. Figure 4 shows 2H21 (HIP @ 2150°F, 5 hours) after forging and clean up. It is apparent that the HIP process temperature had a considerable effect on forgeability. As shown in a "side-by-side" comparison in Figure 5, a HIP temperature of 2250°F resulted in "large" edge cracks with "large" shear displacement. HIP at 2200°F reduced this effect and HIP at 2100°F produced relatively "fine" edge cracks uniformly dispersed around the circumference. The depth of radial penetration was also least for the lowest HIP temperature 2150°F. It should be noted that a basic assumption in this analysis is uniformity of forging practice among the three pieces.

The trend in reduced edge cracking at lower HIP temperature indicates that HIP of this powder at 2100°F or even 2050°F might produce even greater forging plasticity. The present billets have been forwarded to Task III for fatigue and fracture toughness studies. Additional hot plasticity material (IN-100 LC) will be produced to determine whether lower HIP temperature would increase hot plasticity.

3. Extrusions

Three alloy powders were produced as $\sim 1/2" \phi$ core extruded rods for Task III. All extrusions were produced from hot isostatically pressed extrusion billets (see Table III). Successful extrusions were obtained for Mar M 509 Homogeneous Metals, Inc. fine powder, Can No. 2139; Co-Hf, CH8-C1 Chemstrand powder, Can No. 2J62; and IN-100 LC Chemstrand powder, Can No. 2J62. Can No. 2149, containing steam atomized and cleaned Mar M 509, bulged and ruptured on heat up for extrusion and could not be extruded. Can No. 2K39 (IN-100 LC) was extruded but the die insert failed, and a cracked $\sim 2" \phi$ bar resulted instead of the required $1/2" \phi$ core

extrusion. A brief summary of extrusion conditions is given in Table IV.

4. Microstructures

As previously shown^{1,2} one characteristic of the structure material consolidated by hot isostatic pressing of powder is the presence of particles which have undergone little or no deformation. Other particles undergo heavy deformation and recrystallize producing fine grains. The resulting compact thus has grain sizes covering a range of $\approx 10:1$.

With IN-100 LC, which in addition to having a mixed grain size HIP structure, (Figure 6, left), undergoes γ' coarsening at 2235°F, subsequent hot work (extrusion) has caused internal fracture, (Figure 6, right, lower center). The origins of the fracture appears in one case to be at the head-and-tails of a prior powder particle which did not deform during HIP. The original dendrite structure appears intact and has not realigned in the extrusion direction. Extrusion is a high strain rate process which accentuates the difference in plasticity of coarse and fine grain material and has caused internal tearing for the processing conditions employed.

From the behavior of the IN-100 LC system during HIP and extrusion, it would appear useful to consider limiting the maximum powder particle size allowable for a given set of processing conditions. This would reduce the grain size range after HIP and, consequently, the variability in plasticity between the "coarse" and "fine" grain size local volumes of the structures.

Opportunity to examine the effects of a finer powder mesh size on processing response occurred with Mar M 509 "fine" powder. Figure 7, left, shows the structure after HIP; and Figure 7, right, shows the HIP structure after extrusion. Note that the magnification is 500X as opposed to 100X for IN-100, Figure 6. In the HIP structure an undeformed "cast" particle structure is shown in the upper half of the figure as quarter-circle. Carbide coarsening did not occur during HIP. The extruded

¹ Semi-Annual Technical Report No. 3, ARPA Contract No. DAHC1570C0283, Page 4.
² Effect of Processing Variables on Powder Metallurgy Rene 95, S. F. Barker & E. H. VanDerMolen, Proceedings 2nd International Conference Superalloys Processing, September, 1972, Pg. AA19.

structure showed no signs of internal tears. The conclusion is that a "fine" powder size and absence of "2nd" phase coarsening during HIP have produced a Mar M 509 structure which exhibits uniform plasticity during extrusion and no internal tearing.

C. Gas Studies

Task III investigation of heat treatment response of consolidated cobalt P/M alloys (Semi-Annual Technica' Report No. 4, pages 89, 92) has indicated that swelling and distortion may occur during high temperature heat treatment. Since residual gas, including argon, was suspected as a cause of the above behavior, an analytical survey was conducted on a variety of powders and consolidated materials. Table V lists the "critical" gas analyses obtained during the current reporting period.

Analysis of all Homogeneous Metals powders (as received) and all Chemstrand powders (as received) indicated no detectable argon (powder analyses 1,3,4 and 5). Although the powders were handled in air which is ~1% argon, insufficient adsorption took place to be detectable analytically. Next, it is to be noted that analyses 1 and 2 show 12 ppm and 84 ppm argon in consolidated bar material. In these cases the extrusion billets were prepared by hot isostatic pressing at 26 ksi and 28 ksi respectively, with argon as the pressurization fluid. It is to be further noted that bar produced by extrusion of billets HIP'ed at 15 ksi showed no detectable argon.

It would appear plausible to assume that argon gas may enter the powder compact during hot isostatic pressing. The mechanism (s) remain in doubt. Possibilities may include:

1. Permeation through microporosity in weld metal areas of the HIP can.
2. Permeation through HIP can wall defects traceable to original ingot practice, i.e., slag stringers, unwelded pipe, folds in rolling, cold shuts, etc.

3. Diffusion through "sound" material:
 - a. grain boundary diffusion
 - b. bulk diffusion.

Since Task III work has indicated that residual gas in consolidated material may adversely affect high temperature heat treatment response (and properties) and since this gas may be argon introduced in hot isostatic pressing, investigation of the above possibilities is currently being carried out.

III. CONCLUSIONS

IN-100 LC R.E.P. powder can be hot isostatically pressed to 7" ϕ x 3 1/2" high, 33 lb. forging billets. Press forging can "successfully" convert these billets to \sim 12" ϕ x 1" thick discs with edge cracking least for prior HIP @ 2150°F, and most for prior HIP @ 2250°F. Plasticity of material HIP'ed at lower temperatures warrants further test.

Extrusion of HIP billets at \sim 23 x R.A. resulted in internal fracture initiation near "coarse" powder particles. This finding suggests that reduction in upper mesh size of powder to be consolidated may eliminate this type of defect. Avoidance of internal tears at high extrusion R.A. occurred with -80 mesh (\leftarrow 177 μ) Mar M 509 "fine" powder.

Chemical analysis showing argon in material compacted by HIP requires further immediate study. The powders in these tests were "non-argon atomized", and to date no model has yet been established to explain the observations.

TABLE I

Atomization Runs

Heat No.	Alloy	Atomization Steam, Argon	Top Pressure	Side Pressure	Tundish Nozzle	Top Temperature	Objective	Result
247	Mar M 509 + Hf	S	60 mmg 8 psi	2 1/2 x 100 mmf 10 psig	13/32" \diamond ZrO ₂	2995°F	Produce coarse powder for cleaning and consolidation.	Coarse rounded powder. Shells and "nested" particles. Chemistry, see Table II.

TABLE II

Coarse Powder Chemistry

Heat No.	Sample Description	Analysis, Wt. Percent
247	Mar M 509 + Hf. Steam atomized -4/+30 mesh. Four chemical cleaning cycles and inhibited aqua regia.	Cr 26.69, Ni 9.50, W 8.17, Mn 0.004, Ta 3.12, Hf 0.46, Ti 0.22, C 0.76.

TABLE III

Hot Isostatic Pressing Runs

No.	Can No.	Powder	Billet Size at start	Pressing Conditions	Remarks
1.	2G10	VM-300, R.E.P. Lot #6278, -35 mesh.	5" x 7" x 14" Rectangular sheet bar.	2300°F, 14,500 psi, 3 hrs.	Completed to 3 3/4" x 5 1/2" x 12".
2.	2H24	CH2-01-HE, 2 pcs.	5/8" ϕ x 8" Extrusion.	2300°F, 27,000 psi, 2 hrs.	Cannon-Muskegon Ht. No. VE-2
3.	2H20	IN-100 LC, R.E.P. Lot #6140, -35 mesh.	8" ϕ x 4" high.	2250°F, 14,900 psi, 5 hrs.	
4.	2H19	IN-100 LC, R.E.P. Lot #6140, -35 mesh.	8" ϕ x 4" high.	2200°F, 14,600 psi, 5 hrs.	
5.	2J61	Co-Hf, CH8-Cl Chemstrand I Exp. 21, I Exp. 23.	3 1/4" ϕ x 3 15/16"	2235°F, 14,600 psi, 2 hrs.	
	2J62	IN-100 LC Chemstrand I Exp. 17, I Exp. 19.	3 1/4" ϕ x 7 1/4"	2235°F, 14,600 psi, 2 hrs.	Extrusion billet. Median powder particle size \sim 400 μ for all Chemstrand powders.
	2J33	Co-Hf, CH8-Cl Chemstrand I Exp. 23.	3/4" ϕ x 3"	2235°F, 14,600 psi, 2 hrs.	
	2J34	IN-100 LC Chemstrand I Exp. 17	3/4" ϕ x 3 1/2"	2235°F, 14,600 psi, 2 hrs.	Cannon-Muskegon Ht. No. VE-2 Extrusion billet.
	2I39	Mar M 509 Homogeneous Metals, Inc., A-371 -80 mesh, C52-H1.	3 1/4" ϕ x 9"	2235°F, 14,600 psi, 2 hrs.	

TABLE III (Continued)

No.	Can No.	Powder	Billet Size at start	Pressing Conditions	Remarks
5.	2142	Mar M 509 Homogeneous Metals, Inc., A-371 -80 mesh, C52-H1.	5/8" ϕ x 13"	2235°F, 14,600 psi, 2 hrs.	Extrusion billet.
	2144	Mar M 509 Homogeneous Metals, Inc., A-371 -20/+80 mesh. C52-H1	5/8" ϕ x 13"	2235°F, 14,600 psi, 2 hrs.	
	2149	Mar M 509 IMT 30-247. Steam atomized & cleaned. -4/+30 mesh.	3 1/4" ϕ x 13"	2235°F, 14,600 psi, 2 hrs.	
	2H21	IN-100 LC, R.E.P. Lot #6140. -35 mesh.	8" ϕ x 4" high.	2150°F, 14,400 psi, 5 hrs.	
6.	2K27	IN-100 LC, R.E.P. Lot #6355, -50 mesh.	1" x 3" x 13" Flat bar.	2150°F, 14,400 psi, 5 hrs.	See Figure for can ready for processing.
	2K31	3 pcs. IN-100 Cast bar. (R.E.P. stubs).	2 1/2" ϕ x 2" high.	2150°F, 14,400 psi, 5 hrs.	
	2K02 2K06 2K07 2K10	IN-100 LC, R.E.P. Lot #6355, -50 mesh.	3/4" ϕ x 13"	2150°F, 14,400 psi, 5 hrs.	
	2K01 2K03 2K04 2K08 2K12	IN-100 LC, R.E.P. Lot #6355, -50 mesh.	3/4" ϕ x 13"	2150°F, 15,600 psi, 2 hrs.	

Cannon-Muskegon Ht. No. VE 372.

TABLE III (Continued)

No.	Can No.	Powder	Billet Size at start	Pressing Conditions	Remarks
8.	2K05}	IN-100 LC, R.E.P. Lot #6355, -50 mesh.	3/4" ϕ x 13"	2200°F, 14,800 psi, 2 hrs.	Extrusion billet.
	2K09}				
	2K11}				
	2K39				
9.	2L40	IN-100 LC, R.E.P. Lot #6355, -50 mesh.	3 1/4" ϕ x 9"	2200°F, 16,900 psi, 5 hrs.	Extrusion billet.
	2L42}				
	2L51}				
	2L52}				
10.	2L53}	IN-100 LC, R.E.P. Lot #6355, -50 mesh.	3/4" ϕ x 13"	2250°F, 15,100 psi, 5 hrs.	Gas permeability test sample.
	2L54}				
	2L43}				
	2L46}				
11.	2L47}	304 S. S. Bar, Solid	1 1/4" ϕ x 2"	2250°F, 17,700 psi, 2 hrs.	Gas permeability test sample.
	2L50}				
	2L55}				
	2L120}				
	2L121}	IN-100 LC, R.E.P. Lot #6355, -50 mesh.	3/4" ϕ x 13"	2250°F, 17,700 psi, 2 hrs.	Gas permeability test sample.
	2L122}				
	2L44}				
	2L45}				
	2L49}	304 S. S. Bar, Solid	1 1/4" ϕ x 2"	2250°F, 17,700 psi, 2 hrs.	Gas permeability test sample.
	2L54}				
	2L150}				
	2L151}				
	2L152}				

TABLE IV

Extrusion Runs

Billet No.	Die	Reduction	Speed	Upset (tons)	Runs (tons)	Remarks
2J-61	.630"	23.4:1	400 ipm	750	580	See Table III for can and powder identification.
2J-62	.630"	23.4:1	400 ipm	790	570	" " "
2I-39	.610"	25:1	100 ipm	800	770	" " "
2I-49	.610"	25:1	100 ipm	800	770	Billet ruptured before extrusion.
2K-39	.610"	25:1	100 ipm	800	770	Stalled.

Press: 1400-ton.

Liner: 3.050-inch @ 900°F.

Cutoff: C.R.S. @ 1500°F.

Temperature: 2050°F under nitrogen atmosphere.

TABLE V

Gas Analysis

No.	Sample Description	Vacuum Fusion - Mass. Spec. Readout, ppm						Remarks
		O	N	H	He	Ar		
1.	Ch6-H1-HE. Co-Hf alloy. Homogeneous Metals, Inc. powder. HIP @ 2300°F, 26 Ksi, 4 hrs. + Ext. @ 2200°F, 22:1 R.A.	305 (310)	27 96	6 10	ND,4* ND,.1	12 ND,.5)	Solid bar after consolidation. Analysis of powder as received from HMI, Inc.	
2.	CH7-H2-HE. Co-Hf alloy. Homogeneous Metals, Inc. powder. HIP @ 2325°F, 28 Ksi, 2 hrs. + Ext. @ 2050°F, 20:R.A.	150	11	5	ND,4	84	Powder analysis not avail- able but estimated as ~ same as (1) above.	
3.	CH8-C1-H, Co-Hf alloy. Chemstrand powder. HIP @ 2235°F, 15 Ksi, 2 hrs.	5.6 (9	ND,10 ND,10	5.5 ND,1.0	ND,2 ND,4	ND,.2 ND,.2)	Solid bar after consolidation. Analysis of powder as rec'd from Chemstrand.	
4.	C51-H1-H, Mar M509 Homogeneous Metals, Inc. powder Ht. No. A-371, -80 mesh HIP @ 2235°F, 15 Ksi, 2 hrs.	23 (31	ND,10 ND,10	4.2 9.6	ND,2 ND,2	ND,.2 ND,.2)	Solid bar after consolidation. Analysis of powder as rec'd from HMI, Inc.	
5.	IN-100 LC Chemstrand I Exp. 19 powder. HIP @ 2235°F, 15 Ksi, 2 hrs. Can No. 25-34.	21 (19	ND,10 ND,10	25 ND,1	ND,2 ND,4	.2 ND,.2)	Solid bar after cons lidation. Analysis of powder as rec'd from Chemstrand.	
* N.D. = none detected, less than x.								

*N.D. = none detected, less than x.



Figure 1. HIP billet IN-100 LC. 8" diameter x 4" high
ready for pressing. Can No. 2H21.

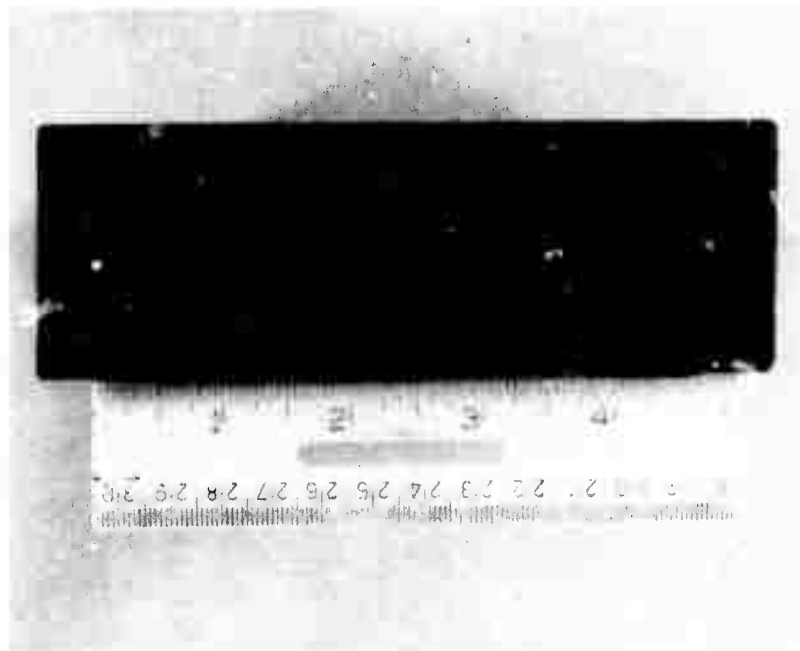


Figure 2. VM-300 sheet bar. Hot isostatically pressed and press forged. Transverse section. Can No. 2G10.

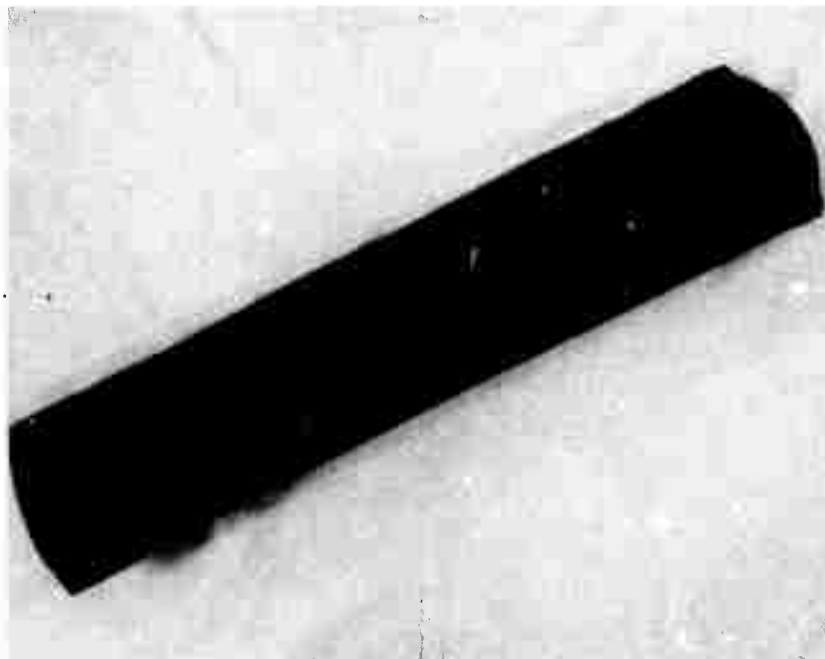


Figure 3. VM-300 sheet bar. HIP, press forged and hot rolled to 5/8" thickness. Can No. 2G10.

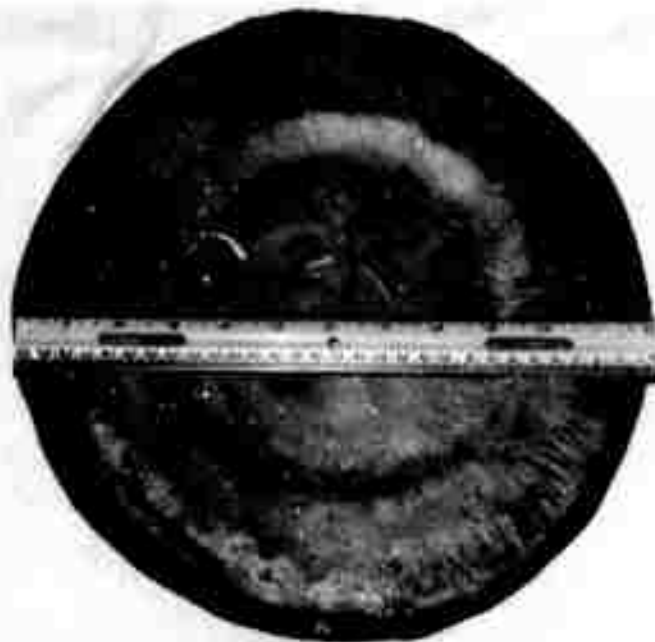


Figure 4. IN-100 LC. 33 lb. billet HIP'ed at 2150°F, 15 ksi, 5 hrs. and press forged to ~12" diameter disc. Can No. 2H21.



Figure 5. IN-100 LC press forged HIP billets. Top: 2H21, HIP'ed at 2150°F, 15 ksi, 5 hrs., middle: 2H19 HIP'ed at 2200°F, 15 ksi, 5 hrs., bottom: 2H20, HIP'ed at 2250 F, 15 ksi, 5 hrs.

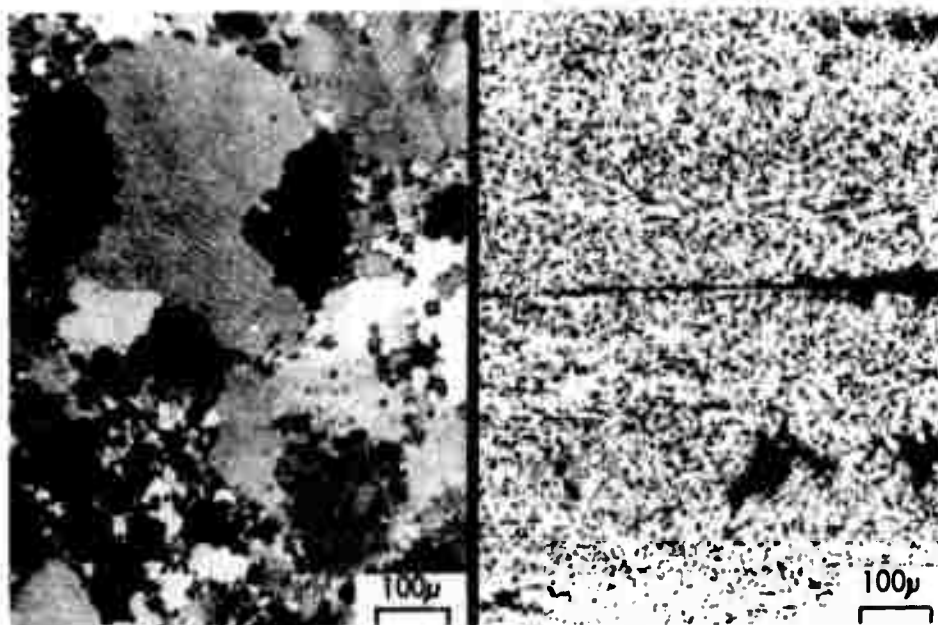


Figure 6. Left half: IN-100 LC HIP'ed at 2235°F, 15 ksi, 2 hrs. Chemstrand 400 μ powder. Can No. 2J34. Etched. Right half: IN-100 LC HIP'ed at 2235°F, 15 ksi, 2 hrs. plus extrusion at 2050°F, ~24X R.A. Can No 2J62. Internal tearing at prior particle boundary. Etched.

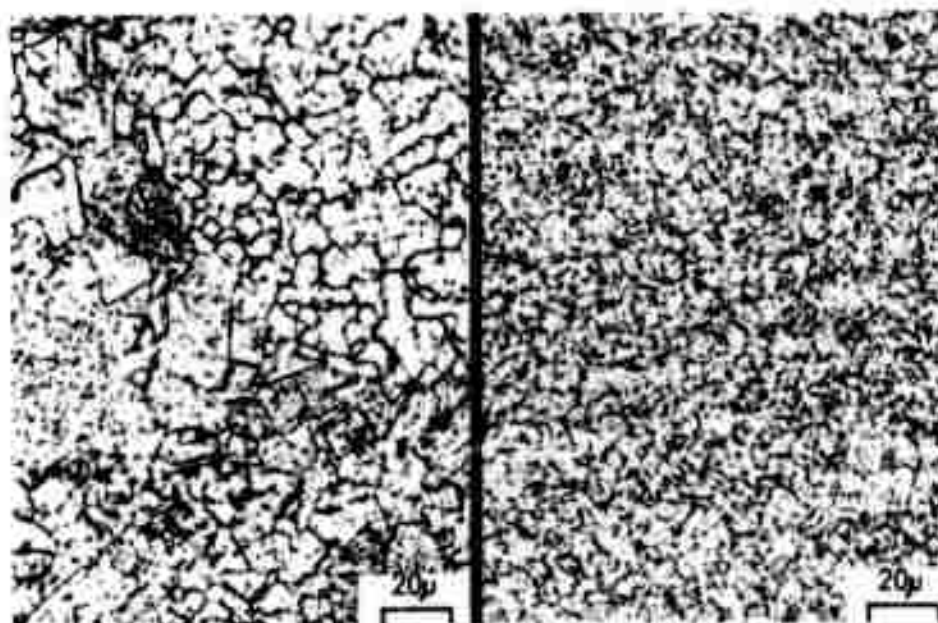


Figure 7. Left half: Mar M 509 HIP'ed at 2235°F, 15 ksi, 2 hrs. Homogeneous Metals -80 mesh powder. Can No. 2142. Etched. Right half: Mar M 509 HIP'ed at 2235°F, 15 ksi, 2 hrs. plus extrusion at 2050°F, ~5X R.A. Can No. 2139. Etched.

-18-

TASK II

SOLIDIFICATION RESEARCH

R. Mehrabian

P.A. Joly

M.C. Flemings

TASK II - SOLIDIFICATION RESEARCH

by

R. Mehrabian, P. A. Joly, M. C. Flemings

In this part of the program, work was continued on developing and evaluating new processes for atomization of metal powders. Specific aspects of these investigations have included:

1. The effects of the independent variables in the new Filatomization process, developed in this part of the program⁽¹⁾, on the formation and solidification of alloy powder particles were determined. A patent application based on this process was filed through the M.I.T. patent office.

2. Prealloyed powders of Maraging 300 alloy, IN-100 alloy, and a Mar-M-509 type alloy, produced by different atomization processes, were evaluated with respect to chemistry, morphology, and segregate spacings. Powder particles produced by spin atomization, a new process, were compared to powder particles produced by older, more established atomization processes.

1. Filatomization

Details of a new process for atomization of metal powders, developed in this part of the program, were reported earlier⁽¹⁾. The process, called Filatomization, entails filtration and subsequent atomization of alloy melts by forcing them through porous ceramic filters.

Experiments were continued to investigate the effects of the governing

parameters (i.e., temperature, filter material, pore size, pressure, etc.) on the mechanism of formation and size of the resulting powder particles. Sintered Al_2O_3 and SiO_2 disc filters, 87-150 μ pore size, were utilized to atomize powders of aluminum and tin alloys. The apparatus was modified, such that formation of the alloy powder particles could be observed and photographed using a set of magnifying lenses.

Experimental observations showed that successful formation of spherical powder particles depends on detachment of the liquid drops from the filter prior to growth and coalescence of adjacent drops. Conditions that permit liquid drops exiting from adjacent pores to coalesce result in formation of large liquid drops that do not completely solidify in flight and splat in the collector container. The different variables that affect formation and subsequent solidification of the alloy powder particles are; (a) pressure differential across the ceramic filter, (b) superheat in the melt, (c) the wetting angle between the melt and the ceramic filter, (d) the average pore size of the ceramic filter, and (e) the free flight time available for complete solidification.

(a) Pressure

Observations to date show that during Filatomization liquid metal flows preferentially through paths of least resistance, causing a channeling phenomenon to occur. Hence, only a small fraction of the available pores are utilized for drop formation. In general, increasing the pressure head on the melt, above a critical maximum, results in flow through greater number of pores accompanied by consolidation of drops, or streams, from adjacent pores (i.e., less than one drop diameter apart).

(b) Superheat

Direct observations during drop formation, below the filter, have shown that formation of consolidated large drops, or streams, can be correlated to superheat in the melt. In general, increasing the superheat in the melt results in formation of larger drops before detachment from the filter occurs.

(c) Wetting

Increased wetting between the ceramic filter and the molten alloy has an adverse effect on Filatomization. When the melt partially wets the porous filter, as in the case of aluminum alloy melts and SiO_2 filters, liquid drops forming below the filter spread out more easily and result in frequent formation of consolidated drops.

(d) Filter Pore Size

As expected, the diameter of filatomized powders decrease with decreasing average pore size of the filters used. However, variations in superheat, pressure, and wetting angle between the alloy melt and the filter, mentioned above, influence the average particle size in important ways.

(e) Heat Flow and Solidification

Heat flow analysis previously reported⁽²⁾, in this part of the program, was refined and extended to permit calculation of free fall times and distances necessary for complete solidification of Filatomized powders. Calculations were made for the Maraging 300 steel alloy for which heat transfer coefficients were previously determined⁽²⁾. Figure 1 shows plots of solidification times and free fall distances versus drop diameter calculated using a heat transfer coefficient $h=0.0095 \text{ cal/cm}^2 \text{ sec}^\circ\text{C}$.

Apparatus Modification

Detachment of liquid drops, prior to consolidation of adjacent drops, from the ceramic filters is the critical step for successful Filatomization. Understanding the effects, and subsequent control, of the variables listed above has been the major aim of this investigation. However, other processing techniques have also been developed to aid in detachment of the liquid drops from the ceramic filters. As example, one successful method has been to direct low velocity inert gas jets transversely across the base of the ceramic filters. A ring shaped, multiple hole, gas nozzle was located directly below, and around the circumference, of the ceramic filters. The slight disturbance of the forming liquid drops, induced by the inert gas flow, resulted in their early detachment. Other methods presently being investigated are vibration and application of electric and magnetic fields. Finally, other apparatus modifications have been made to study formation and detachment of liquid drops, from the base of the porous ceramic filters, by high speed photography.

2. Evaluation of Powder Particles Produced by Different Atomization Processes

In this part of the work, prealloyed powder particles of Maraging 300 steel alloy, IN-100 alloy, and a Mar-M-509 type alloy, produced by different atomization processes were evaluated. The different atomization processes were:

(a) Spir-atomization - A new proprietary atomization process that has been developed at Chemstrand Corporation.

(b) Inert gas atomization - A prealloyed ingot is remelted in argon or vacuum, and atomized by a stream of high purity argon gas.

(c) Vacuum atomization - The remelted alloy is pressurized and saturated with hydrogen. Atomization is obtained through a "pressure nozzle" operating between the hydrogen filled chamber and a vacuum chamber.

(d) Rotating Electrode Process - The end of a rotating electrode is arc melted in inert atmosphere and fine droplets are flung off by centrifugal force.

(e) Steam atomization - The prealloyed ingot is remelted in an atmosphere and atomized by a stream of low pressure steam.

Powder particles of the three alloys were characterized by chemical analysis, morphology, size distribution, and segregate dendrite arm spacings. Results of this study are presented in Table I and Figure 2. The spin atomized powder particles were by far the cleanest and most spherical particles obtained in all three alloys combined. However, in each individual type of alloy there were other comparable processes. For example, R.E.P. atomized powder particles of IN-100 and vacuum atomized powder particles of Maraging 300 steel alloy both contained less than 100 ppm of oxygen as did the spin atomized powder particles. Table I also lists nitrogen, argon, and hydrogen contents of the powders. As expected, steam atomization resulted in the highest oxygen and nitrogen contents. Figure 2 shows the measured secondary dendrite arm spacings in the different powder particles of the Maraging 300 steel alloy. Average secondary dendrite arm spacings in spin atomized powders is ~6 microns, and in coarse steam and argon atomized powders is ~10 microns. Results of dendrite arm spacing measurements in the other two alloys show the same trend.

Figure 3 compares scanning electron micrograph views of representative powder particles of IN-100 produced by three processes. The spin atomized

powder particles are smoother, more spherical, and more uniform in size than powder particles obtained by the other two processes.

Figure 4 shows scanning electron micrograph views and a photomicrograph of a polished and etched cross-section of Maraging 300 steel powder. The same type of smooth, well rounded and uniform powder particles were also obtained in the Mar-M-509 type alloy.

In summary then, comparison of atomized powder particles obtained by different atomization processes show that the new spin atomization process is quite promising and should be explored further. Powders of the three alloys were supplied to other groups in this study for hot isostatic pressing and extrusion into billets. Some of the properties of the billets thus produced are reported in this volume.

REFERENCES

1. Semi-Annual Technical Report No. 4, Task II, ARPA Order No. 1608.
2. Semi-Annual Technical Report No. 2, Task II, ARPA Order No. 1608.

TABLE I - POWDER DESCRIPTION

Alloy	Atomization Process	Median size μ	Gas content, p.p.m.				Shape of powders
			O	N	H	Ar	
Cobalt base alloy MAR-M-509-type alloy	spin atomized	340	45	<10	<1.0	<.2	solid spheres
	vacuum atomized	110	250-310*	10-100	5-10	<.2	flakes, solid spheres °
	steam atomized	2000	200-1200	100-600	11-24	<.2	flakes, hollow spheres °
Nickel base alloy IN-100	spin atomized	400	85	<10	<1.0	<.2	solid spheres
	R.E.F. atomized	170	70	10	56	.3	solid spheres
	argon atomized fine powder	75	170	7	17	1.6	solid spheres, with fine particles attached to coarser particles
Iron base alloy Maraging steel VM-300	spin atomized	430	42	-	-	-	solid spheres
	vacuum atomized	300	53	10	5.6	<.2	flakes, solid spheres
	steam atomized	1980	150-2000	-	-	-	solid spheres with porosity
	argon atomized + coarse powder	2590	630	-	-	-	solid spheres with porosity

* probably from retained slag.

+ further quenched in water tank.

° From Ray Robinson, Task III, this report.

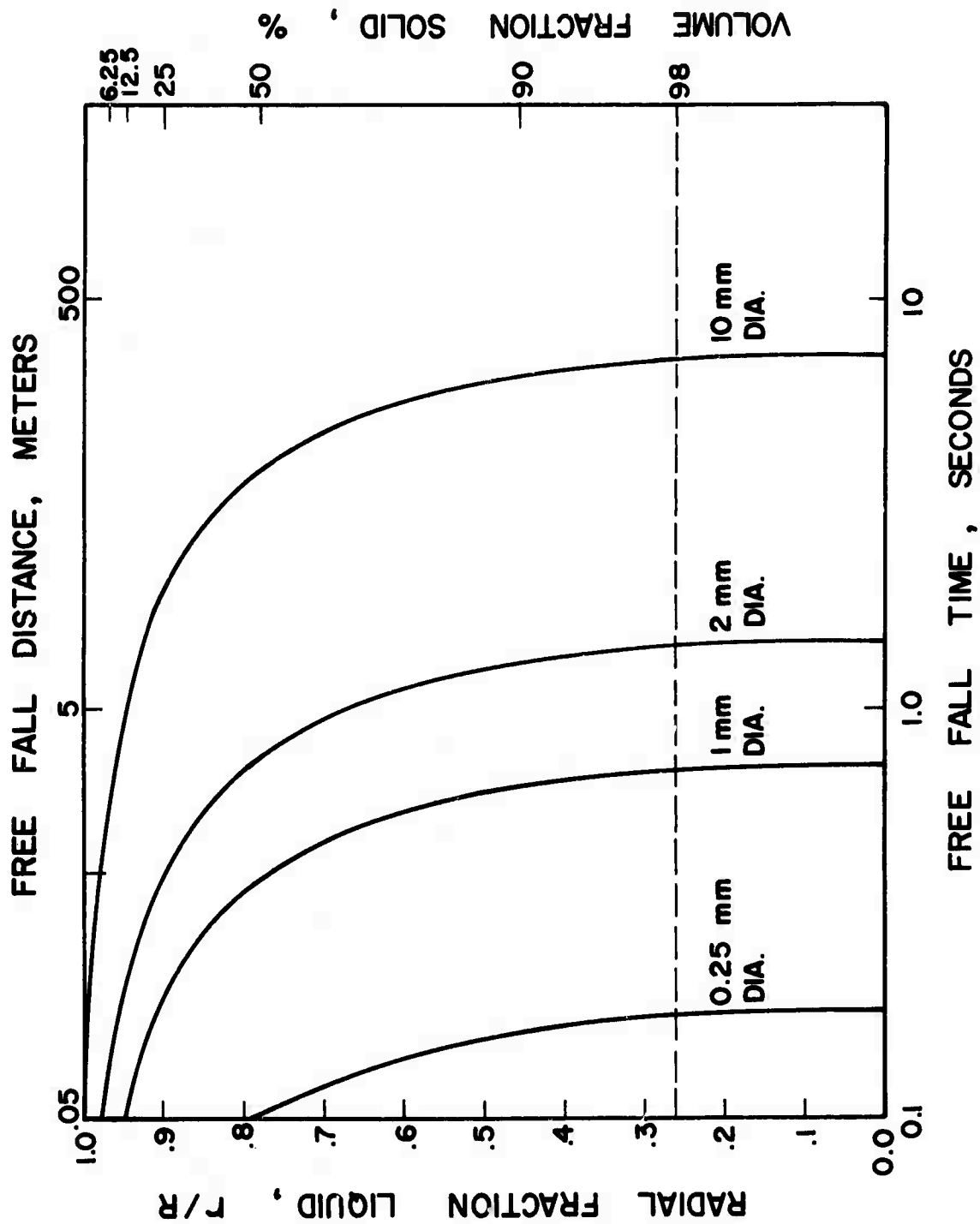


Figure 1. Calculated radial fraction liquid and volume fraction solid versus free fall time and distance for different size powder particles of Maraging 300 steel alloy.

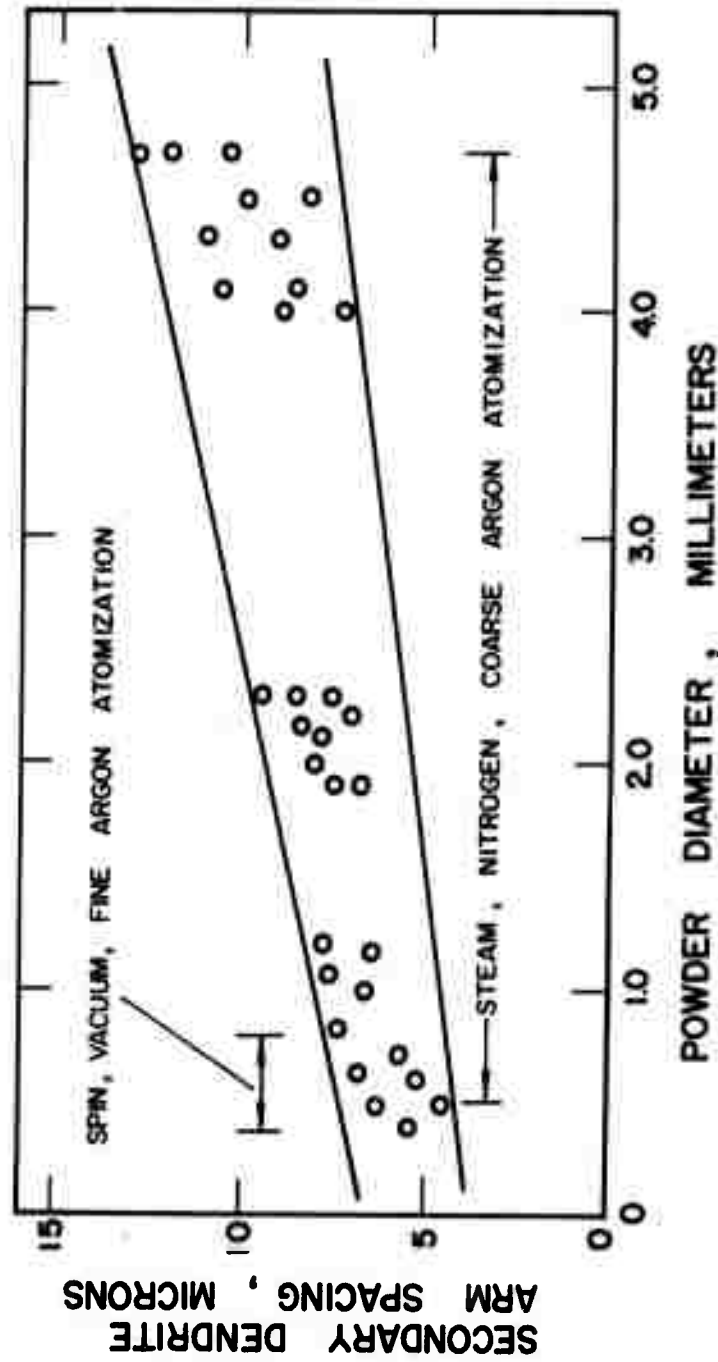


Figure 2. Secondary dendrite arm spacings versus powder particle diameter of Maraging 300 steel alloy obtained by different atomization processes.

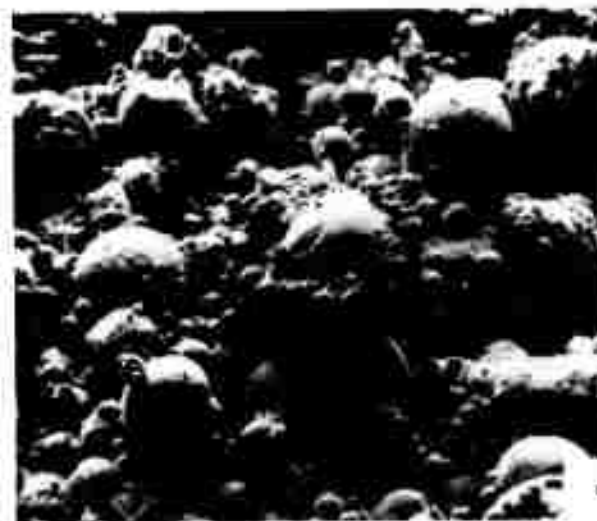
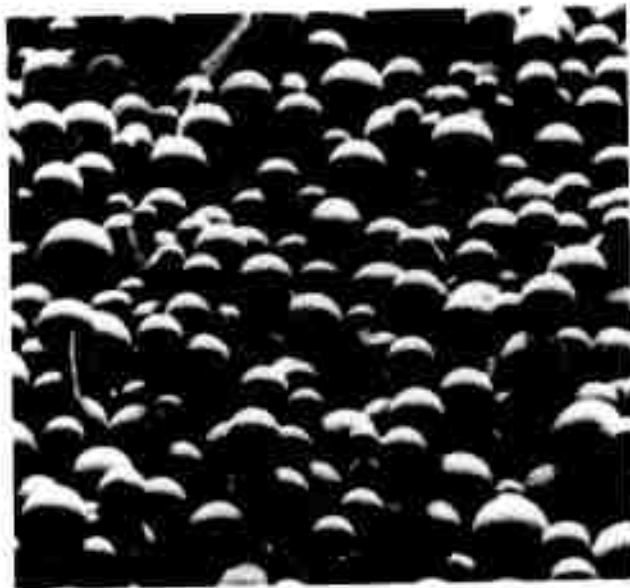
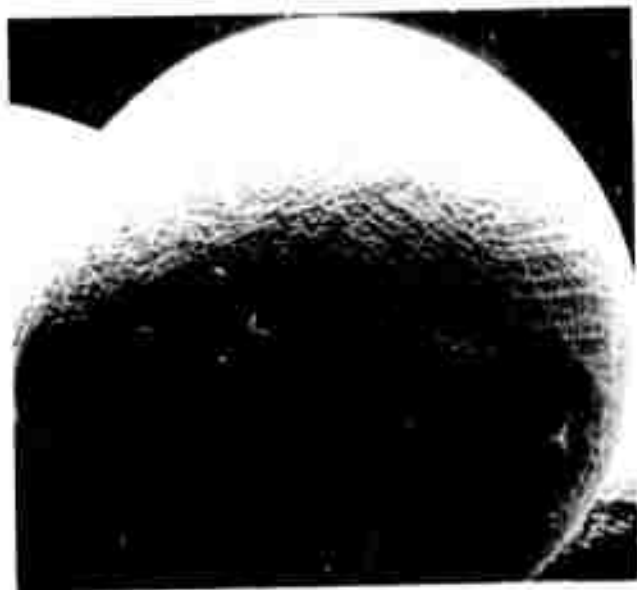


Figure 3. SEM micrograph views of atomized powder particles of IN-100 alloy; (a) and (b) show spin atomized powders at 56X and 215X, respectively, (c) and (d) show vacuum atomized powders at 57X and 22.5X, respectively, (e) and (f) show inert gas atomized fine powders at 210X and 1050X, respectively.



a



b



c

Figure 4. Spin atomized powders of Maraging 300 steel alloy; (a) and (b) are SEM micrograph views at 19X and 240X, respectively, (c) is a photomicrograph of a polished and etched cross-section at 200X.

Reproduced from
best available copy.



TASKS III AND IV

THERMOMECHANICAL TREATMENT, MICROSTRUCTURE
AND MECHANICAL PROPERTIES

L.F. Van Swam

R.K. Robinson

S.J. Berman

J. Im

R.M. Pelloux

A.S. Argon

N.J. Grant

MECHANICAL PROPERTIES OF 300 GRADE MARAGING STEELS

A. INTRODUCTION

An improvement of fracture toughness was previously shown to occur by decreasing the grain size of commercially available VASCOMAX 300. We have now carried out more tests on grain size refinement and the resulting tensile and fracture toughness properties are reported. Tensile and fracture toughness testing of HIP and hot-rolled high purity rotating electrode powder have been continued. Whereas delamination of powder particles was a problem in earlier testing, we have now succeeded in producing a material completely free of this kind of defect.

Research on the fatigue properties of 300 grade maraging steel has been expanded. Both annealed and aged Vascomax 300 were studied. The determination of the cyclic stress strain curves and the parameters n' and k' show that a large degree of cyclic softening takes place. The S-N curves for annealed and aged Vascomax 300 tested in dry argon (dewpoint -70°F) are reported. Strain controlled low cycle fatigue data for annealed material were obtained. The elastic and plastic strain components of each test were measured and the results are plotted together with the high cycle fatigue data and monotonic tensile data.

B. TENSILE AND FRACTURE TOUGHNESS PROPERTIES

In our last report it was shown that an increase in fracture toughness from 62 ksi $\sqrt{\text{inch}}$ to 71 ksi $\sqrt{\text{inch}}$ could be accomplished without decreasing the yield-strength by refining the grain size from 25 microns to 5 microns. In an attempt to still further improve the fracture toughness, 1-1/4 inch

plates of Vascomax 300 with a grain size of 25 microns were hot-rolled at 1600, 1500 and 1400°F to .3 inch thickness in 10% passes. The materials were air cooled after hot rolling and the resulting grain sizes were respectively 5 microns at 1600°F and 1 micron for the 1500 and 1400°F rolled material.

Tensile testing in a direction parallel to the rolling direction was done after the following heat treatments:

1. As received specimens 3014, 3015, 3016
2. As received + 3 hours 900°F ageing specimens G3014, G3015, G3016
3. 1 hour 1500°F anneal specimens A3014, A3015, A3016
4. 1 hour 1500°F anneal + 3 hours 900°F ageing
specimens AG3014, AG3015, AG3016

Table I shows a summary of the testing results. The yield and ultimate tensile strengths of the aged material in both conditions are higher than for the commercial material. The R.A. of all AG specimens shows an improvement from the commonly observed 50% to 62%. These same specimens also have a higher work-hardening exponent than the G specimens or commercial material. This is of significance since in general materials with a higher work-hardening exponent show better fracture toughness values.

Table I also gives the tensile data for two powder metallurgical products. Both were produced from high purity spinning electrode powder. The materials designated ER3014, ER3015 and ER3016 were extruded and subsequently hot-rolled at 1400, 1500 and 1600°F, respectively. The resulting grain sizes were 1 micron for ER3014 and ER3015 and 5 microns for ER3016. The material is completely free of banding or inclusion stringers. The tensile fracture surfaces of all these materials showed delamination

between the original powder-particles. Previous testing has shown that such delamination impairs the fracture toughness.

The last alloy for which data are given in Table I is designated HR 91. This material was made by hot isostatically pressing (28,000 psi at 2200°F) high purity powder in a 4 inch X 6 inch X 12 inch can. The compacted powder was then hot-rolled at 1900°F to 1/4 inch thickness. The total reduction accomplished was 91%. Materials made in a similar way but with lower reductions have repeatedly shown incomplete bonding between the powder particles. This high reduction produced for the first time a product which did not delaminate. HR 91 showed good tensile properties and a slightly improved R.A.

Table II lists the fracture toughness values for commercial, fine grained and powder metallurgy materials. In all tests the fracture surface was parallel to the rolling direction. Testing was carried out following ASTM E399 70T. The specimen thickness is 0.25 inch and the load to propagate the last .025 inch of the crack and the total number of cycles to propagate the fatigue crack are indicated. Rolling Vascomax 300 at 1600°F results in a material with a grain size of 5 microns and a K_{IC} of 71 ksi $\sqrt{\text{inch}}$. The yield strength for this material was the same as that for commercial stock. Rolling at 1400 or 1500°F resulted in slightly lower K_{IC} values but increased yield-strength from 280 ksi to 300 ksi. Specimens undergoing a 1 hour 1500°F anneal prior to ageing show a fracture toughness well over 70 ksi $\sqrt{\text{inch}}$, regardless of the rolling temperature. These materials show the best combination of yield strength (280 ksi) and fracture toughness (≈ 74 ksi $\sqrt{\text{inch}}$) so far obtained in this program.

Powder metallurgy products have been HIP pressed and hot-rolled between 2000 and 1800°F with different rolling reductions. K_{IC} values for material rolled 69%, 83% and 91% are given in Table II. HR69 and HR83 showed both extensive delamination between the original powder particles which was thought to impair the toughness. HR91 is completely free from any particle separation but it shows nonetheless a low K_{IC} value. It has been suggested that this might be due to argon pick up during pressing. Argon analysis of this material is now carried out and the results will be published in our next report.

C. FATIGUE OF MARAGING 300 STEEL

Figure 1 shows the high cycle fatigue curves for annealed and aged Vascomax 300. All specimens were tested in dry argon (dewpoint -70°F) and the specimen direction was always parallel to the R.D. of the material. Cyclic stress strain curves for both materials have been determined following the technique of J.D. Morrow. Hourglass shaped specimens .25 inch in diameter are exposed to blocks of increasing and decreasing strain. The strain is the controlled parameter and the increase after each completed hysteresis loop is programmed with a DATATRAK. The stress strain curve is formed by connecting the loop tips from the hysteresis loops. Between 8 and 12 blocks are needed for the material to become cyclically stable. The envelope of the different loop tips is shown in Figure 2 for aged Vascomax 300.

The cyclic stress strain curves for annealed and aged material together with the monotonic curves are plotted in Figure 3. Cyclic softening, especially for the aged material is quite large and is the reason for the

rather poor fatigue limit of this steel. The values of n' and k' from the equation $\sigma = k'(\Delta\epsilon_p/2)^{n'}$ are obtained by plotting the stress versus the plastic strain on log-log coordinates. This plot is shown in Figure 4 and the different values are indicated. Strain controlled low cycle fatigue data have been obtained so far for annealed material only. From the hysteresis loops which are plotted on an X-Y recorder at regular intervals the elastic and plastic components of each test are determined. The total strain and the number of reversals to failure are of course also known. The results can be plotted as $\Delta\epsilon/2$, the strain-amplitude versus the number of load reversals $2N$ on a log-log plot. In Figure 5, the elastic, plastic and total strain curves are plotted for annealed Vascomax 300. Data points at 10^4 or more reversals are high cycle fatigue data from Figure 1. These are obtained by dividing the stress for the data in Figure 1 by the elastic modulus which was assumed to be 26×10^6 psi. Any plastic strain is disregarded in this case and this explains the slightly different slope for the two elastic lines. The points where the elastic line and the plastic line intersect the one reversal line should be the same as, respectively, the true fracture stress divided by E and the true fracture ductility as obtained in tensile testing. These points are indicated by σ_f/E and ϵ_f and excellent agreement was found to occur.

Table I
Tensile Test Data 300 Grade
Maraging Steel

Specimen	U.T.S. ksi	0.2% Offset ksi	R.A. %
3014	153	120	72
3015	155	121	64
3016	142	113	65
A3014	148	116	74
A3015	136	110	75
A3016	140	110	72
G3014	304	301	57
G3015	302	297	49
G3016	289	284	53
AG3014	288	284	53
AG3015	286	280	63
AG3016	289	284	61
ER3014	167	120	79
ER3015	160	122	67
ERG3016	148	115	60
ERG3014	278	276	49
ERG3015	293	290	31
ER3016	292	290	46
HR91	146	114	74
HRG91	284	277	55

G indicates 3 hours ageing at 900°F
A indicates 1 hour anneal at 1500°F

Table II

Fracture Toughness of Several 300
Grade Maraging Steels

Specimen	Load lbs.	Cycles	K_{IC}	Average K_{IC}
VASCOMAX 300	700	28500	61.6	62.6
	625	19500	62.7	
	625	20500	63.3	
HR 69 (1/2" specimen)	1750	34150	49.3	51.1
	1500	35500	52.5	
	1500	40000	51.4	
HR 33	625	24000	53.9	54.8
	625	20000	53.7	
	625	21500	56.9	
HR 91	500	9000	41.3	40.0
	400	30000	39.7	
	450	25500	39.1	
G3014	500	18000	57.7	57.4
	500	16000	56.7	
	500	17000	57.4	
G3015	500	17000	61.5	62.3
	500	16000	62.8	
	500	9000	65.1	
G3016	500	15000	72.2	71.9
	500	16000	71.5	
	500	17000	75.0	
AG3014	500	18700	72.5	72.5
AG3015	500	12500	75.1	74.4
	500	14300	73.8	
AG3016	500	23700	74.3	75.1
	500	14700	77.5	
	500	17500	76.5	

STRESS
KSI

MARAGING
STEEL 300

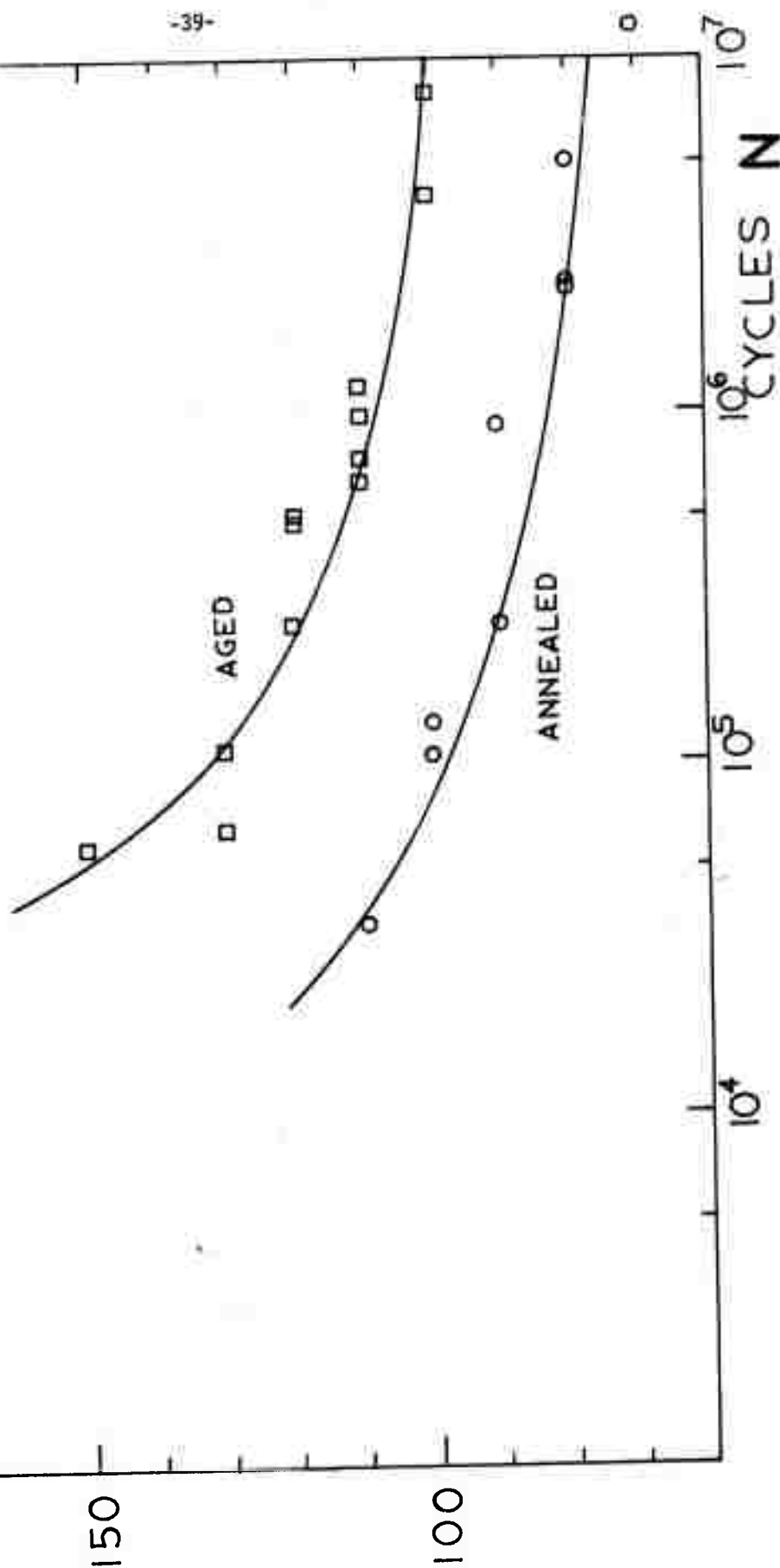


Figure 1 - Tension-Compression S-N curves for Vascomax 300 tested in dry argon.

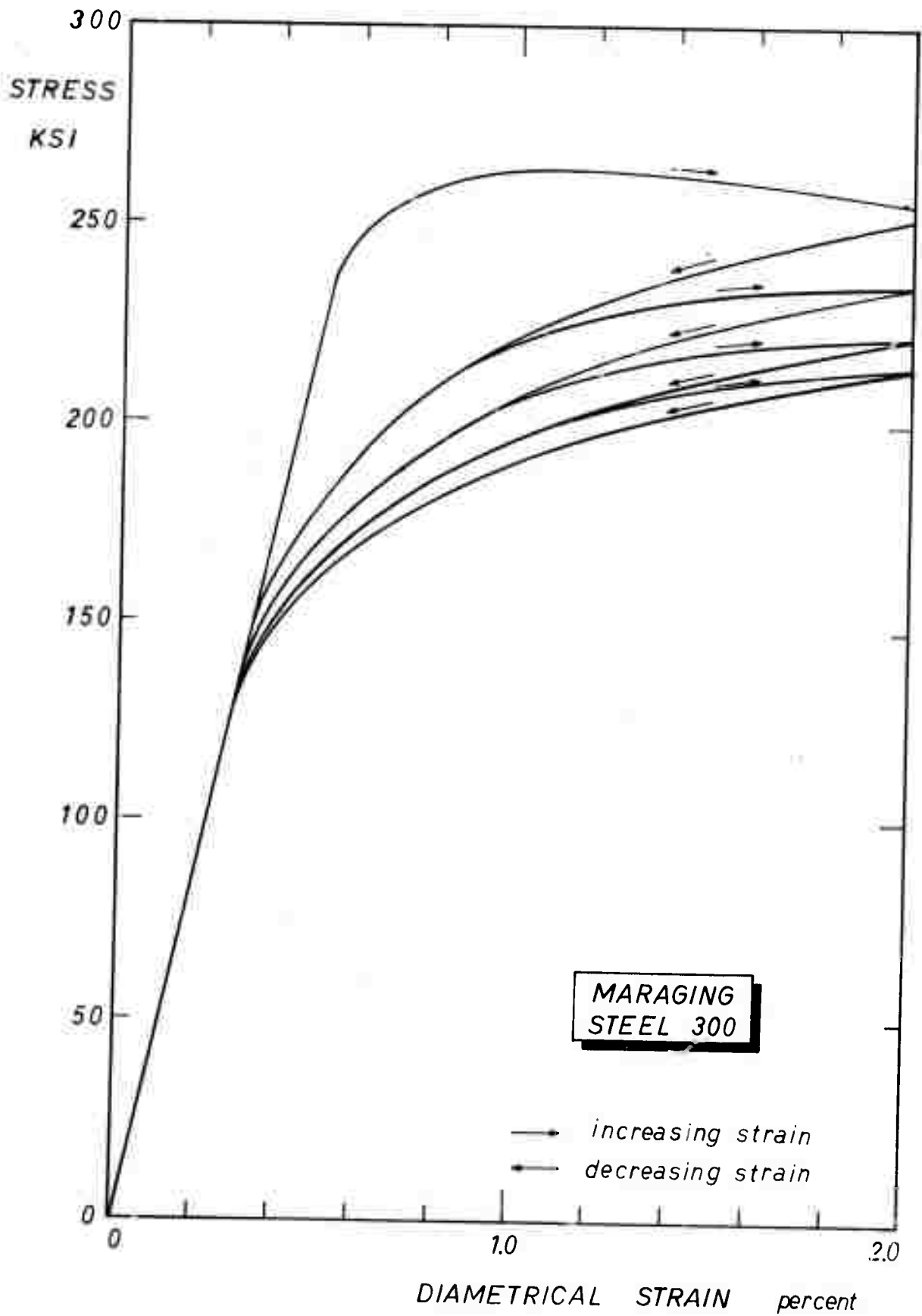


Figure 2 - Development of hysteresis loop tips of aged Vascomax 300 exposed to blocks of increasing and decreasing strain.

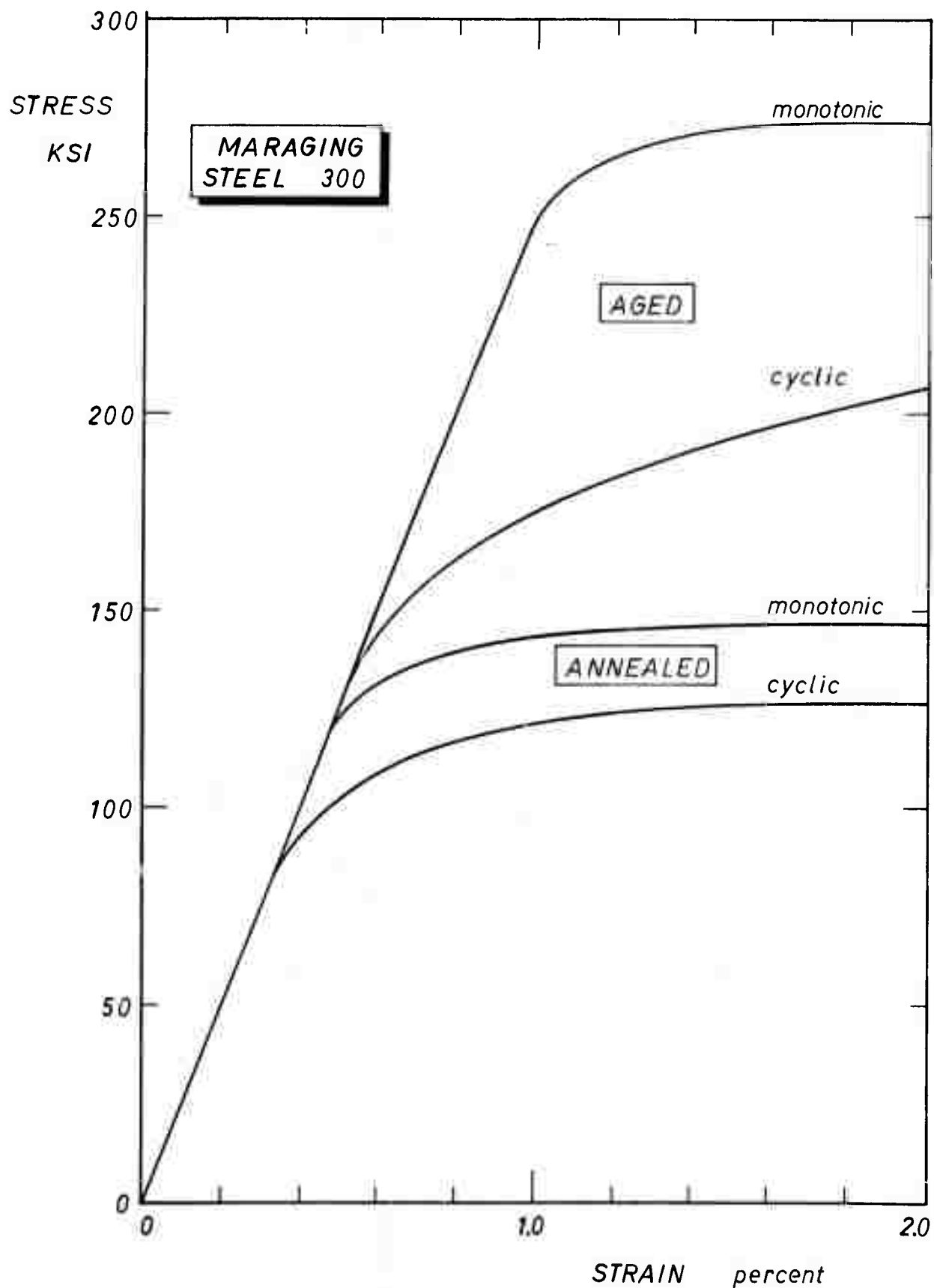


Figure 3 - Monotonic and cyclic stress strain curves for aged and annealed Vascomax 300.

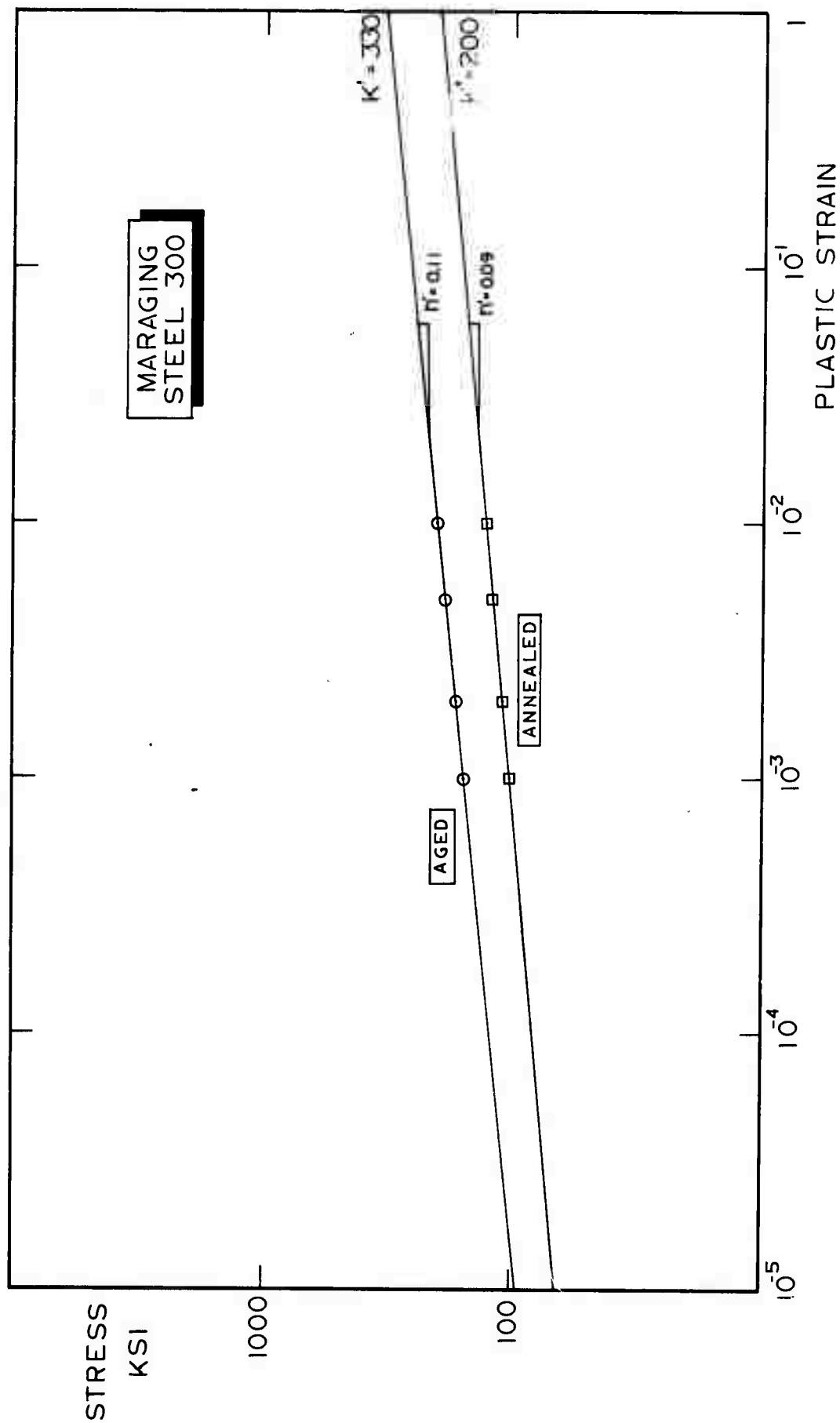
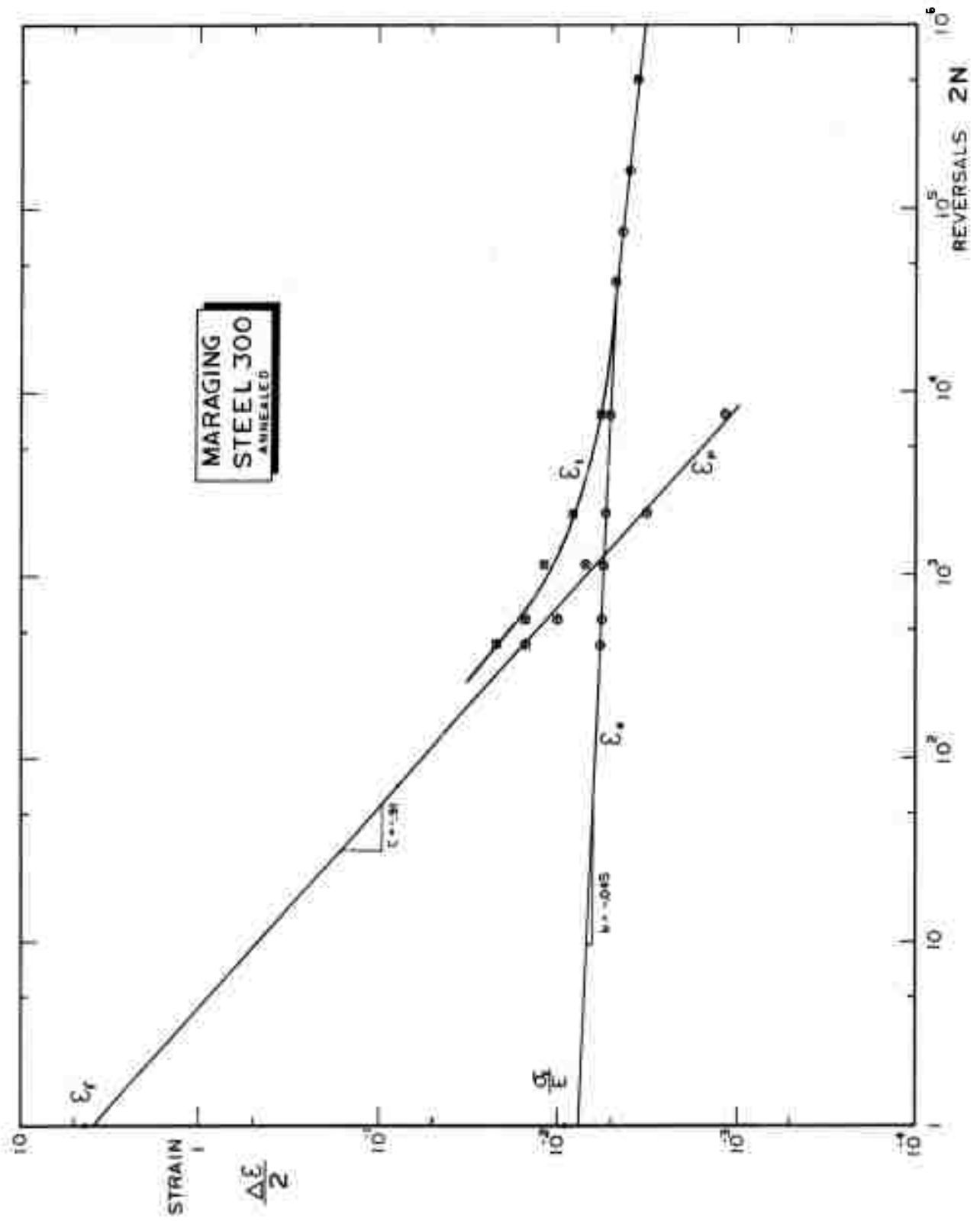


Figure 4 - Cyclic workhardening exponent and annealed Vascomax 300 as determined from the cyclic stress strain curve.



DEVELOPMENT OF P/M COBALT-BASE ALLOYS
USING RAPIDLY QUENCHED, PRE-ALLOYED POWDERS

Progress made in this program area since the last report includes the following:

1. Powder Processing and Alloy Consolidation

Steam, vacuum, and spin atomization resulted in powders differing in shape, mean size, size distribution, and impurity content. Powder morphologies in this program can be grouped into three classes: irregularly shaped flakes, rounded solid particles and rounded hollow particles which often contained large openings or holes through the wall. Examples of each of these morphologies were presented in Figures 2 and 3, and in Figure 1. Steam atomization with its coarse rounded powder product, economic potential, and rapid cooling rate was selected for the first atomization trials. Steam atomized M-509 alloys resulted in coarse rounded hollow and solid powders. Silicon additions up to 0.8wt %, which had been found to aid spheroidization of another cobalt base alloy (X-45), had little effect on M-509 spheroidicity (Figure 1), but appeared to be extremely beneficial in minimizing oxygen contamination, as shown

IMT HT #	Alloy	Silicon Wt %	Oxygen ppm
30-225	M-509	0	960
30-226	M-509	0	1000
30-227	M-509	0	916
30-112	Hi-Zr	.08	700
30-241	Hi W+Cr	.4	350
30-111	M-509	.83	200

The atomization pre-heat temperature for the above alloys was $2980 \pm 40^\circ\text{F}$ ($1640 \pm 22^\circ\text{C}$).

Steam atomized Cl-1 atom % HfC alloy was converted from a sharp, flaky powder to a rounded powder by increasing the pre-atomization melt temperature from 2850°F (1566°C) to 3100°F (1704°C) and by adding 0.8 wt % silicon. At the 3 atom % HfC level (9 wt % HfC), high superheats and silicon additions were only partially successful in spheroidizing the sharp, flaky powder (Figure 1). Again, oxygen levels were lower in the powder containing silicon additions. On a weight % basis, silicon, boron, and carbon also lower the melting point of cobalt more than any other common alloying addition ($\approx 100^\circ\text{F}$ (55°C)/1 wt %). Details of size, shape, and impurity analyses, are summarized below:

Atomization Process	Median Size μ 's	DAS μ 's	Impurities, ppm.			Shape
			O	N	H	
Steam	2000	2.5	200-1200	100-600	11-24	flaky, hollow solid spheres
Spin	340	1.5	40-50	<10	<1	solid spheres
Vacuum*	110	2.5	250**-300	10-100	5-10	flaky, solid spheres

* H_2 solubility method

** probably from retained melting slag

No argon or helium was found in any atomized powder; nor was any nitrogen or hydrogen detected in the spin atomized powder. DAS values are approximate since powder particles of random sizes were selected for measurement.

Full densification of all atomized powders, as determined by

metallography , was achieved by HIP except for Co-1 atom % HfC (CH₂) which was HIP at 2100°F (1149°C) and 14 ksi for one hour. Consequently all subsequent HIP runs were made at higher temperatures (to 2300°F, 1260°C) and pressures (to 28 ksi) for up to four hours. Argon contamination was introduced into several alloys during the HIP cycle (Table I). Density changes after annealing argon contaminated samples at 2300°F (1260°C) were noted in Table II. These data are summarized as a function of increasing HIP temperature as follows:

Alloy	Ar, ppm	DENSITY		HIP CONDITIONS		
		Decrease %	Time at 2300°F hrs	Temp °F	Time hrs	ksi
C51-03,4	1.9	5.1	20	2000	2	28
C51-04	0.7	3.3	20	2150	2	27
C51-H1	.2	0.1	20	2235	2	15
CH8-C1	.2	0.3	1	2235	2	15
C51-05	.2	15.3	36*	2300	1	28
C51-03	112	5.4	20	2300	2	28
CH6-H1	12	6.0	7	2300	4	26
CH7-H2	84	6.8	20	2325	2	28

* 2275°F

Powders which were HIP at 15 ksi (2200 ± 35°F (1204 ± 20°C)) did not pick up argon during the HIP cycle nor did the consolidated alloys swell during subsequent high temperature annealing. All powders analysed which were HIP at 2300°F (1260°C) or higher picked up argon except for the HIP + hot rolled alloy, C51-05-HR. All alloys consolidated at 2300°F (1260°C) swelled except for the W + Cr modified M-509 alloy C52-06-HE. Two M-509 alloys which were HIP at 2000°F (1093°C) and 2150°F (1177°C) picked up argon and swelled during annealing but to a lesser extent. All annealed

alloys which contained argon and/or swelled exhibited rounded porosity similar to that shown in Figure 4 for C51-05-HR. There is substantial evidence indicating that argon penetrates the previously evacuated and welded mild steel can surrounding the powders during the HIP cycle, and heat entrapped argon later causes swelling (density decrease) and gross internal porosity upon high temperature annealing.

Duplicate vacuum fusion analyses were made on the anomalous HIP plus hot rolled alloys, C51-05-HR, with 100 ppm of nitrogen being the only significant change in the results of Table I. A dark gray phase was observed around the edges of some of the voids shown in Figure 4. X-ray diffraction analysis of extracted phases (Table III) was inconclusive in identifying this gray phase. Abundant quantities of Ta-rich MC and Cr_{23}C_6 were identified, but a moderately intense peak corresponding to a d-spacing of 2.32 \AA was not identified. A similar peak was observed in both M-509 modifications, CA1-01-HE and C-52-06-HE, at about 1/3 the intensity (Table IV). Neither of these latter two alloys swelled after annealing for 7 hours at 2300°F (1260°C).

There is no simple explanation as to how argon penetrated the mild steel HIP can at a sufficient rate to correspond to a final concentration up to 100 ppm. Fissures or interconnected porosity in the TIG weld, incompletely sealed out-gas tubes, and defect structures such as grain boundaries, which could admit small amounts of argon throughout the pressing cycle or which could become sealed during the cycle after initial argon penetration, are potential candidates for rapid diffusion paths. If the density data of Table II reflect quantitative differences in argon contamination, it is interesting to note that the argon concentration was found

to increase in going from the outer radius towards the billet center of alloy C51-03. This trend is consistent with the view of argon penetration early in the cycle and then stopping or slowing down as the outer billet radius compresses and densifies with the last densification occurring in the center of the billet.

2. High Temperature Treatments

a. Annealing, Solutionizing, and Ageing

Each of the six HIP + extruded P/M alloys is discussed separately. Annealing, solutionizing, and ageing experiments were not conducted on the hot rolled or cast alloys.

i) M-509

One hour anneals up to 2100°F (1149°C) did not affect the room temperature hardness, grain size, or apparent size or distribution of the carbide precipitates. Changes in the lattice parameter indicated that some carbide solutionizing was occurring. X-ray diffraction analyses of the 111 and 220 peak shapes and the relative intensities on polished transverse sections did not reveal any significant changes; the 200/111 and 220/111 intensity ratios remained about the same as for randomly oriented pure cobalt (0.40 and 0.25, respectively; ASTM card #15-806). Softening occurred over the temperature range 2100°F (1149°C) to 2350°F (1288°C) with abnormal grain growth occurring at $2250 \pm 50^\circ\text{F}$ ($1232 \pm 28^\circ\text{C}$). The lattice continued to expand as the degree of solutionizing increased with temperature until a maximum lattice expansion of 0.09 \AA ($3.659 - 3.569 \text{ \AA}$, Table V) was achieved at 2350°F (1288°C). Abnormal grain growth is characterized by a significant degree of texturing in the 220 direction as

evidenced by ten-fold or greater increases in the 220/111 intensity ratio and by increases and decreases in the height-to-width ratios of the 111 and 220 peaks, respectively. Analysis of Cr_{23}C_6 and tantalum rich MC carbides, which were extracted from samples before and after solutionizing (Table XIII), indicated that about half of the Cr_{23}C_6 carbides present in as-extruded alloys remained in solid solution after water quenching from the solutionizing temperature. The actual carbide weight changes as determined by semi-quantitative extraction compared favorably with the calculated carbide weight fractions indicated in Table VI.

Room temperature hardness of fully solutionized M-509 was $R_C 30 \pm 2$ as compared to a $R_C 42$ hardness value in the as-extruded condition. Ageing experiments were conducted to determine an optimum heat treatment cycle with the data tabulated in Tables VII and VIII. Samples solutionized at 2325 to 2350°F (1274 to 1288°C) were aged at 1650°F (899°C) for 1, 4, 20 and 40 hours, and at 1800 and 2000°F (982 and 1093°C) for 1, 25 and 100 hours.

Some interesting results can be extracted from Table VIII. M-509 softened after a 1 hour exposure at 2300°F (1260°C) but did not re-harden after the standard ageing cycle. X-ray data indicated abnormal grain growth had occurred, but maximum solutionizing of chromium carbide had not yet occurred (Table V). Evidently grain size strengthening was removed by this particular heat treatment without being replaced by the same precipitation hardening which occurs after the higher temperature solutionizing treatments. Longer exposures (25 and 100 hours) at 2300°F (1260°C) restored a degree of age hardening response to M-509, but at reduced hardness values.

TMT generally stabilized the alloy grain structure to higher temperatures. The hardness values of all TMT M-509 alloys after annealing at temperatures in excess of 2200°F (1204°C) were higher than those for the as-extruded condition except for the alloy given 20% RA with 1500°F (816°C) intermediate anneals (Table VIII). Abnormal grain growth occurred between 2250 and 2300°F (1232 and 1260°C) except for S15N20 and S40N15 (final I.A. at 2100°F (1140°C)) which exhibited abnormal grain growth between 2100 and 2250°F (1149 and 1232°C) and no abnormal grain growth up to 2350°F (1288°C), respectively. The degree of (220) texturing for all TMT alloys was about the same as that of the as-extruded alloy except for the S40N15 alloy which was significantly less pronounced.

ii) Modified M-509 Alloys

The Zr and W-Cr modifications (CZ1 and C52) of M-509 exhibited greater resistance to softening, lattice expansion, abnormal grain growth and texturing during high temperature annealing treatments than that of the M-509 alloy. Despite their respective differences in chemistry and carbide content (Table VI), the modified alloys responded similarly to annealing, solutionizing, and ageing treatment. Alloy CZ1 had an excess of MC carbides and C52 had an excess of Cr_{23}C_6 compared to M-509. The lattice parameters for C51, C52 and CZ1 alloys were 4.44, 4.40 and 4.53 Å, respectively, as compared to that of pure TaC of 4.455 Å (ASTM card #19-1292). The expansion of the parameter for CZ1 can be accounted for by enhanced zirconium substitution in the lattice (ZrC : $a_0 = 4.698$, ASTM card #19-1487).

TMT enhanced abnormal grain growth and texturing in C52-S25N18 and reduced it in C52-S15N18 and 52-S30N21. TMT similarly enhanced abnormal grain growth and texturing in the CZ1 alloys, S20N15 and S22N15 (final I.A.

at 2100°F (1149°C)), and reduced it in S20N18.

iii) Co-1 and 2 atom % HfC Alloys (CH2 and CH7)

The Co-HfC alloys responded differently to heat treatment compared to the M-509 type alloys. The major difference was due to the lack of a solutionizing phase, i.e., the Co-HfC alloys contained only a HfC precipitate which did not undergo significant solutionizing-ageing reactions. Alloys CH2 and CH7 did not show any lattice change (after cooling) with annealing temperature up to the maximum 2300°F (1260°C) temperature of study.

CH2 was re-HIP at 2300°F (1260°C) early in the program to close up porosity; this treatment generated a duplex grain size and λ 20 textured structure similar to that of M-509. Care must be taken in comparing the as-formed properties of the six P/M alloys since CH2 has a heat treated (duplex) structure. The lower hardness values of CH2 are attributed both to its coarse grain structure and to its relatively small amount of precipitate (2.5 - 3 vol % calculated and 3.2 - 4.8 wt % measured values). The low volume fraction of carbides in CH2 probably made possible the abnormal grain growth during re-HIP. No annealing conditions were found which would allow a similar effect to occur in CH7 (or CH6). Alloy CH7 formed internal porosity when annealed for short time periods at temperatures above 2200°F (1204°C), which caused the apparent softening. Argon analysis on this alloy indicated a concentration of 84 ppm.

TMT was very effective in hardening CH2 (re-HIP) at annealing temperatures up to 1800°F (982°C), after which the hardness fluctuated about the re-HIP values, presumably caused by a combination of recrystallization (normal or secondary) and partial solutionizing of HfC. TMT was effective in raising the low temperature hardness values of CH7 and in delaying the

softening due to internal porosity formation.

iv) Co-3 atom % HfC (CH6)

This alloy had the best high temperature stability of all of the alloys studied in this program (Table VIII). A small but perceptible amount of lattice expansion occurred upon annealing for 1 hour up to 2400°F (1316°C). Abnormal grain growth, solutionizing-ageing reactions, and 220 texturing were not observed under any heat treatment conditions. Long term annealing at temperatures of 2300°F (1260°C) and higher resulted in porosity forming in the immediate vicinity of carbide precipitates. TMT affected the properties of this alloy substantially more than the hardness and X-ray data reveal. Discussion on TMT for this alloy is reserved for the mechanical properties section.

b. Grain Coarsening

Uniform grain coarsening was predictable for M-509 type alloys up to $2250 \pm 50^\circ\text{C}$ ($1232 \pm 28^\circ\text{C}$), for CH2 only after TMT had recrystallized the duplex re-HIP structure, and for CH7 and CH6 up to their incipient melting points. TMT of the M-509 type alloys raised the uniform coarsening range about 50°F (28°C), but had no significant effect on CH6. These observations are based on the evaluation of literally hundreds of metallographic specimens, but are qualitative in nature due to the difficulty in resolving grain boundaries in some of the highly worked or textured samples. In those cases where uniform grain coarsening occurred, the rate of coarsening was extremely slow with the extruded grain size only increasing by a factor of 2-4 after exposures of 100-125 hours. Uniform grain coarsening appeared to be controlled by the coarsening or solutionizing rate of the carbides, which were observed to be uniformly distributed throughout the grains and grain

boundaries. The stability of CH6 to coarsening is illustrated in Figure 5 which shows the change in grain and precipitate structure after a 1 hour exposure just below its incipient melting point ($\approx 2450^{\circ}\text{F}$, 1343°C).

Abnormal grain growth in the M-509 type alloys yielded unpredictable grain sizes especially for the size range of the coarse grains and for the fraction of coarse versus fine grains. Examples of the grain sizes (mean intercept diameter, \bar{L}) found after various annealing treatments in alloys C51, CH2, and CH6 are listed in Table IX. Duplex grain sizes are indicated by an average high and low grain size; single grain size numbers are indicative of a uniform grain size.

c. Oxidation

The cumulative weight gain data in cast and P/M alloys which were exposed to static air at 2000°F (1093°C) for times up to 100 hours are summarized below:

Alloy	$\frac{k}{\text{mg}} \frac{\text{cm}^2}{\text{t}^n}$	n	$\frac{G}{\text{mg}} \frac{\text{cm}^2}{\text{cm}^2}$	$\frac{g}{\text{mg}} \frac{\text{cm}^2}{\text{cm}^2}$
C51 P/M	2.5	.3	8.3	10.9
C51 Cast (Lit. ¹²⁰)	.65	.5	7	
C52 P/M	.3	.7	7.6	26.9
CZ1 P/M	.9	.5	7.2	5.5
CH2 P/M	10	.3	43.7	195
CH2 Cast			11.6	95
CH7 P/M	.25	.8	8.8	26
CH7 Cast			2.7	13.5
CH6 P/M	.5	.3	2.5	.6
CH6 Cast	.25	.8	10.3	49

where: G (total weight gain) $\approx kt^n$ (hours) and
 g = total loose scale weight, each after 100 hours

The oxidation resistance and scale adherence of P/M CH6 is comparable

to, if not better than, the best commercially available cobalt base super-alloy, FSX-414, which relies upon 30% Cr additions for oxidation resistance. Furthermore, this improved resistance was obtained with an alloy containing 9 weight % Hf, which points out the complexity of alloying for oxidation resistance; Hf (or Zr) additions are commonly believed to be either innocuous (below 1 wt %) or deleterious to oxidation resistance unless high Cr contents (≈ 30 wt %) are used. None of the other Hf based alloys compared favorably with cast or P/M M-509 except for cast CH7. The only alloy exhibiting parabolic rate behavior was P/M CZ1 which closely matched the kinetics of cast M-509 alloy.

De-carburization occurred in a wide band beneath the partially oxidized matrix containing the surface scale for all M-509 type alloys. The only scale identified on CZ1 was the cobalt chromite spinel, CoCr_2O_4 , which can be either protective or non-protective. P/M alloys, C52 and C51, had a Cr_2O_3 scale present in addition to the chromite spinel.

The Co-HfC P/M alloys were rich in the two scales, CoO and CoCr_2O_4 . CH2 had preferential oxidation at grain boundaries; CH7 underwent localized attack accompanied by severe spalling (Figures 6 and 7). Both CH2 and CH6 have carbon contents in excess of those needed for stoichiometric HfC formation; CH7 is hafnium-rich. The cause (s) for the unusual protection and adherence afforded by the CoO and CoCr_2O_4 scales on CH6 were not identified.

3. Mechanical Properties

a. Room Temperature Tensile Tests

i) M-509 Alloys

The refined structure (grains and precipitates) of as-extruded P/M

M-509 resulted in UTS and YS values about 70% higher, and elongation values about 500% higher than those of cast M-509 (Table X). High temperature anneals which coarsened the P/M structure reduced the degree of improvement over cast values but in all cases tensile properties exceeded those of the cast alloy. The lowest rupture elongation value (1%) occurred in a specimen containing eutectic carbides at isolated grain boundaries as a result of prior annealing above the incipient melting temperature. Upon ageing this sample, secondary carbides having a marked degree of preferred orientation presumably along 111 matrix habit planes precipitated within the grains.

TMT did not affect UTS or ductility, but it did increase YS for reductions in area up to 20-30%, at which point saturation of a stable dislocation sub-structure probably occurred. A decrease in YS for alloy S30N15 was attributed to extra I.A.'s which had to be used on this alloy to achieve 30% RA. Stored energy of TMT was removed by annealing for 4 hours at 2300°F (1260°C) except for samples swaged 40% which exhibited a greater resistance to softening during high temperature annealing.

The modified alloys, C52 and CZ1, behaved in a similar fashion except these alloys had lower ductilities in the as-extruded condition. Since precipitate size, volume fraction, and distribution of carbides for these two alloys were similar to those of M-509, lower ductility values are attributed to the nature of the carbide-matrix interface (coherency, orientation) or to the solid solution matrix. These alloys were much more difficult to swage without generating edge or circumferential cracks.

HIP and HIP plus rolled M-509 alloys exhibited limited ductility except for the vacuum atomized plus HIP alloy, C51-H1, which was the only alloy with low oxygen content (e.g., all others had ≈ 1000 ppm vs. 280 ppm

for C51-H1). The low ductility values associated with the strongest alloy, C51-05, were attributed to a relatively high content of dark gray stringer material believed to be residual steam atomized surface scale. The fracture surface was laminated, with large cracks being generated along the prior stringers. Porosity which formed during annealing was concentrated in regions having a high density of the dark gray phase. X-ray diffraction analysis did not provide positive identification of the gray phase.

ii) Co-HfC Alloys

UTS and YS values of P/M HIP plus extruded alloys increased as the volume fraction of HfC increased, and these values were higher than those of comparable cast alloys. TMT increased room temperature strength values of the 1 and 2 atom % HfC alloys (CH2 and CH7) in a predictable fashion, and annealing for four hours at 2300°F (1260°C) restored the as-extruded strength levels but with significantly higher ductilities. TMT of the 3 atom % HfC alloy, CH6, resulted in the highest strength values and greatest resistance to recovery and recrystallization (Table XI). Intermediate annealing at 1500°F (816°C) was the most effective treatment with nearly 90% of the 200 and 250 ksi Y.S. and UTS values, respectively, being retained after a 4 hour exposure at 2300°F (1260°C).

The greater stability of HfC in CH6 relative to Cr_{23}C_6 (and to a much lesser extent, TaC) in M-509 allowed HfC precipitates to be more effective barriers to dislocation movement over a much wider temperature range. The ability of CH6 to retain stored energy of cold work up to a homologous temperature of 0.95 is reminiscent of the characteristics of oxide dispersed alloys.

b. Stress Rupture

i) M-509

Grain size played a key role in determining the stress rupture properties at the temperatures evaluated (1200, 1500 and 1800°F)(649, 816 and 982°C). For 1800°F (982°C) exposures, negative slopes of (log stress versus log rupture life curves) less than 0.2 (Tables XII, log ksi/log hrs) corresponded to coarse (usually duplex) grain sizes (Table IX), while values equal to or exceeding 0.2 had grain sizes, \bar{L} , in the 3-10 μ range. Similarly, at 1500 and 1200°F (816 and 649°C), the critical slopes occurred at -0.1, i.e., coarse grained alloys had stress rupture slopes less than this value. The best stress rupture factors (stress for 100 hr life/slope) for M-509 at each of the three temperatures were from as-extruded alloys which had been given a grain coarsening treatment (\bar{L} = 15-300 μ 's) consisting of 4 hours exposure at 2300°F (1260°C). A slightly better rupture strength value (but a steeper slope) was obtained by heat treating at the incipient melting temperature (2350°F (1288°C) for 1 hour, causing eutectic carbides to form at grain boundaries). Rupture elongation and reduction of area values were significantly reduced by this treatment compared to the 2300°F (1260°C) treatment with intergranular cracking occurring along the grain boundary carbides.

TMT did not improve any of the stress rupture properties of M-509 type alloys except for alloy CZ1-S22N21723 which relied on the TMT and a final 2300°F (1260°C) anneal to coarsen the grain structure into duplex sizes. As-extruded M-509 exhibited large elongations at 1800°F (982°C) with the largest (102%) occurring at a stress of 10 ksi and a minimum creep rate of 0.4 hour⁻¹.

ii) Co-HfC Alloys

Grain size was not a prime consideration in the stress rupture performance of CH6 alloy since the grain size was stabilized by HfC precipitates at \bar{L} 's of 3-20 μ for all TMT and annealing treatments (Table IX). Alloy CH2 had a duplex structure and hence grain size effects were important. Alloy CH7 could be recrystallized by high temperature annealing, but the grain size appeared to be more stable than in CH2.

The best 1800°F (982°C) stress rupture properties for P/M CH6 resulted from a TMT consisting of 30% RA using the maximum I.A. temperature (2100°F (1149°C)). In general, the best 1800°F (982°C) stress rupture strengths (and factors, i.e., 100 hr σ /slope) were obtained by TMT without a final high temperature grain coarsening treatment. The 1500°F (815°C) stress rupture properties were better if the grain coarsening anneal was used. The 1200°F (649°C) stress rupture properties on as-extruded CH6 with and without the anneal were about the same. CH6 alloy S40N18 exhibited anomalous behavior by reversing the above 1800 and 1500°F (982 and 815°C) trends. High temperature annealing tended to remove some of the stored energy of TMT and to enhance formation of fine precipitates having a marked degree of preferred orientation presumably along 111 matrix habit planes.

The best stress rupture properties at 1800°F (982°C) for alloys CH2 and CH7 were obtained by recrystallizing TMT specimens into uniform grain structures via annealing at 2300°F (1260°C) for 4 hours. The 1800°F (982°C) stress rupture strengths of P/M Co-HfC alloys could be increased to that of their cast counterpart using TMT, but the slopes of the cast alloys were flatter.

c. Other Aspects

Hot workability of these alloys was assessed using high strain rate tests. All HIP plus extruded alloys exhibited elongations in excess of 26% at strain rates up to 20 sec^{-1} at 2100°F (1149°C) except for CH2 and CH7. CH2 was not fully dense and CH7 was susceptible to swelling and void formation at the test temperature. Elongations of about 10% were obtained with the only low oxygen as-HIP M-509 alloy. Interference by impurities such as argon or residual oxide scale may have masked the high strain rate results on steam atomized-plus-HIP M-509 powder. Preliminary hammer forging tests on P/M C52-HE at 1800°F (982°C) and 2100°F (1149°C) and on P/M CH6-HE at 1500°F (815°C) and 1800°F (982°C) were not encouraging. Severe end cracking occurred which indicated that more work needs to be done in this area to determine the optimum forging conditions. The potential for cold or hot working these alloys appears good; M-509 was solutionized and swaged 40% (RA) at room temperature, without intermediate anneals, before end cracking was observed, and no difficulty was experienced in any of the hot or warm rolling.

P/M Co-HfC alloys demonstrated a clear superiority in impact resistance compared to P/M M-509 alloys. Comparisons among all the alloys are valid, e.g., grain sizes, precipitate sizes and distribution, UTS and YS values were similar, except for CH2 which had a duplex structure and significantly lower UTS and YS values.

SUMMARY

1. Steam, vacuum, and spin atomization methods provide acceptable means of producing highly alloyed, multiphase cobalt base superalloy powders with good refinement of dendrites, grains, excess phase precipitates and melt

impurities. Steam atomization of cobalt-base alloys which have a high reactive metal content, e.g., M-509, can be used successfully provided minor additions of deoxidizers such as silicon are made and an adequate cleaning treatment is used after atomization.

2. Hot isostatic pressing (HIP) provided an effective means of consolidating all sizes and shapes of powder particles into a fully dense billet suitable for evaluation or suitable for hot working by extrusion or rolling. In some cases, the high pressure argon used in HIP penetrated the impaction containers and contaminated the densified alloy with unacceptably high levels of argon which subsequently is believed to have caused some of the swelling and void formation found during high temperature annealing of the contaminated alloys.
3. HIP plus extruded P/M alloys having extremely fine grain and carbide precipitate sizes, had room temperature YS and UTS values which far exceeded those of both cast and wrought contemporary cobalt base superalloys.
4. Ductilities, as indicated by percent elongation and RA, of P/M alloys at all temperatures and at strain rates up to 20 sec^{-1} were significantly better than their cast counterpart.
5. The as-extruded 1200, 1500, and 1800°F (649, 816, and 982°C) stress rupture properties of P/M M-509 were increased by a solutionizing-ageing treatment which allowed abnormal (parasitic) grain growth to occur generating a coarse-fine duplex grain size. The 1800°F (982°C) stress rupture properties were improved four-fold by this heat treatment but did not equal those of cast M-509.
6. TMT via swage-anneal was not effective in strengthening M-509 alloys but was very effective in increasing room and elevated temperature tensile

and stress rupture properties, respectively, of the P/M Co-HfC alloys. The 1800°F (982°C) stress rupture strength of P/M Co-HfC alloys could be increased to that of their cast counterpart using TMT but the slopes of the log stress-log rupture life curves of the cast alloys were flatter.

7. In addition to solid solution strengthening in both alloy systems, M-509 alloys were strengthened by two precipitates, Cr_{23}C_6 and a tantalum-rich MC carbide while the Co-HfC alloys contained only HfC precipitates. Cr_{23}C_6 precipitates in M-509 solutionized sufficiently at $2250 \pm 50^\circ\text{F}$ ($1232 \pm 28^\circ\text{C}$) to allow abnormal grain growth to occur generating a preferred 220 texture in the extrusion direction. HfC precipitates in P/M Co-HfC alloys stabilized the fine, equi-axed, as-extruded grain structure at temperatures in excess of 2400°F (1316°C) and retained much of the stored energy of TMT up to 2300°F (1260°C) for short term (1-4 hour) exposures. The oxidation resistance, as determined by interrupted exposures up to 100 hours in duration at 2000°F (1093°C), of P/M M-509 was comparable to that of cast M-509. The oxidation resistance of P/M Co-3 atom % HfC was comparable to or exceeded that of the best commercially available cobalt base superalloy.

TABLE I

HIP ALLOYS AND SOME IMPURITY ANALYSES BEFORE AND AFTER HIP

Alloy	Atomization Process	Impurities (ppm)*			Temp °F	HIP Conditions Time hrs	ρ ksi
		O	N	Ar			
C51-01-powder-HIP	steam	200 140	610 -	<0.2 -	2175	1	15
C51-03,4-powder-HIP	steam	980 630	- 13	- 1.9 3.6	2000	2	28
C51-04-powder-HIP	steam	1000 -	- <10	- 0.7 17	2150	2	27
C51-03-powder-HIP	steam	960 1190	115 <10	<0.2 112 2.9	2300	2	28
C51-05-powder-HIP + Hot Roll	steam	916 770	- <10	- <0.2 5.2	2300	1	28
C51-H1-powder-HIP	vacuum	- 280	<10 <10	<0.2 <0.2	2235	2	15
CZ1-01-powder	steam	700	-	-	2175	1	15
C52-06-powder	steam	350	-	-	2300	2	28
CH2-01-powder	steam	460	-	-	2100	1	14
CH7-H1-powder-HIP	vacuum	253	- 11	- 84	2325	2	28
CH8-C1-powder-HIP	spin	45 -	<10 <10	<0.2 <0.2	2235	2	15
CH6-H1-powder-HIP	vacuum	310 270	96 27	<0.2 12	2300	4	26

* Oxygen analyses using a LECO oxygen analyzer and calibrated standards. N, Ar, He, H analyses using vacuum fusion method. No helium was detected in any powder or consolidated alloy to the 2 ppm detectability limit.

TABLE II
DENSITY CHANGES DURING ANNEALING

<u>Alloy</u>	<u>Annealing Temp(°F)</u>	<u>Treatment Time(hrs)</u>	<u>Density Decrease (%)</u>
<u>MAR-M-509 Alloys</u>			
C51-01-H	2350	16	0.1
C51-03,4-H2000	2200	5	-0.1
	2300	1	1.7
	2300	20	5.1
	2350	16	7.6
C51-04-H2150	2200	5	0.3
	2300	1	0.6
	2300	20	3.3
	2350	16	5.9
C51-03-H2300	HIP Billet		4-3/4" dia. X 4-3/4" high
sample: outer radius	2300	1	2.5
	2350	16	5.3
3/4 radius	2300	1	3.1
	2350	16	7.2
1/2 radius	2300	1	3.2
	2350	16	7.5
1/4 radius	2300	1	3.6
	2350	16	8.3
Billet Center	2200	5	0.3
	2300	1	3.7
	2300	20	5.4
C51-H1-HT22(5)	2300	1	0.4
	2300	20	0.1
C51-01-HE	2300	4	0.1
	2300	64	0
C51-05-HR	2250	2	5.0
	2275	36	15.3
	2325	27	14.8
C52-06-HE	2300	7	0.5
CZ1-01-HE	2300	7	0.1

(continued)

Table II, continued

	<u>(°F)</u>	<u>(hrs)</u>	<u>(%)</u>
<u>Co-HfC Alloys</u>			
CH2-01-HE	2300	20	1.9
CH2-01-HEH	2300	4	0.4
CH7-H2-HE	2200	5	2.2
	2300	1	4.2
	2300	20	6.8
CH6-H1-HE	2300	7	6.0
	2400	2	17.6
	2425	2	17.9
CH6-M1-C	2425	17	1.5
CH8-C1-HT22(5)	2300	1	0.3

TABLE III

X-RAY POWDER DIFFRACTION PATTERNS OF PHASES ELECTROLYTICALLY
EXTRACTED FROM HIP AND HIP + HOT ROLLED MAR-M-509 P/M ALLOYS

$\frac{C51-03-H}{d(\text{\AA})}$	$\frac{I}{I}$	$\frac{C51-05-HR}{d(\text{\AA})}$	$\frac{I}{I}$	$\frac{C51-05-HRTR1}{d(\text{\AA})}$	$\frac{I}{I}$	$\frac{C51-05-HRTR2}{d(\text{\AA})}$	$\frac{I}{I}$	$\frac{C51-05-HRTR3}{d(\text{\AA})}$	$\frac{I}{I}$	$\frac{C51-05-HRTR4}{d(\text{\AA})}$	$\frac{I}{I}$
2.584	100	2.584	100	2.575	100	2.575	100	2.575	100	2.579	100
		2.392	24	2.392	20						
		2.318	18	2.311	35	2.311	30	2.311	32	2.311	24
2.236	62	2.236	64	2.226	60	2.229	50	2.229	56	2.232	63
		2.182	22	2.185	15					2.148	8
2.061	12	2.055	56	2.058	50	2.052	16	2.055	23	2.055	24
				2.037	25	2.034	30	2.037	26	2.037	24
		1.887	13								
		1.802	11								
		1.766	9	1.763	15	1.759	9	1.763	14	1.763	11
		1.608	9								
1.574	34	1.577	36								
1.341	41	1.344	40	1.573	30	1.572	25	1.573	30	1.573	29
1.286	19	1.289	18	1.343	30	1.340	27	1.342	30		
		1.255	18								
		1.230	7								

TABLE IV

X-RAY POWDER DIFFRACTION PATTERNS OF PHASES ELECTROLYTICALLY
EXTRACTED FROM HIP + EXTRUDED MAR-M-509-TYPE ALLOYS

C51-01-HE			C52-06-HE			CZ1-01-HE			ASTM Index	
d (Å)	I	I_{100}	d (Å)	I	I_{100}	d (Å)	I	I_{100}	d (Å)	I_{100} (hkl)
2.570	60	100	2.543	50	100	2.616	41	100	2.571	100
2.226	40	67	2.200	42	84	2.265	30	73	2.227	65
1.570	28	47	1.554	25	50	(1.600	16	39)	1.575	45
(1.338	37	62)	$a_0 = 4.40$			1.563	17	41	1.344	40
1.282	15	25				1.305	7	17	1.287	14
$a_0 = 4.44$						$a_0 = 4.53$				
									TaC #19-1292	

Table IV, continued

			C52-06-HE			CZ1-01-HE					
d (Å)	I	I ₁₀₀	d (Å)	I	I ₁₀₀	d (Å)	I	I ₁₀₀	d (Å)	I ₁₀₀	(hkl)
									ZrC	8F	#19-1487
1.685	8		2.32	7	27	2.31	5	100	2.706	100	111
			1.688	26	100	1.688	4	80	2.345	80	200
			1.628	12	46	1.629	4	80	1.659	50	220
						1.325	4	80	1.415	45	311
									1.355	18	222
									1.174	10	400
									ZrN		#2-956
									2.64	100	
									2.29	100	
									1.62	80	
									HfN	8F	#6-516
									2.62	100	
									2.26	70	
									1.60	40	

() means two or more peak overlaps

TABLE V
X-RAY DIFFRACTION DATA AFTER ISOCHRONAL (ONE HOUR) ANNEALING TREATMENTS

Alloy	Temp °F	2θ		Intensity 220/111	Height 220/111	Width _{1/2} 220/111	H/W _{1/2}	
		111	220				111	220
C51-01-HE HIP + Extruded	1500	67.3	130.0	0.18	0.11	1.7	28	1.8
	1800	67.4	130.4	0.24	0.12	2.0	16	1.0
	2100	67.4	130.2	0.13	0.09	1.5	22	1.2
	2250	67.2	130.0	0.18	0.10	1.9	26	1.3
	2300	67.3	129.5	0.31	0.2	1.8	12	1.0
	2350	67.2	129.5	2.0	1.3	1.5	10	9.2
	2400	67.2	129.2	6.3	4.2	1.5	4.4	12
		67.1	129.4	1.06	0.51	2.1	10	2.4
C52-06-HE HIP + Extruded	1500	67.2	129.9	0.4	0.17	2.4	17	1.2
	2250	67.4	130.0	0.35	0.16	2.2	21	1.6
	2300	67.1	129.7	0.31	0.17	1.8	12	1.1
	2350	67.1	129.6	0.35	0.21	1.7	18	2.2
		66.9	129.1	1.1	0.7	1.6	9.7	4.2
CZ1-01-HE HIP + Extruded	1500	67.4	130.1	0.32	0.13	2.4	21	1.2
	2250	67.3	130.1	0.30	0.13	2.4	21	1.1
	2300	67.1	129.8	0.23	0.15	1.6	22	2.2
	2350	67.2	129.8	0.63	0.31	2.03	19	2.9
		67.2	129.4	0.75	0.41	1.8	18	2.5
CH2-01-HEH HIP + Extr + HIP	1500	67.2	129.9	1.1	0.55	2.1	10	2.7
	2300	67.3	130.0	0.82	0.39	2.1	23	4.3
		67.3	129.8	0.70	0.41	1.7	21	5.0

(continued)

Table V, continued

Alloy	Temp °F	2θ		Intensity 220/111	Height 220/111	Width _{1/2} 220/111	H/W _{1/2}	
		111	220				111	220
CH7-H2-HE HIP + Extruded		67.2	129.5	0.40	0.2	1.7	16	2.3
	1500	67.1	129.6	0.40	0.25	1.6	13	2.0
	1800	67.0	129.5	0.44	0.27	1.6	16	2.6
	2100	67.3	129.8	0.35	0.24	1.5	13	2.0
	2300	67.1	129.5	0.37	0.27	1.4	10	2.0
CH6-H1-HE HIP + Extruded		67.4	129.7	0.14	0.1	1.7	21	1.0
	1500	67.5	130.0	0.23	0.11	2.1	14	0.7
	1800	67.2	129.8	0.05	0.14	1.2	14	0.5
	2300	67.0	129.6	0.33	0.17	2.0	20	1.8
	2350	67.1	129.7	0.12	0.08	1.5	30	2.3
	2400	67.2	129.6	0.10	0.08	1.2	25	1.8

TABLE VI
CALCULATED CARBIDE WEIGHT AND VOLUME FRACTIONS BASED ON STOICHIOMETRIC PHASES

Alloy	Basis: 100 grams* "C" (gr-atom)		"M" (gr-atom)		Carbide Weight** (grams)	(%)	Carbide Volume*** (cc)	(%)	Average Density (gr/cc)
C51-01-HE									
Cr ₂₃ C ₆	0.02966		0.1137		6.2681	64.1	0.8967	75.0	
TaC	0.01520		0.0152		2.9326	30.0	0.2025	16.9	
ZrC	0.00384		0.00384		0.3961	4.1	0.0604	5.1	
TiC	0.00292		0.00292		0.1751	1.8	0.0356	3.0	
					9.7719	100.0	1.1952	100.0	8.176
CZ1-01-HE									
Cr ₂₃ C ₆	0.01841		0.07057		3.8905	39.3	0.5566	46.0	
TaC	0.01697		0.01697		3.2670	33.0	0.2256	18.7	
ZrC	0.02456		0.02456		2.5353	25.6	0.3865	32.0	
TiC	0.00334		0.00334		0.2001	2.1	0.0407	3.3	
					9.8929	100.0	1.2094	100.0	8.180
C52-06-HE									
Cr ₂₃ C ₆	0.04166		0.1597		8.82	82.0	1.263	85.3	
TaC	0.00608		0.00608		1.173	11.0	0.0810	5.5	
ZrC	0.00219		0.00219		0.226	2.0	0.0345	2.3	
TiC	0.00835		0.00835		0.500	5.0	0.1016	6.9	
					10.72	100.0	1.479	100.0	7.25
CH2-01-HE									
Cr ₂₃ C ₆	0.00208		0.00797		0.4394	13.7	0.06286	22.3	
HfC	0.01457		0.01457		2.7756	86.3	0.21907	77.7	
					3.2150	100.0	0.28193	100.0	

(continued)

Table VI, continued

Alloy	Basis: 100 grams*		Carbide Weight** (grams)	Carbide Volume*** (cc)	Average Density (gr/cc)
	"C" (gr-atom)	"M" (gr-atom)			
CH7-H2-HE HfC	0.0358	0.0358	6.8306	0.5391	12.67
CH6-H1-HE Cr ₂₃ C ₆ HfC	0.00184	0.00705	0.3887	0.0556	6.6
	0.04978	0.04978	9.4979	0.7496	93.4
			9.8866	0.8052	12.28

* C x 3.833 = Cr, C x 1.0 = M
 ** (gr-atom x molecular wt.) = wt.
 *** wt/density = volume

TABLE VII

AGEING DATA ON MAR-M-509-TYPE ALLOYS

Alloy	Age		2 θ		220/111 Ratios		H/W _{1/2}		I 220/111	Hardness R _C
	T (°F)	t (hrs)	111	220	Ht.	W _{1/2} max.	111	220		
C51-01-HE	none	none	67.3	130.0	0.11	1.7	28	1.8	0.18	42
	water quench		67.2	129.2	4.2	1.5	4.4	12	6.3	32
	1650	1	67.3	130.1	2.93	1.6	3.3	6.1	4.7	42
	1650	20	67.4	130.4	9	1.32	1.7	12	12	41
T2350	air cool		67.2	129.4	0.9	2.0	8.5	3.6	1.8	31
	1650	40	67.3	130.2	0.38	2.1	10	1.8	0.8	38X
T2325	air cool		67.1	129.3	0.33	2.0	13	2.1	0.64	32
	1800	1	67.1	129.9	0.71	2.3	6.9	2.1	1.6	38
	1800	25	67.3	130.1	0.67	2.0	16	5.3	1.3	37
	1800	64	67.3	130.1	0.86	2.3	12	4.3	2.0	36X
	2000	1	67.1	129.1	0.63	2.0	18	5.7	1.3	33X
	2000	25	67.2	130.0	11.0	1.1	3.7	36	12.0	36
	2000	100	67.4	130.5	1.1	1.9	8	4.9	2.2	34
	2350		67.1	129.6	0.1	1.8	33	1.2	0.2	46X/30*
	1650	40	67.3	130.3	0.015	1.6	44	0.4	0.02	38
	2350		67.2	129.4	0.3	1.7	32	5.3	0.5	46X/32X
S30N18T	1650	40	67.3	130.3	0.19	2.0	35	3.1	0.38	39X
S40N18T	2350		67.3	129.6	1.1	1.6	12	8.5	1.7	45/33
	1650	40	67.3	130.3	0.8	1.8	17	8	1.4	39X
S20N15T	2350		67.2	129.4	1.3	1.6	2.4	2.0	2.1	50/32
	1650	40	67.2	130.1	2.9	2.0	4.3	7.0	5.8	39X
S30N15T	2350		67.2	129.5	3.5	1.3	4.4	12	4.3	48X/30
	1650	40	67.3	130.2	2.8	1.8	4.6	7.1	5.1	38X
S40N15**T	2350		67.2	129.5	0.3	1.8	29	4.6	0.5	46/33X
	1650	40	67.4	130.1	0.16	1.9	26	2.3	0.31	39X

(continued)

Table VII, continued

Alloy	Age		2θ		220/111 Ratios		H/W _{1/2}		I 220/111	Hardness R _C
	T (°F)	t (hrs)	111	220	Ht.	W _{1/2} max.	111	220		
C52-06-HE T2350	none	none	67.2	129.9	0.17	0.24	17.4	1.2	0.4	42
	air cool									
	1800	1	67.0	129.2	1.0	1.6	11	7	1.6	33
	1800	25	67.2	129.8	0.29	1.6	6.2	1.1	0.46	38
	1800	64	67.2	129.8	0.38	1.9	12	2.3	0.72	38X
	2000	1	67.3	130.1	0.43	2.2	15	3.0	0.94	41
	2000	25	67.1	129.6	0.52	2.0	24	6.2	1.0	38X
	2000	25	67.1	129.7	0.79	1.8	15	6.4	1.4	39
	2000	100	67.3	130.1	0.83	1.9	6	2.7	1.6	35
	none	none	67.4	130.1	0.13	2.4	20.8	1.2	0.32	42
CZ1-01-HE T2350	air cool									
	1800	1	67.1	129.5	0.23	1.7	7.3	1.0	0.39	30X
	1800	25	67.1	129.8	0.12	2.0	4.0	0.2	0.24	35
	1800	64	67.3	130.1	0.28	2.0	13	1.8	0.56	36
	2000	1	67.3	130.0	0.58	2.0	12	3.5	1.2	37
	2000	25	67.2	130.0	0.20	1.9	16	1.7	0.38	35X
	2000	25	67.2	129.9	0.14	2.0	9.3	0.7	0.28	34X
	2000	100	67.1	129.8	0.32	2.5	9.7	1.2	0.8	37X
	none	none								
	air cool									

* xx/xx hardness before/after solutionizing treatment
 ** Except for final I.A. at 2100°F

TABLE VIII
SOLUTIONIZING AND AGEING DATA

Alloy	Hardness R _c	Solutionize at 2300°F				Solutionize at 2350°F				
		R _c 1 hr.	A6	25 hr.	R _c A6	100 hr.	R _c A6	R _c 1 hr.	Age at 1650°F 4 hrs 20 hrs 40 hrs	
C51-01-HE	42			water quenched						
C51-01-HE	42	31X	31	24	32	10	18X	32	42	-
S20N18	46X							31	35	38X
S30N18	46X							30	34X	38
S40N18	45	38	38	33	35X	16	27	32X	37	39X
S20N15	50							33	38X	39X
S30N15	48X							32	38X	39X
S40N15*	46	38	38X	34	37	17X	24	30	33	38X
C52-06-HE	42	40	-	36	38	11	17X	33X	37	39X
S30N21	46	40X	-	38	39X	14	30			
CZ1-01-HE										
T2350A18(1)	36	38X	-	29	33X					
T2350A18(25)	35					31X	34			
S22N21	45X	37	-	34	36	28	36			
CH2-01-HEH										
S40N18	31	29X	30	24	29	21	22			
S40N21	45X	32	30X	26	26X	22	22			
	44	31	32	28	29	25	25			
CH7-H2-HE										
S40N18	33X	15	13	11	13X	10	10			
S30N15*	45	24X	22	17	15	10	13			
	39	28	28	24	26	<1	1			
CH6-H1-HE										
S30N21	42	40X	-	38	38	33	32			
S30N18	46	39	-	37	37	33	34			
S40N18	51	41X	-			34	33			
S20N15	46	39		38X	38X					
S30N15	50	40X								
S30N15	50	40X		37X	36X	34	34			

* Except for final I.A. at 2100°F

TABLE IX
EXAMPLES OF GRAIN SIZES IN P/M COBALT BASE ALLOYS
AFTER ANNEALING AT 2300°F (1260°C)

Prior Treatment	Time at 2300°F	Grain Size, (\bar{L} , μ 's)		
		C51	CH2	CH6
<u>As Extruded</u>	0	3.8	10-75	4
	1	10-500	15-100	
	25		20-200*	4.5
	100	60-800	20-70	20
<u>S20N15</u>	0	4		3
	1	25-150		4.5
	100			16
<u>S30N15</u>	0	4		3
	1	x**-1000		4.5
	25			5.5
<u>S40N15</u>	0	2.5		4
	1	10-40		
	100	60-1000		
<u>S20N18</u>	0	3		3
	1	x-1000		3
<u>S30N18</u>	0	6		
	1	8		
	100			18
<u>S40N18</u>	0	10		4.5
	25	80		6
	100	200-1500		
<u>S30-40N21</u>	0		13	3.5
	1		20	
	25		25	7
	100		40	7

Note: Low-high range of grain sizes is indicated for duplex grain structures. Single value indicates uniform grain size.

* few isolated grains are larger

** letter "x" means finer grain size was not measured

TABLE X

ROOM TEMPERATURE TENSILE PROPERTIES OF
MAR-M-509-TYPE P/M ALLOYS

Alloy	YS (0.2%) ksi	UTS ksi	Elong. %	R.A. %
<u>HIP + EXTRUDED ALLOYS</u>				
<u>MAR-M-509 P/M Alloy</u>				
C51-01-HE	135	190	11	8
C51-01-HE	123	195	17	14
T2280(116)A6	94	166	11	8
T23(4) no age	96	166	24	21
T23(4)A6	110	155	10	10
T23(64)A6	114	134	2.8	1.0
T2350(1)A6	92	120	1.0	1.0
S20N15A6	169	202	13	18
S30N15A6	154	193	14	21
S30N15T23(4)A6	114	153	7.6	10
S40N15*A6	166	193	13	15
S40N15*T23(4)A6	130	162	4.3	3
S20N18A6	143	195	20	19
S20N18T23(4)A6	93	127	9.6	8.0
S30N18A6	164	200	14	12
S30N18T23(4)A6	122	170	11	10
S40N18A6	165	195	13	12
S40N18T23(4)A6	122	166	9.4	6.0
<u>H1 W, Cr, and C Modification</u>				
C52-06-HE	138	182	3	2
T23(4)A6	130	174	15	12
S30N21A6	166	198	12	14
S30N21T23(4)A6	137	162	4	4
<u>Hi Zr Modification</u>				
CZ1-01-HE	129	188	6	7
T23(7)A6	135	164	4.2	6
S22N15*A6	158	190	7.6	2
S22N15*T23(4)A6	117	161	11	10
<u>HIP'ed MAR-M-509 P/M Alloys</u>				
C51-034-H2000(2)	98	119	0.7	<1
H20(2)H2325(2)	72	104	2.1	1
C51-04-H2150(2)	78	110	1.5	1.2
C51-03-H2300(2)	68	94	1.2	<1
H23(2)H23(4)	108	113	1.4	0.7
C51-H1-H2235(2)	122	161	6	6

(continued)

Table X, continued

	<u>YS</u>	<u>UTS</u>	<u>Elong.</u>	<u>R.A.</u>
<u>HIP'ed + Hot Rolled MAR-M-509 P/M Alloys</u>				
C51-05-HR'(6:1 RA at 2100)				
Longitudinal direction	150	188	2	2
Long transverse direction	155	193	2	2
C51-05-HR'T2260(1)A6	97	158	4.7	3.8
C51-05-HR'R(2:1 RA at 1800)	239	251	<2	<1
HR'R(2:1 RA at 1600)	271	271	<1	<1
HR'R(2:1 RA at 1400)	305	307	<1	<1
HR'R(2:1 RA at 1200)	298	308	<1	<1

* except for final I.A. at 2100°F (1149°C).

TABLE XI
ROOM TEMPERATURE TENSILE PROPERTIES OF
Co-HfC P/M AND CAST ALLOYS

Alloy	YS (0.2%) ksi	UTS ksi	Elong. %	R.A. %
<u>Co-1 atom % HfC</u>				
CH1-M1-cast	60	82	12	-
CH2-01-HE(HIP + Extr)	98	142	4	6
CH2-01-HEH'2200(4)	97	137	11	10
CH2-01-HEH2300(1)	70	111	5	5
CH2-01-HEHT23(4)A6	≈90	134	8.6	6
HEHT2350(4)A6	100	130	9	5
HEHS30N18A6	132	160	5.2	7.8
HEHS30N18T23(4)A6	80	105	6.2	4
HEHS40N21A6	168	186	11	12
HEHS40N21T23(4)A6	101	131	4.8	3
<u>Co-2 atom % HfC</u>				
CH7-M1-cast	80	101	1.2	1
CH8-C1-HIP only	117	117	<1	<1
CH7-H2-HE(HIP + Extr)	105	154	7	5
CH7-H2-HE S30N15*A6	139	183	22	19
HE S30N15*T23(4)A6	97	151	23	21
CH7-H2-HE S30N18A6	169	204	5	6
HE S30N18T23(4)A6	96	141	15	4
<u>Co-3 atom % HfC</u>				
CH6-M1-cast	≈60	77	1.5	1
CH4-M1-C**H2275(2)H2300(2)	113	145	4	4
CH4-M1-CR(5:1 RA at 2100)A6	148	170	12	8
CH6-H1-HE(HIP + Extr)	132	187	4	4
T23(4)A6	136	188	26	23
T2426(17)	75	104	8	7
S20N15A6	203	250	9	10
S20N15T23(4)A6	151	216	18	17
S30N15A10	255	255	<1	<1
S30N15A6	200	250	13	14
S30N15T23(4)A6	174	235	13	14
S40N15***A6	163	202	14	8
S40N15***T23(4)A6	126	154	5.1	3
S20N18A6	151	201	26	24
S20N18T23(4)A6	140	185	18	16

(continued)

Table XI, continued

	<u>YS</u>	<u>UTS</u>	<u>Elong.</u>	<u>R.A.</u>
CH6-H1-HES30N18A10	279	299	1	1
S30N18A6	143	198	19	18
S30N18T23(4)A6	132	186	18	18
S40N18A6	134	190	25	16
S40N18T23(4)A6	120	180	32	22
S20N21	210	222	7.2	12
S20N21T23(4)A6	134	170	10	10
S30N21A6	176	238	16	12
S30N21T23(4)A6	126	181	26	19

* except for final I.A. at 2100°F (1149°C)

** quench cast into copper molds

*** except for final I.A. at 2300°F (1260°C)

TABLE XII
STRESS FOR 10 AND 100 HOUR RUPTURE LIFE

Alloy	Temp (°F)	Stress for Life		Slope ¹ (-)
		10 hr. ksi	100 hr. ksi	
<u>MAR-M-509-Type Alloys</u>				
<u>C51-01-HE</u>	1800	4.8	2.5	0.285
T2280 (116)		8.1	4.6	0.245
T2290 (1)		11.0	7.5	0.167
T2300 (4)		13.0	9.2	0.150
T2300 (64)		14.0	9.2	0.183
T2350 (1)		15.5	10.5	0.170
S40N15*		9.0	4.5	0.302
S40N15T23**		11.0	7.1	0.192
S40N18		7.4	3.5	0.326
S40N18T23		11.5	7.4	0.192
<u>C51-01-HE</u>		1500	22.5	15.5
T23	32.5		28.0	0.065
S40N15	29.5		19.5	0.180
S40N15T23	36.5		29.5	0.096
S40N18	29.0		19.5	0.172
S40N18T23	34.5		25.5	0.130
<u>C51-01-HE</u>	1200	92.0	66.0	0.150
T23		86.0	74.0	0.065
S40N15		100.0	-	-
S40N18		79.0	50.0	0.128
<u>C51-05-HR</u>	1800	7.4	3.4	0.337
R18		4.6	2.0	0.362
R16		3.9	2.0	0.290
R14		4.0	1.9	0.324
R12		3.7	1.6	0.365
<u>C52-06-HE</u>	1800	4.5	2.2	0.312
T23		6.6	3.6	0.264
S30N21T23		9.0	3.2	0.450
<u>C52-06-HE</u>	1500	20.5	12.0	0.232
T23		30.0	16.0	0.274
<u>CZ1-01-HE</u>	1800	8.5	5.4	0.197
T23		9.4	5.7	0.217
S22N21T23		13.7	9.5	0.161
<u>CZ1-01-HE</u>	1500	26.0	16.0	0.213
T23		28.0	20.5	0.135

(continued)

Table XII, continued

<u>Co-HfC Alloys</u>	<u>(°F)</u>	<u>10 hr. ksi</u>	<u>100 hr. ksi</u>	<u>(-)</u>
<u>CH2-01-HE</u>	1800	9.2	3.9	0.374
<u>CH2-01-HEH</u>		10.0	6.2	0.211
T23		11.0	7.3	0.178
T2350 (4)		11.0	5.7	0.287
S40N21T23		12.0	8.3	0.161
<u>CH1-M1-Cast</u>		13.0	9.0	0.161
<u>CH2-01-HEH</u>	1500	36.0	26.5	0.133
T23		33.5	23.5	0.155
<u>CH2-01-HEH</u>	1200	108.0	79.0	0.135
<u>CH7-H2-HE</u>	1800	6.7	3.9	0.234
T23		7.8	4.1	0.280
S30N15T23 (1)		12.3	9.2	0.126
<u>CH7-M1-C</u>		≈11.5	9.3	0.094
<u>CH7-H2-HE</u>	1500	23.5	15.5	0.182
<u>CH6-H1-HE</u>	1800	8.0	5.0	0.161
T23		10.0	5.8	0.235
S40N15***		13.0	8.2	0.198
S40N15T23		13.0	6.8	0.324
S40N18		11.8	6.5	0.260
S40N18T23		12.0	8.0	0.176
S30N21		12.4	9.3	0.126
S30N21T23		8.6	5.5	0.194
<u>CH6-M1-C</u>		12.0	9.6	0.098
<u>CH6-H1-HE</u>	1500	26.0	18.3	0.152
T23		29.5	22.0	0.126
S40N15		30.5	18.0	0.230
S40N15T23		36.0	23.0	0.196
S40N18		30.0	23.3	0.109
S40N18T23		33.5	24.6	0.135
S30N21		33.5	24.6	0.135
S30N21T23		37.0	28.5	0.113

(continued)

Table XII, continued

	(°F)	10 hr. ksi	100 hr. ksi	(-)
CH6-H1-HE	1200	85.0	62.0	0.141
T23		88.0	65.0	0.133
S30N15A10		74.0	47.0	0.196
S40N15		84.0	56.0	0.176
		93.0	63.0	0.169
		86.0	50.0	0.235
S30N21A6	2000	4.8	3.8	0.1
S30N21T23		1.8	-	-

$$l_{\text{slope}} = \frac{\ln \sigma_{10 \text{ hr}} - \ln \sigma_{100 \text{ hr}}}{\ln 100 \text{ hr} - \ln 10 \text{ hr}}$$

* Except for final I.A. at 2100°F (1149°C) for this alloy.

** All 2300°F (1260°C) anneals are for four hours unless indicated

*** Except for final I.A. at 2300°F (1260°C) for this alloy.

Note: all samples aged 20 hours at 1650°F (899°C) unless indicated.

TABLE XIII

ELECTROLYTICALLY EXTRACTED PHASES

Alloy	Extracted Weight %	X-Ray Intensity MC/Cr ₂₃ C ₆ Ratio	
		111/420	200/422
<u>HIP + Extruded</u>			
C51-01-HE	8.9	2.6	1.3
C52-06-HE	12.7	0.46	
CZ1-01-HE	17.5	4.7	3.7
CH2-01-HEH	4.8		
CH7-H2-HE	5.7		
CH6-H1-HE	8.4		
<u>HIP and HIP + Rolled</u>			
C51-05-HRR1800	10.1	6.2	3.5
-HRR1600	9.4		
-HRR1400	6.6		
-HRR1200	7.0		
C51-05-HR	8.7	5.5	3.3
C51-03-H	8.0	12.0	
<u>MAR-M-509 (C51-01-HE + . . .)</u>			
T2325A20(100)	10	3.4	1.8
T2350 water quenched	7.7	5.0	2.6
T2350A6	12	2.2	1.4
T2350A6(50) + S.R.T.* at 1800°F, 10 ksi 137 hrs.	12	2.1	1.6
S.R.T. at 1800°F, 2.75 ksi, 72.5 hrs.	14	2.2	1.5
S30N15T23(4)A6 + S.R.T. at 1800°F, 10 ksi, 16 hrs.	12	2.5	1.8
T23(4) no age	9.2	2.3	1.8
S20N15A6	13	1.55	1.45
T23(4)A6	12	1.95	1.5
as-extruded	13.2		
T23(100) no age	6.7	6.1	3.3
T2325A18(64)	13	2.5	1.5

(continued)

Table XIII, Continued

<u>Co-3 atom % HfC (CH6-H1-HE)</u>	<u>Weight %</u>
T2425(2) no age	7.4
T2300(100) no age	6.5
S.R.T. 1800°F, 5 ksi, 104 hrs.	7.4
T2440A6 + S.R.T. at 1800°F, 10 ksi, 36 hrs.	7.8
S30N15A6 + S.R.T. at 1800°F, 10 ksi, 3.6 hrs.	8.2
S40N23A6 + S.R.T. at 1800°F, 10 ksi, 39 hrs.	8.8

* S.R.T. = stress rupture test specimen





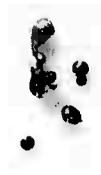




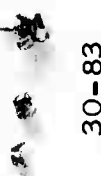
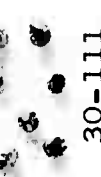


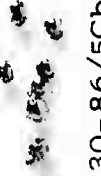
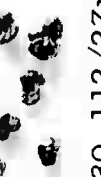
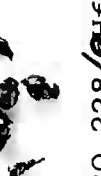
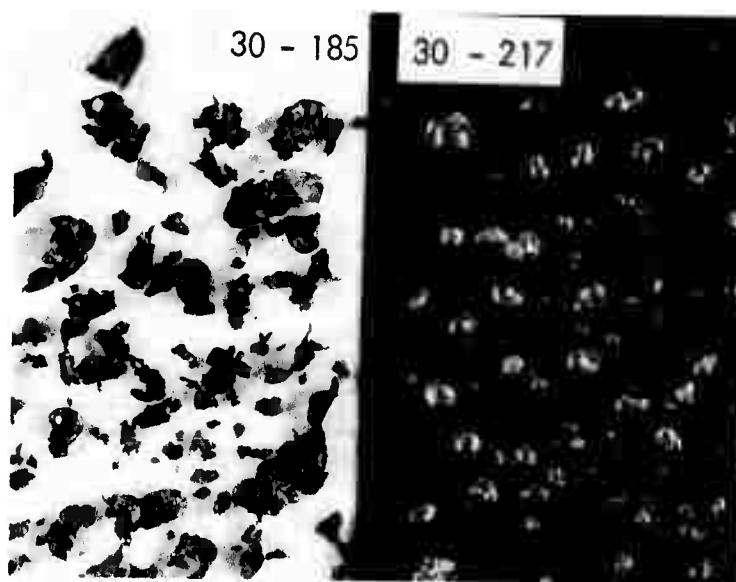
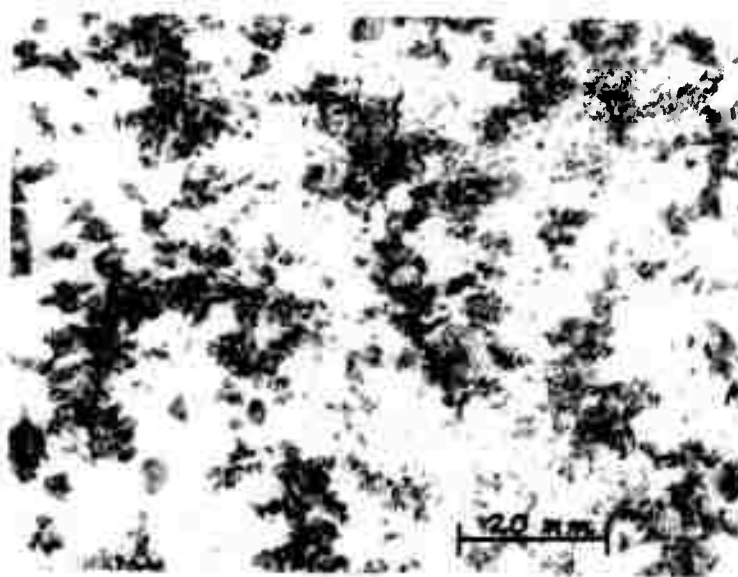
<u>X-45</u> 0.83 Si 0.015 B	<u>X-45</u> 2920°F + 40°F	<u>MAR-M-509</u> 2970°F + 30°F	<u>Co-Hf</u> 2975°F + 125°F
 30-55 2650°F	 30-114 .6Si-.01B	 30-225 0 Si-.05B	 30-185/3Hf No Si/B
 30-57 2740°F	 30-116 .6Si-.01B	 30-226 0 Si-.05B	 30-224/9Hf 0 Si-.05B
 30-83 2960°F	 30-83 .8Si-.02B	 30-111 .8Si-.02B	 30-217/3Hf .8Si-.04B
 30-51,52 3120°F	 30-86/5Cb .8Si-.02B	 30-112/2Zr .8Si-.02B	 30-228/9Hf 1.0 Si-.05B

Figure 1 - Effect of Tap Temperature and Chemistry on the Morphology of Steam Atomized Coarse Cobalt Powders.

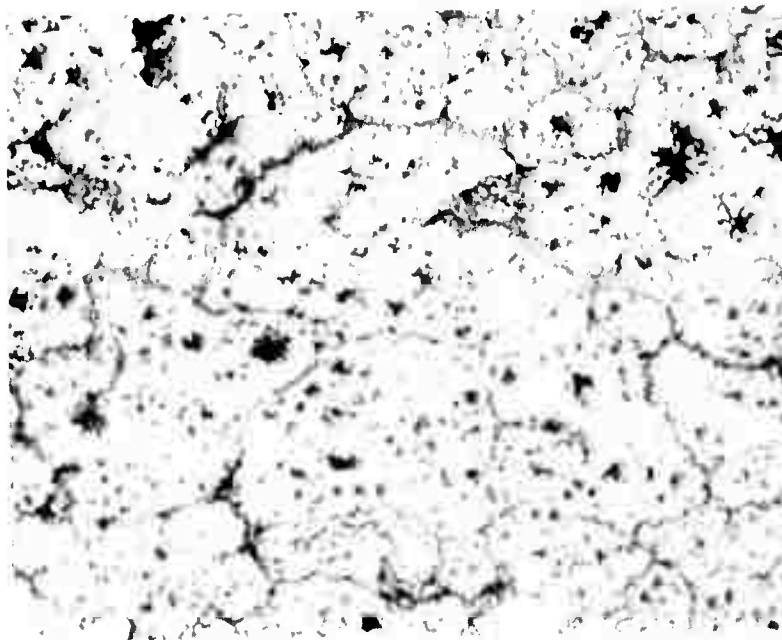


(a)

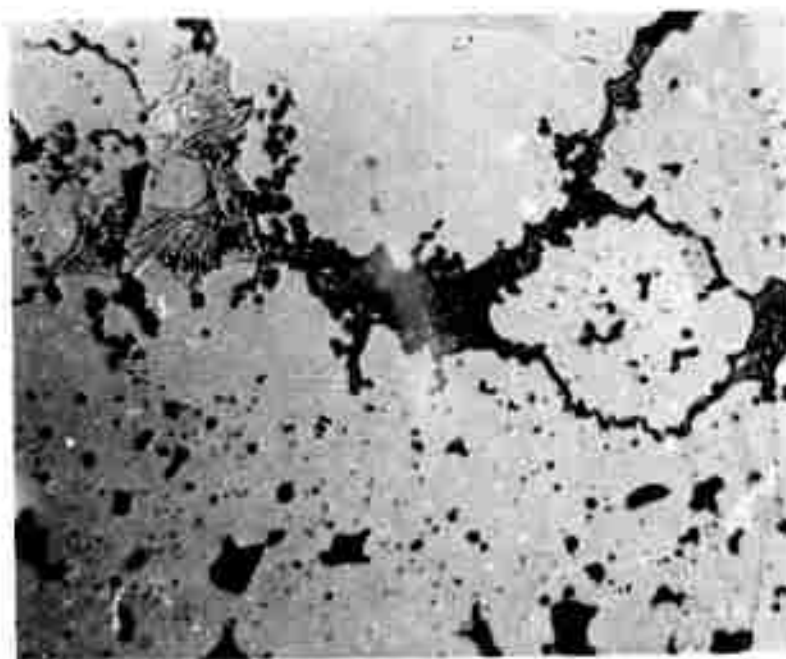


(b)

FIGURE 2. STEAM ATOMIZED Co-HfC POWDERS SHOWING:
(a) Co-1 atom % HfC powder morphology with
(right) and without (left) 0.8% Si additions,
X1; (b) typical morphology of alloys with
greater than about 3% Hf additions, X1.

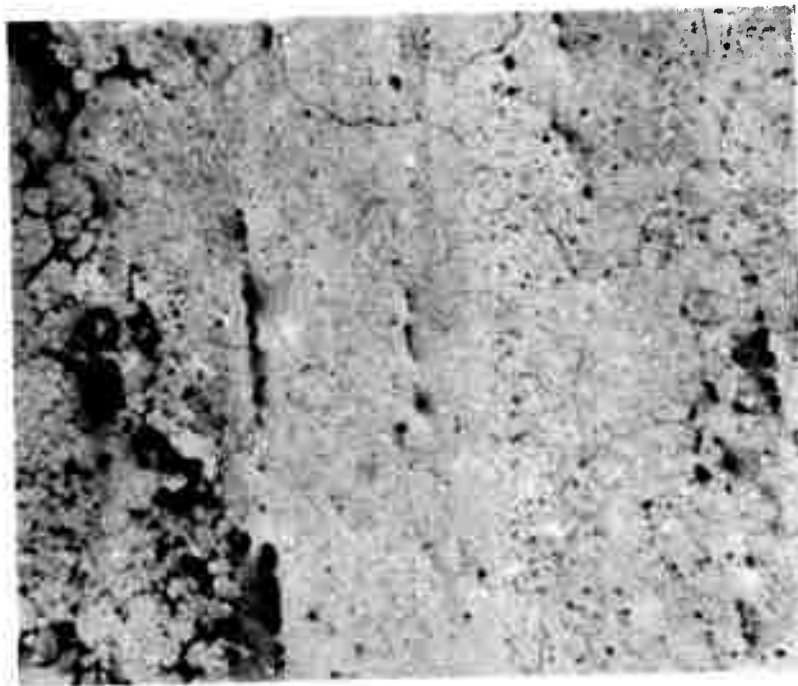


(a)

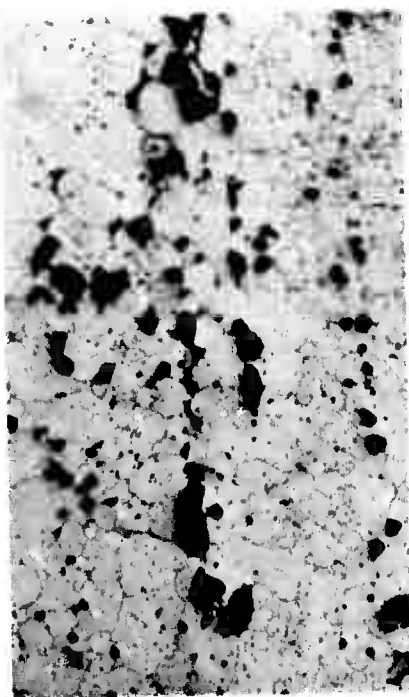


(b)

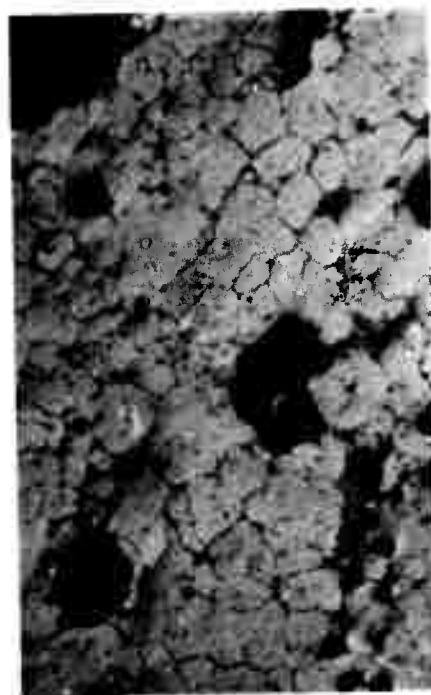
Figure 3 - P/M MAR-M-509 alloy after holding 2 hours at 1330°C (2426°F) and air cooled. (a) Etched. 150X. (b) Etched to reveal four major types of phases after partial melting. 750X.



(a)

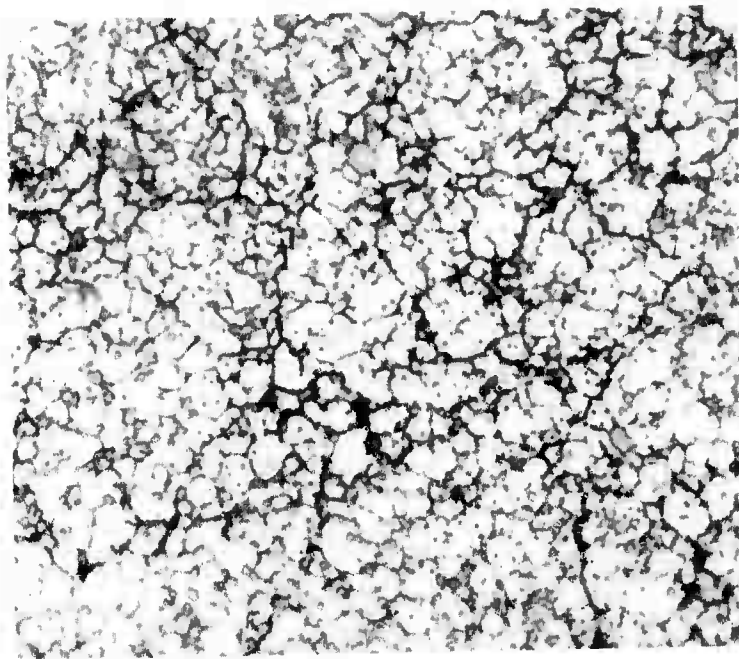


(b)

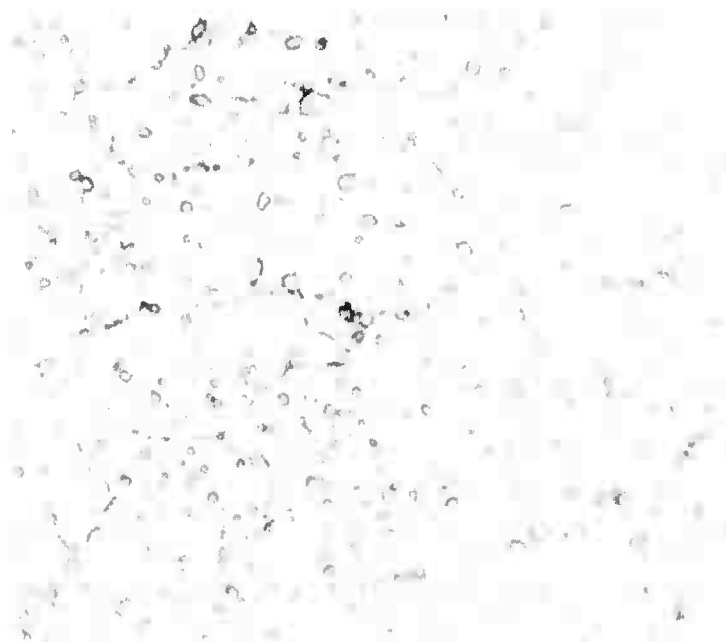


(c)

FIGURE 4 .. POROSITY IN HIP + HOT ROLLED P/M MAR-M-509 AFTER ANNEALING TWO HOURS AT (a) 2265°F (1240°C); (b) 2300°F (1260°C); (c) 2330°F (1280°C), X150. Etched electro. chromic acid.



(a)



(b)

FIGURE 5 . HIP + EXTRUDED P/M COBALT-3 ATOM % HfC IN
(a) as-extruded condition; (b) after one
hour anneal at 2440°F (1340°C). X1500.
Etched electro. Oxalic-HCl acids.

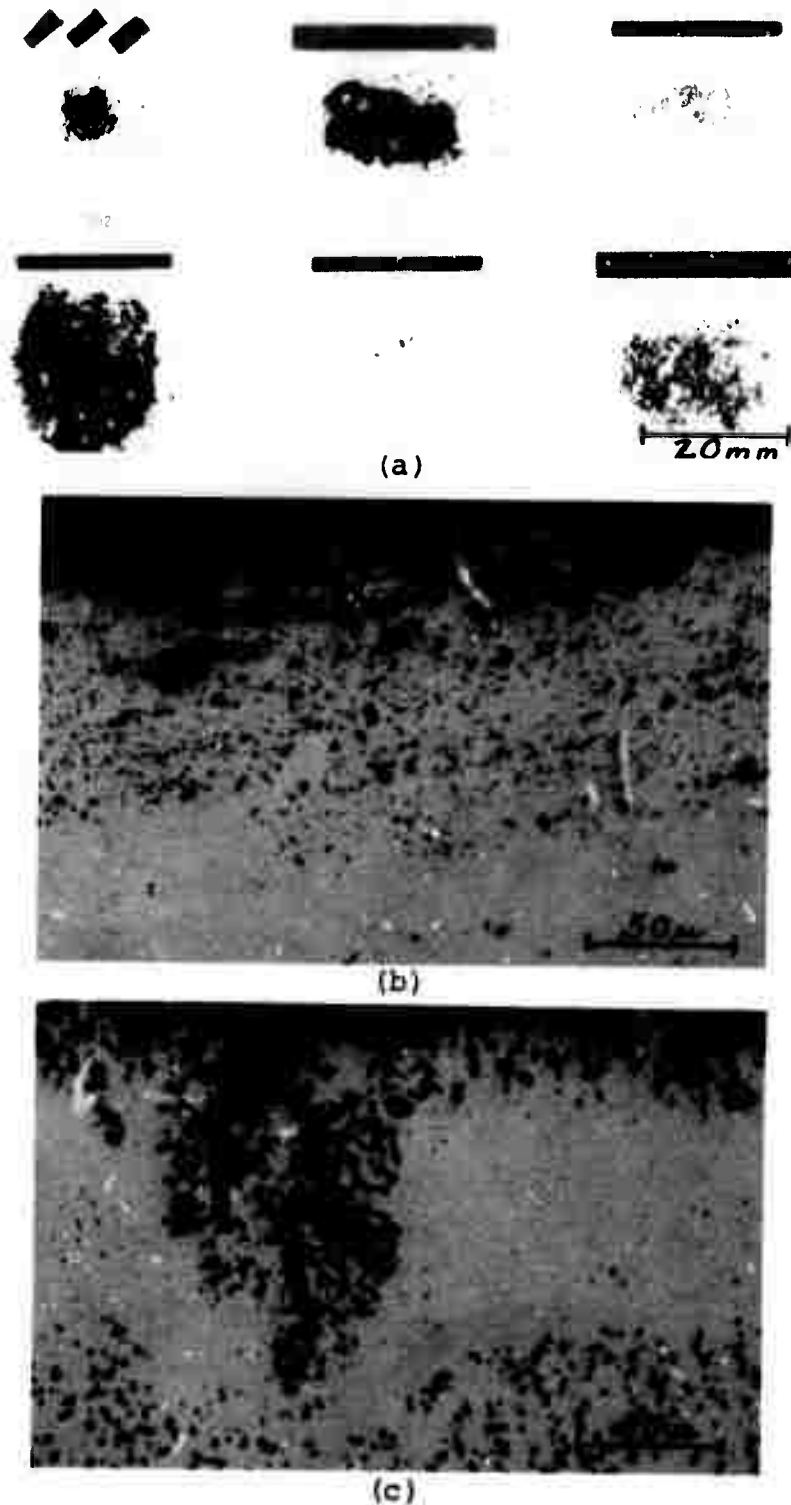
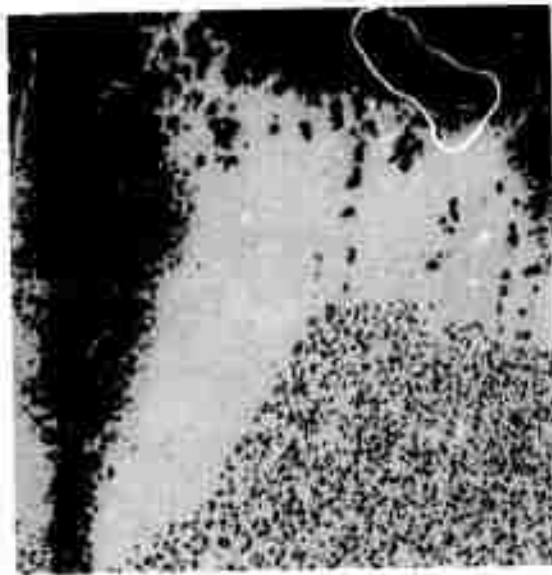
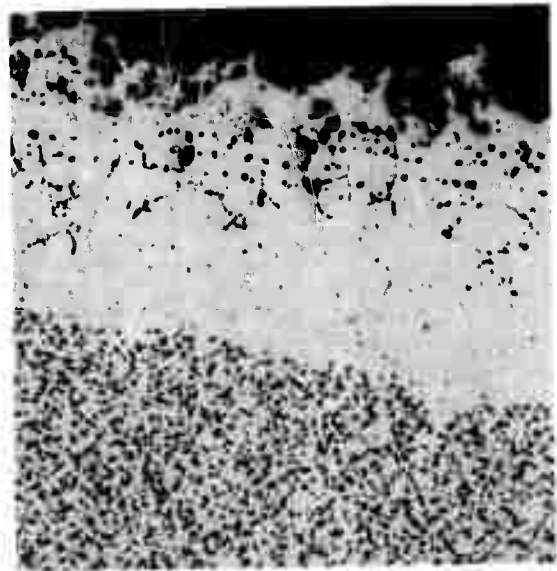


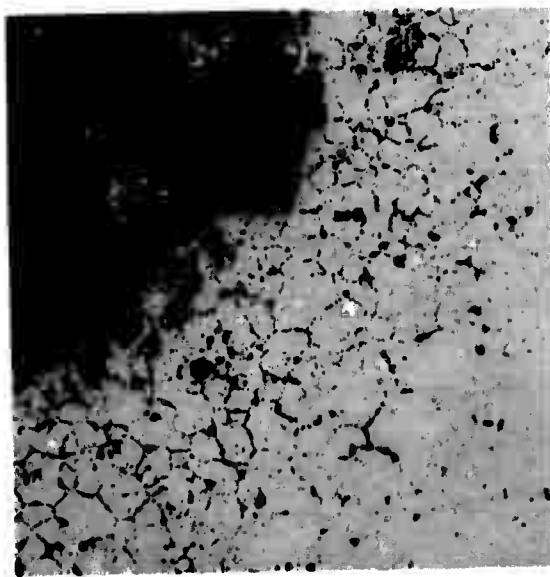
FIGURE 6. OXIDATION SAMPLES, LOOSE SCALE AND CROSS SECTION PHOTOMICROGRAPHS AFTER 100 HOURS AT 2000°F (1093°C). (a) X1; (b) P/M Co-3 atom % HfC (CH6); (c) P/M MAR-M-509 alloy (C51), cross sections, X400. Carbides stained.



(a)



(b)



(c)



(d)

FIGURE 7 PHOTOMICROGRAPHS OF P/M COBALT ALLOYS AFTER 100 HOUR EXPOSURE IN AIR AT 2000°F (1093°C), X200. (a) HiZr-modified MAR-M-509 (CZ1); (b) Hi W + Cr modified Mar-M-509 (C52); (c) Co-1 atom % HfC (CH2); (d) Co-2 atom % HfC (CH7). Carbides stained.

Reproduced from
best available copy.

PROCESSING OF PM IN-100

The following is a brief summary of some of the experimental research carried out during the period of this Technical Report.

A. GRAIN GROWTH STUDIES

In order to evaluate the grain coarsening rates of extruded IN 100 powders, a series of grain coarsening experiments were run at selected temperatures, under the incipient melting temperature. Specimens of extruded Nuclear Metals powder were heated to the appropriate test temperature in an argon atmosphere, and samples were removed from the furnace and air cooled at various time intervals. The specimens were then prepared for metallographic examination and etched in glyceresia, to show both grain boundaries and gamma prime precipitate. Photomicrographs were taken at 150X and the Hilliard Intercept Method was used to determine the average grain size for a given time interval at temperature (see Figure 1).

From this plot of average grain size versus time at temperature, it is seen that the grain coarsening rate of IN 100 is an interface controlled mechanism and can be represented by the linear relationship

$$D - D_0 = Kt$$

where D is the average grain size, D_0 is the initial grain size, t is time and K is a constant of proportionality. This constant K can be replaced as

$$K = K_0 e^{-Q/RT}$$

where K_0 is another constant of proportionality, Q is an empirical heat of activation for the process, T is temperature in °K and R is the international

gas constant.

By plotting the log of the slopes of the grain size versus time plot curves against the reciprocal of absolute temperature (see Figure 2), and finding the slope of the resulting curve, the heat of activation, Q , is found as follows:

$$\log \frac{D - D_0}{t} = Q/2.3R$$

$$7.9 \times 10^3 = Q/(2.3)(1.98 \times 10^{-3})$$

$$(7.9 \times 10^3)(4.554 \times 10^{-3}) = Q$$

$$Q = 35977 \text{ cal/gm atom} \approx 36000 \text{ cal/gm atom}$$

This value shows that the rate of grain growth is extremely temperature dependent, and will hopefully aid in the evaluation of the grain growth rate kinetics.

B. SINTERING

In order to understand the process of hot isostatic pressing of powders, laboratory simulation of the sintering of loose powder was performed. Loose powders of IN 100 were encapsulated in quartz cylinders and placed under vacuum. Figures 3 and 4 illustrate the sintering phenomena under a vacuum of 10^{-6} mm of Hg and show an opening of surface pores and the formation of necks between powder particles. Figures 5, 6 and 7 show the different varieties of oxide that may form when the vacuum is not low enough and/or oxygen enters into the sintering container. A network of oxide particles and oxide whiskers are formed which prevent the proper bonding of the powder particles during sintering.

C. HOT PLASTICITY

One of the major reasons for the use of powder techniques in relation

to superalloys is the improvement in hot plasticity. Therefore an investigation of the hot plasticity of IN 100 as a function of hot isostatic pressing variables was begun.

The study of hot plasticity, or hot workability is preformed with a high strain rate testing machine. For this testing a Nemlab high strain rate, hot tensile testing machine was used.

The data obtained from these preliminary tests is given in Tables I and II. From the data stress versus rupture time stress versus deformation rate and deformation rate versus percent elongation curves were plotted (see Figures 8 through 13).

The stress versus rupture time, and the stress versus deformation rate curves, show a linear relationship on log-log plots. The ductility is less than 3% at all temperatures of testing, but it does increase slightly with slower deformation rates. It was decided that the powder which was hot isostatically pressed at 2150°F for 5 hours exhibited the best hot plasticity if deformed at a temperature just above 2100°F (i.e., 2125°F) and a strain rate of 10^{-3} inches per inch per second. After drawing these conclusions, three billets were prepared and forged satisfactorily. These forgings are now in the process of being evaluated.

D. CRACK PROPAGATION AT ELEVATED TEMPERATURES

Work has just begun on the study of the rate of crack growth in superalloys at elevated temperatures (i.e., 1400 to 1700°F) during both fatigue and creep conditions. A testing procedure, material, grips, equipment, etc. have been set up and work is in progress.

E. FUTURE WORK

Future work will include the following:

- 1) Continued work on the influence of HIP parameters on the hot plasticity of IN 100.
- 2) Crack propagation in cast IN 100 and IN 100 forged from a PM billet under creep and fatigue conditions.
- 3) Grain growth tests with improved alloy powders and at different grain coarsening temperatures.
- 4) An investigation of the diffusion of argon into the powders during hot isostatic pressing operations will be concluded with the Task I research group.
- 5) Hot plasticity tests will evaluate a new powdered IN 100, developed by Professors R. Mehrabian and M.C. Flemings, which is described in Semi-Annual Technical Report #4.

TABLE I

The Hot Plasticity Data of IN 100 PM Under
Varied Hot Isostatic Pressing Conditions

Spec #	HIP Conditions	Test Temp ($\pm 3^\circ\text{F}$)	Rupture Time	Load (Gauge)	Stress Applied (lb/in ²)	% Elong.	Strain Rate sec ⁻¹
2A35-1	at 2325°F, 1 hr; + 2270°F, 1 hr; 2270°F, 1 hr; 25 + ksi	2100°F	>.005 sec	Broke on Preload 15 psi	Broke on Preload 14000	1.7	3.4×10^0
2A35-2		2100°F	.005 sec			.9	1.8×10^0
2A20-1	at 2250°F, 25 + ksi, 2 hr.	2153°F	.005 sec	20 psi	18800	1.3	2.6×10^0
2A20-2		2100°F	24.52 sec	15 psi	14000	1.9	7.75×10^{-4}
2A14-1	at 2150°F, 25 + ksi, 2 hr.	2100°F	4.84 sec	15 psi	14000	1.8	3.72×10^{-3}
2A14-2		2100°F	.198 sec	25 psi	22570	1.3	6.56×10^{-2}
2A18-1	at 2050°F, 25 + ksi, 2 hr.	2100°F	14.306 sec	8 psi	6600	1.9	1.33×10^{-3}
2A18-2		2100°F	1.306 sec	20 psi	18800	1.2	9.19×10^{-3}
2A37-1	at 2000°F, 25 + kis	2100°F	2.754 sec	15 psi	14000	1.6	5.81×10^{-3}
2A37-2	2 hr.	2100°F	.025 sec	20 psi	18800	1.3	5.2×10^{-1}

TABLE II

The Hot Plasticity Data of IN 100 PM Hot Isostatically
Pressed at 2150°F, 15 + ksi for 5 hours Under Varying Testing Temperatures

Spec #	Test Temp (±3°F)	Rupture Time	Load (Gauge)	Stress (psi)	% Elong.	Strain Rate sec ⁻¹
1	2100°F	4.64 sec	15 psi	14000	.82	4.31×10^{-3}
2	2100°F	19.15 sec	10 psi	9600	2.84	3.76×10^{-3}
3	2100°F	.99 sec	20 psi	18800	.61	1.52×10^{-2}
4	2100°F	9.575 sec	12.5 psi	12000	1.61	4.1×10^{-3}
5	2125°F	10.80 sec	11 psi	10500	2.52	5.84×10^{-3}
6	2125°F	8.79 sec	15 psi	14000	2.22	6.5×10^{-3}
7	2125°F	1.731 sec	20 psi	18800	1.18	1.67×10^{-2}
8	2125°F	4.63 sec	18 psi	16800	1.35	7.35×10^{-3}
9	2050°F	29.625 sec	15 psi	14000	2.04	1.74×10^{-3}
10	2050°F	14.712 sec	20 psi	18800	1.74	2.98×10^{-3}
11	2050°F	20.875 sec	18 psi	16800	1.90	2.25×10^{-3}
12	2050°F	11.695 sec	25 psi	22570	1.54	3.34×10^{-3}

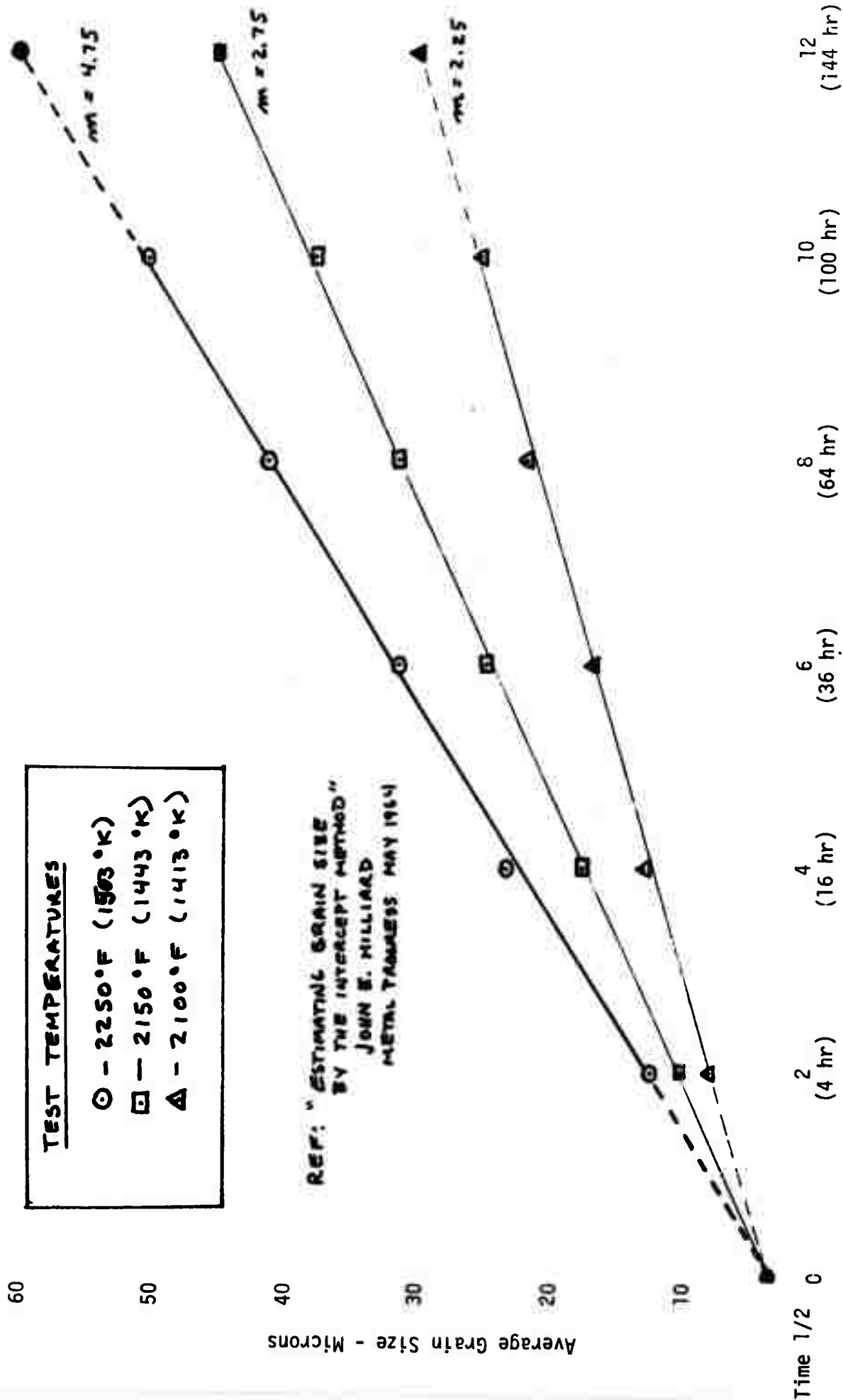


Figure 1 - Effect of Time at Temperature on Average Grain Size for as-extruded IN-100 (N.M.)

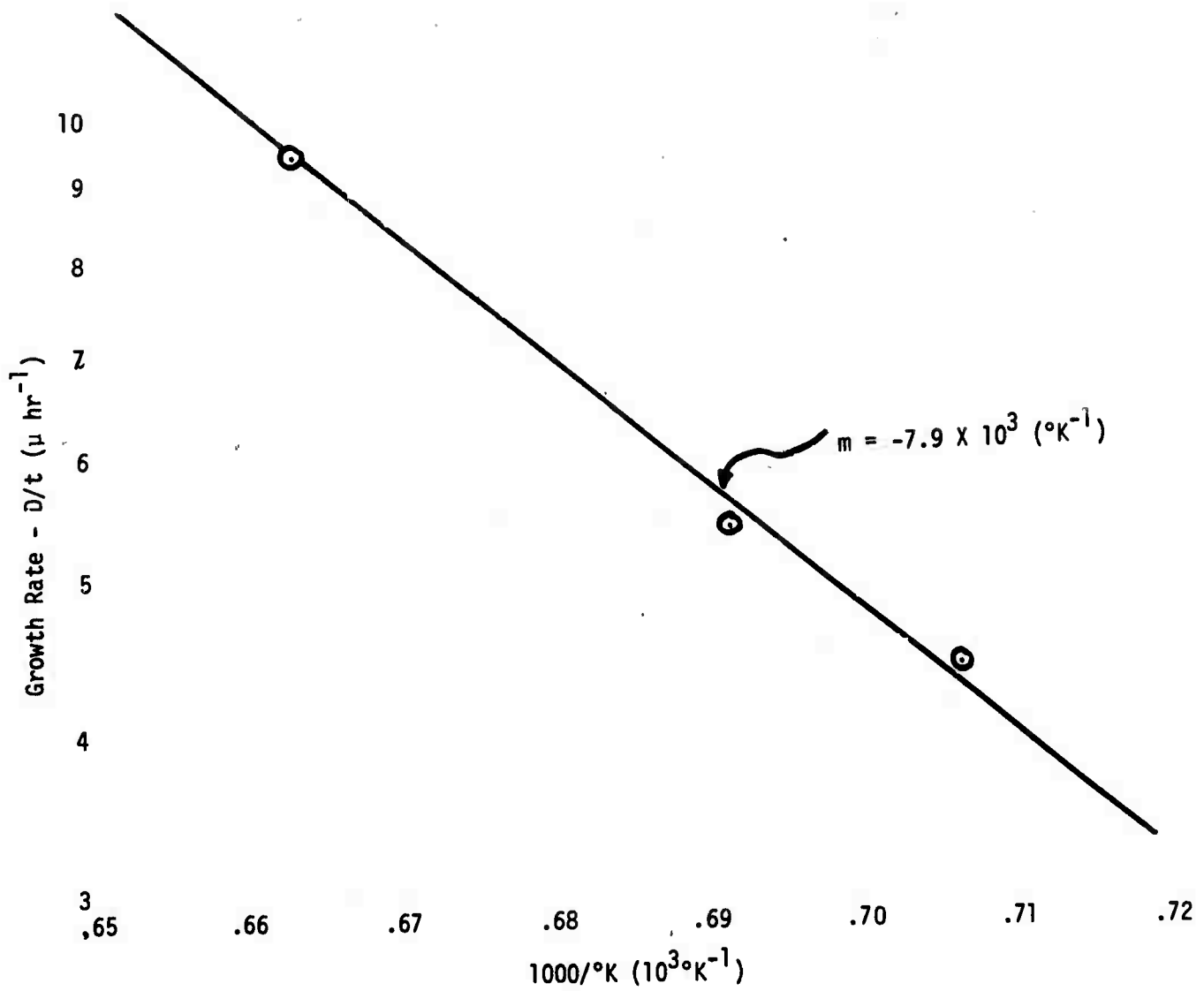


Figure 2 - Logarithm of Growth Rate (Slope of Grain Growth Isotherms) vs. Reciprocal of Absolute Temperature



Figure 3 - The formation of interparticle necks from sintering, at 2150°F, in vacuum, of IN 100 powder. 240X.

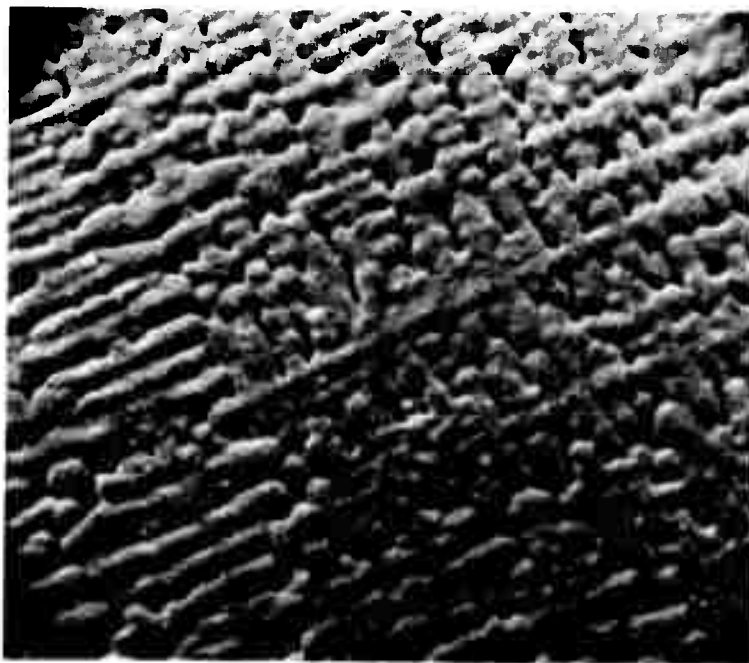


Figure 4 - The surface of IN 100 powder particle after vacuum sintering at 2150°F for 2 hours. 775X.

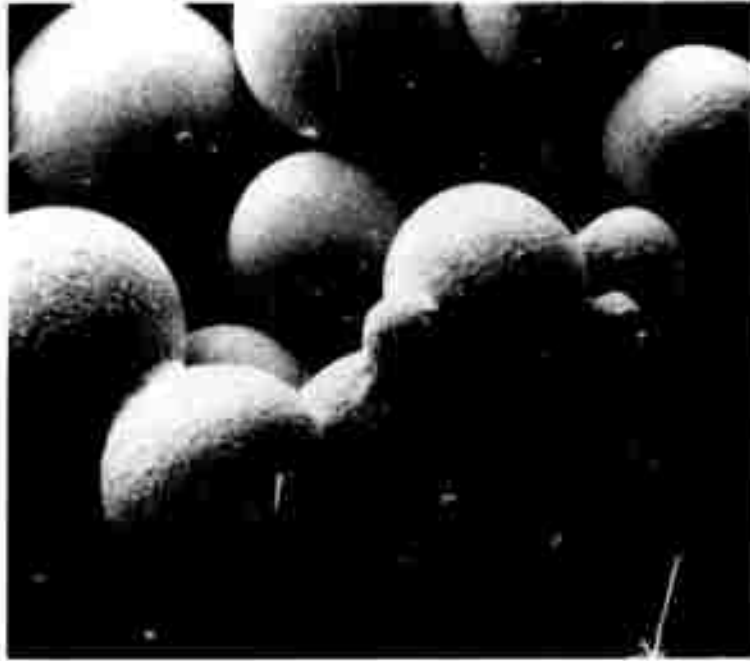


Figure 5 - The oxide formation on the surface of sintered IN 100. 78X

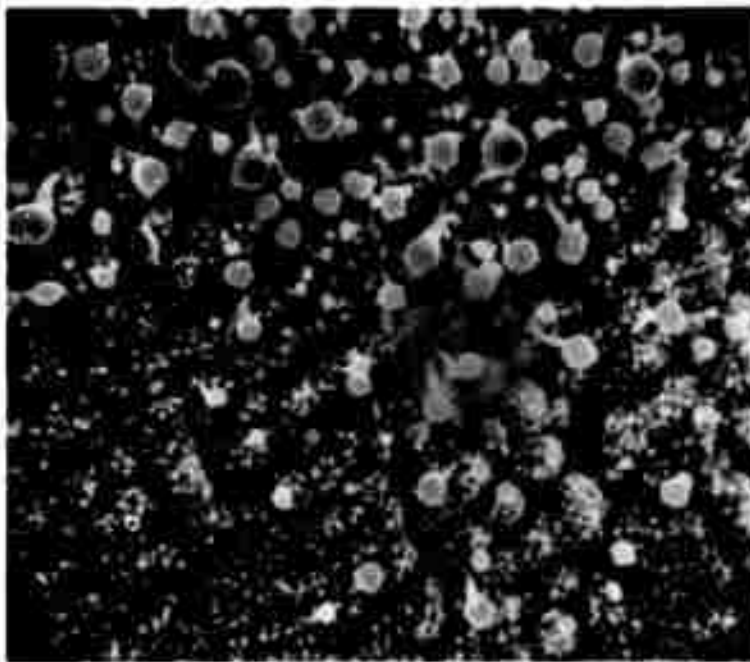


Figure 6 - A nodular and spore type oxide formed on the surface of sintered IN 100. 2420X.



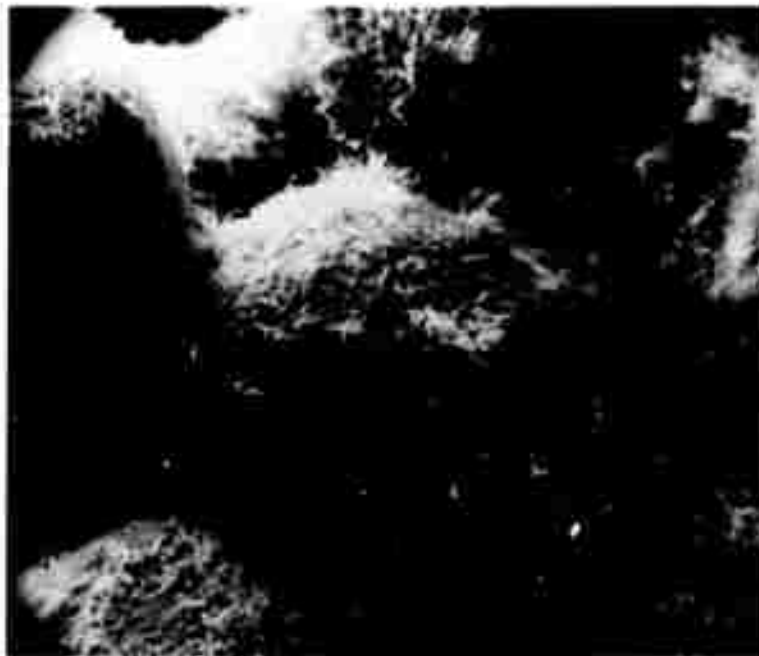
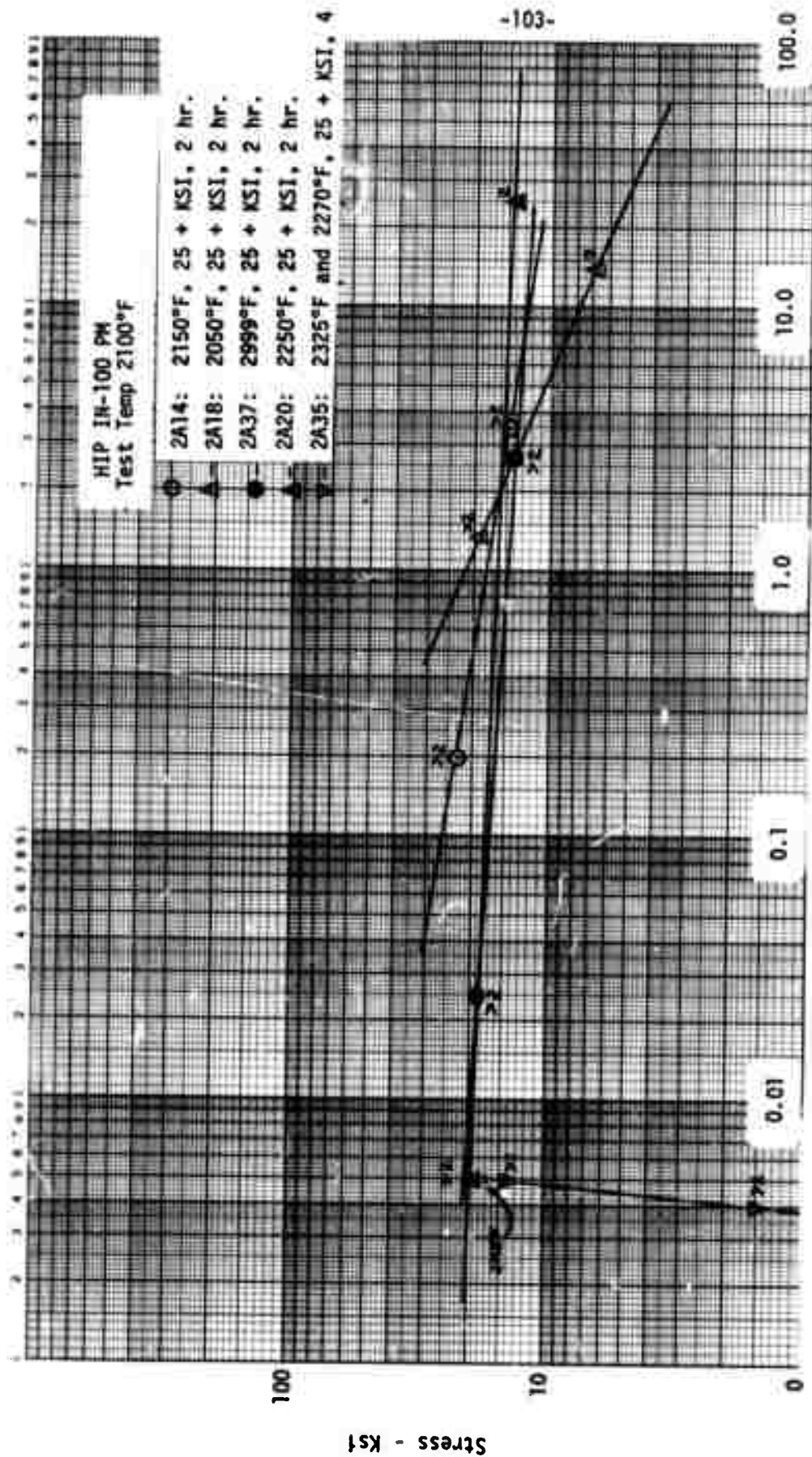


Figure 7 - A whisker type oxide formed on the surface of sintered
IN 100. 800X



Time to Rupture - Seconds

Figure 8 - High Strain Rate Log Stress vs. Log Rupture Time at a Test Temperature of 2100°F

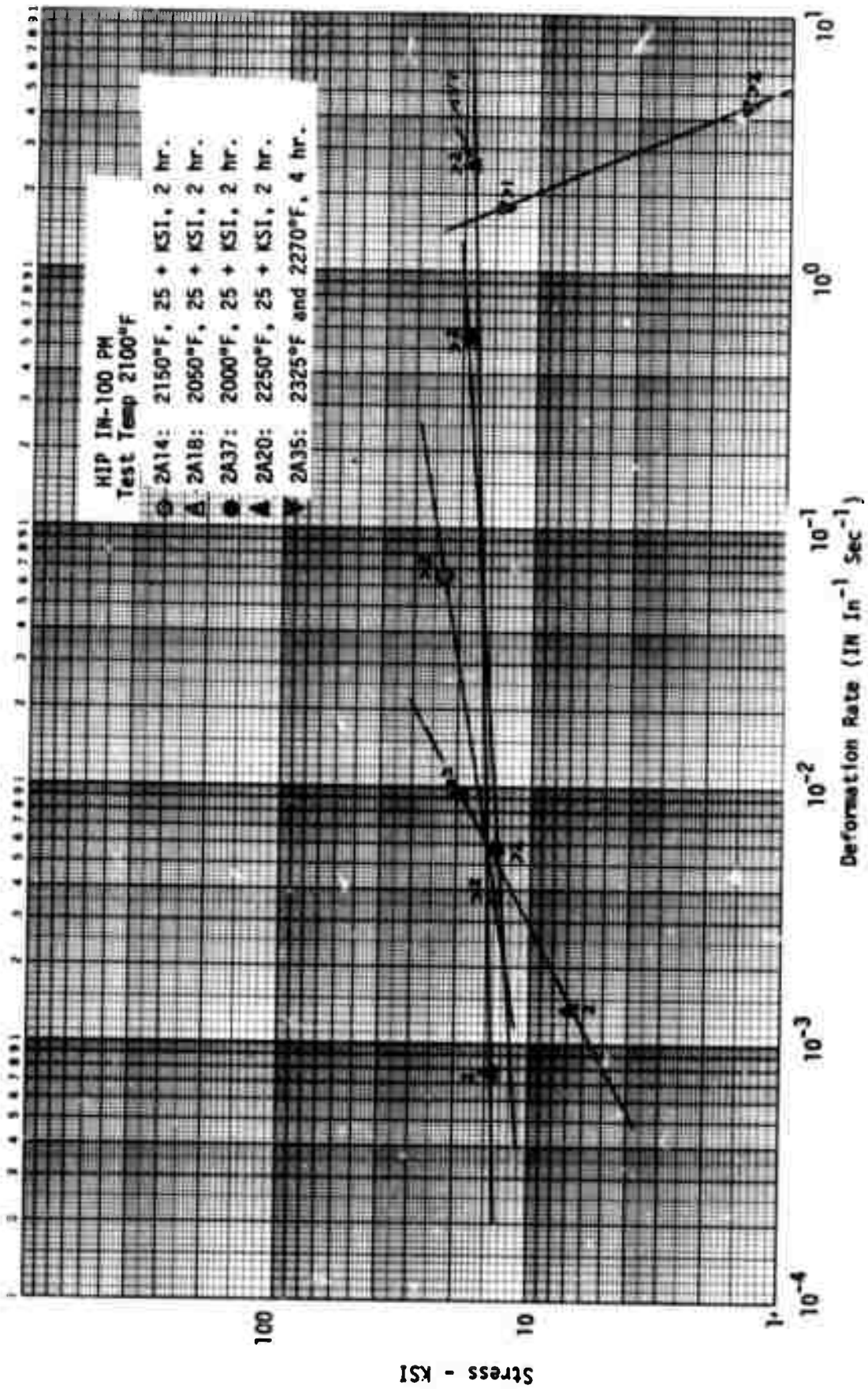


Figure 9 - High Strain Rate Log Stress vs. Log Deformation Rate at Test Temp of 2100°F

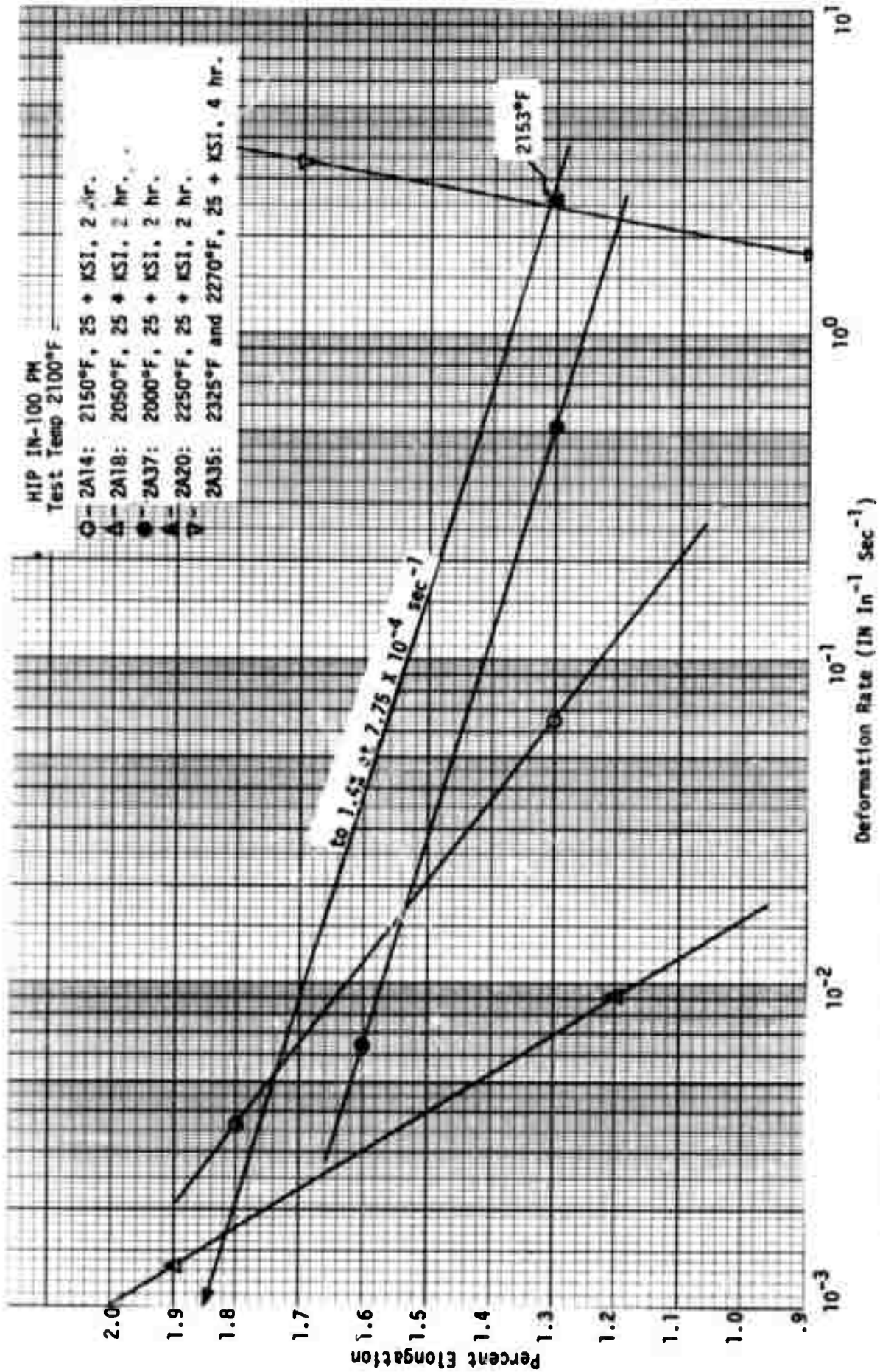


Figure 10 - High Strain Rate Effect of Deformation Rate on Percent Elongation at 2100°F

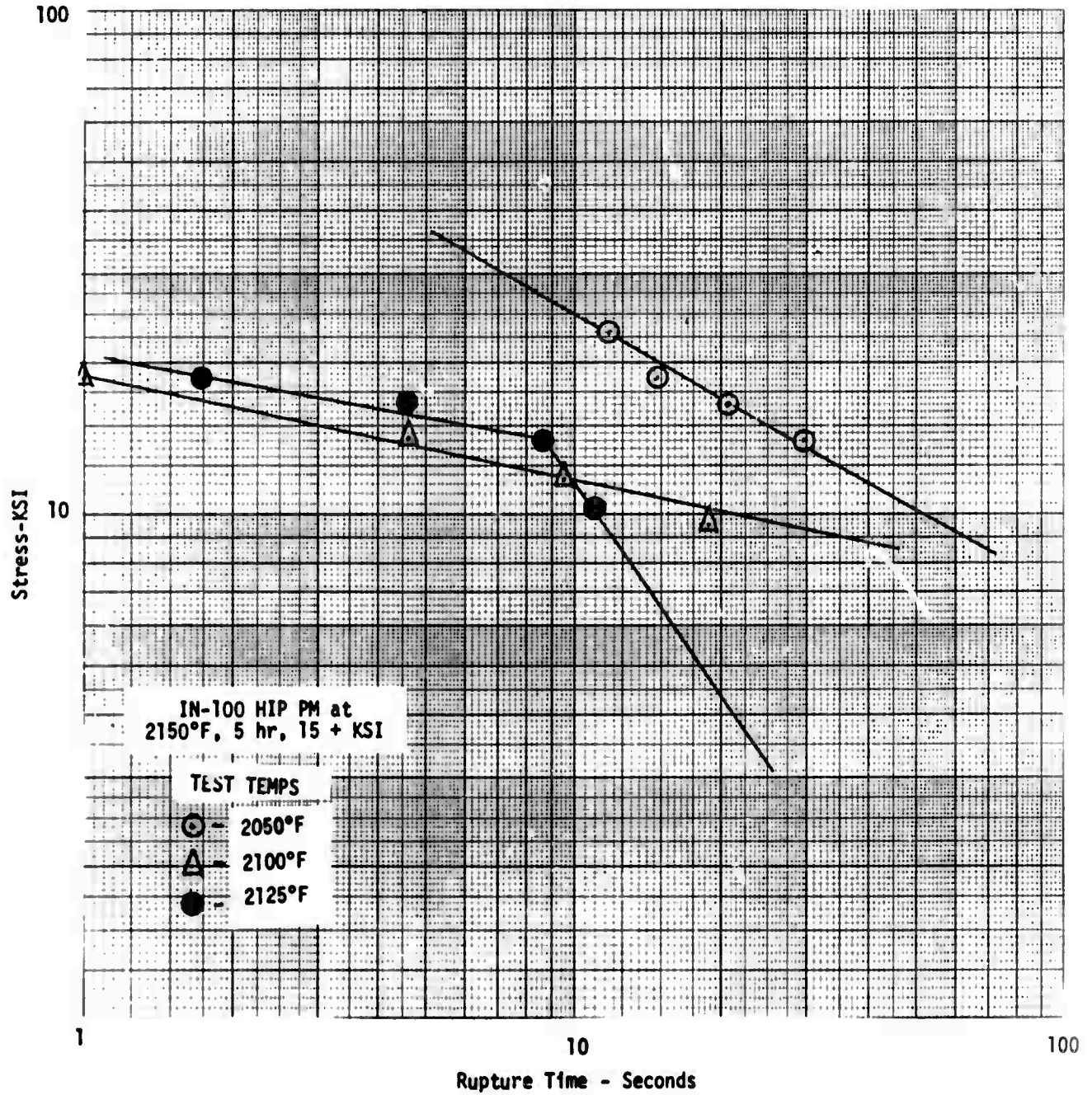


Figure 11 - High Strain Rate Effect of Stress on Rupture Time at Varying Temperatures

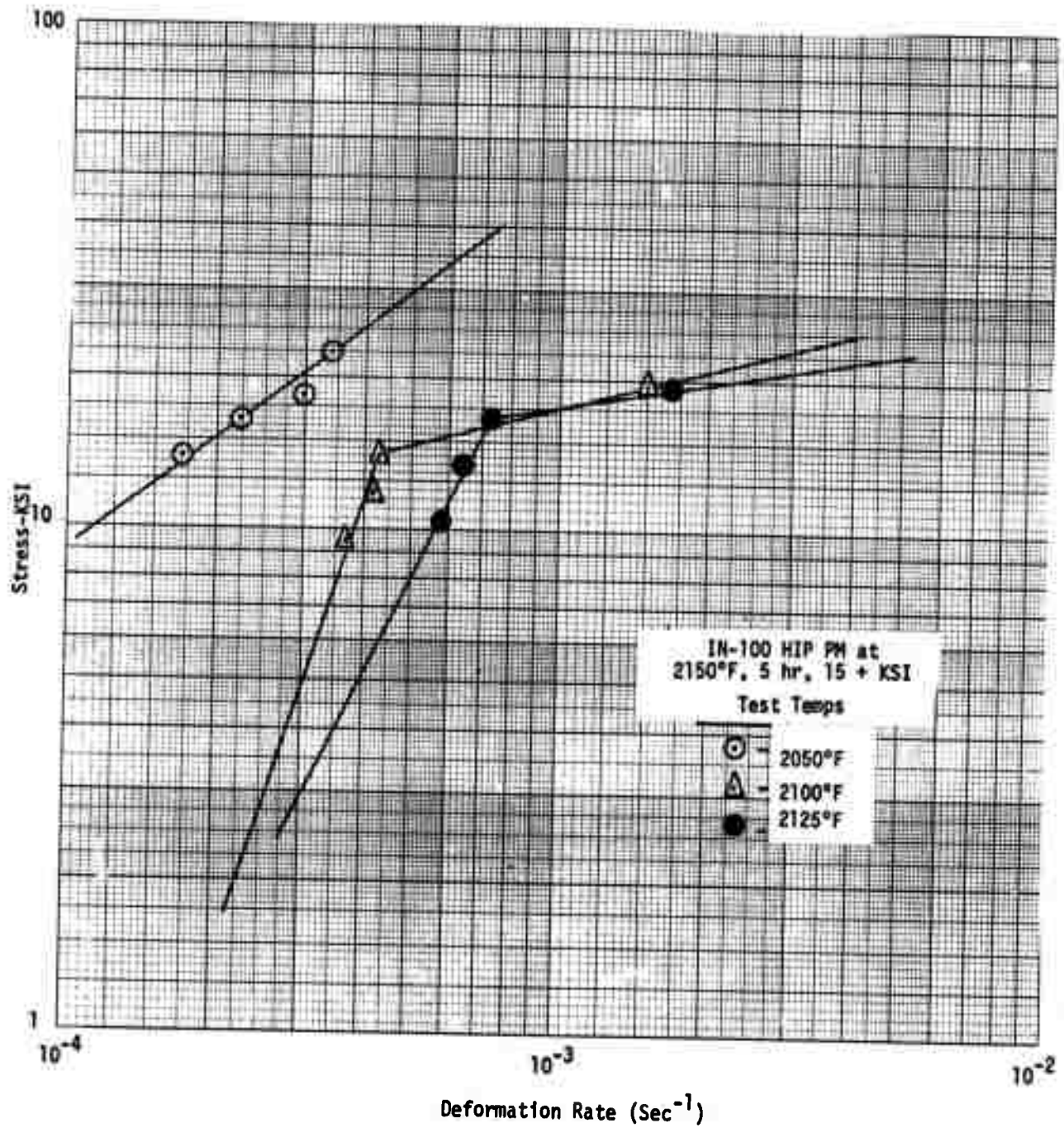


Figure 12 - High Strain Rate Effect of Stress on Deformation Rate at Varying Test Temperatures

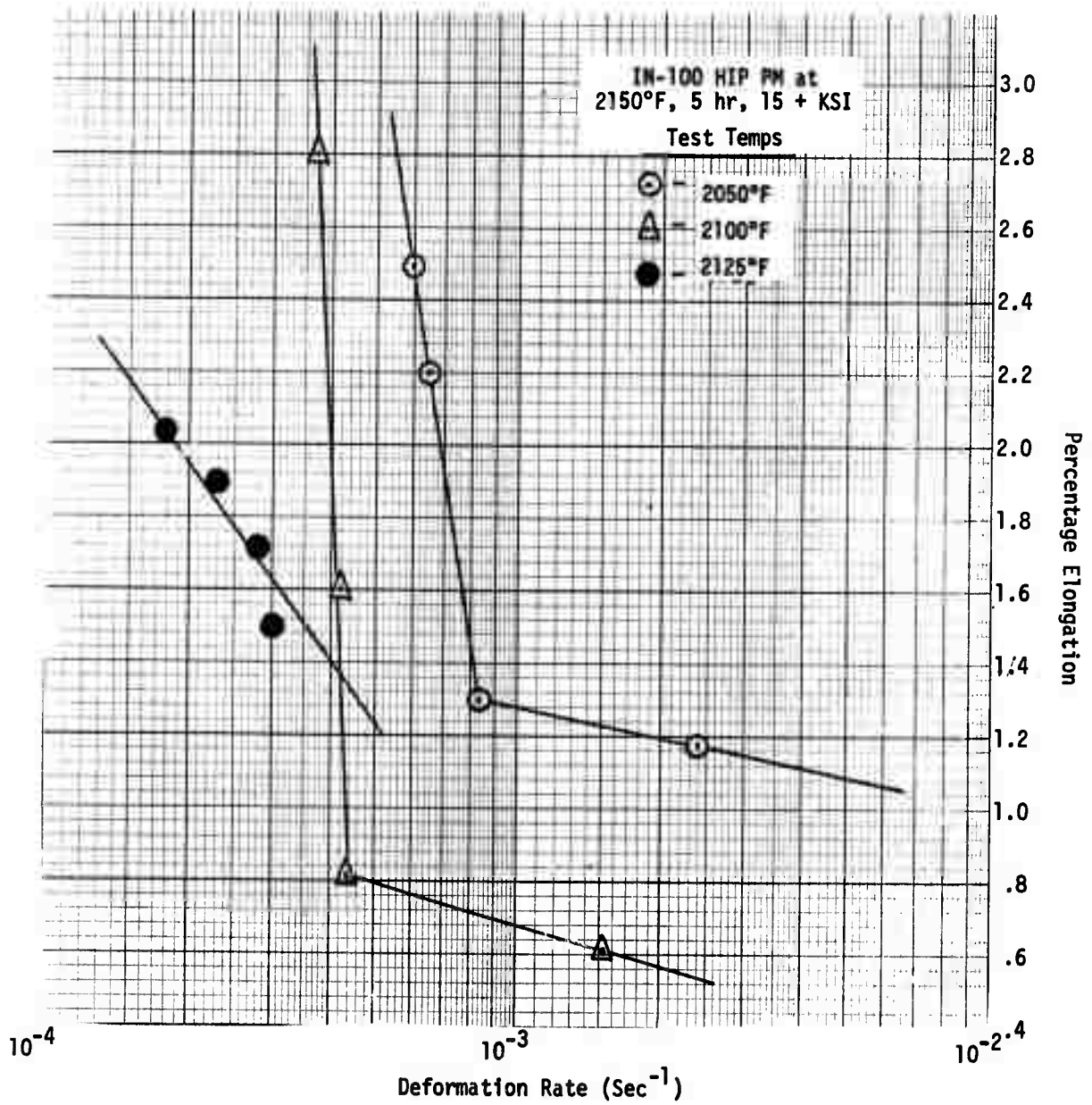


Figure 13 - High Strain Rate Effect on Deformation Rate on Percent Elongation

Inclusion Separation in Ductile Matrices

A. S. Argon
J. Im

A Introduction.

The research on the conditions of separation of inclusions from plastically deformable matrices has progressed in three directions: a) further experiments on inclusion separation on spheroidized medium carbon steel both at room temperature and at elevated temperature just under the ansthenite transition, preliminary experiments on hole formation from elongated inclusions such as coarse pearlite platelets; and b) experiments on inclusion separation in copper with chromium-copper inclusions; c) evaluation of the triaxial stress and equivalent plastic strain distribution in the inhomogeneous plastic flow field in the neck of a tensile bar for a strain hardening elastic-plastic material, by adopting the solution of Needleman (1972) to the materials of interest in the research. The report below gives a short summary of progress in each of these fields.

B .. Inclusion Separation at Elevated Temperature.

The experiments on inclusion separation in spheroidized 1045 steel were extended to elevated temperature to determine the effect of dislocation creep and vacancy creep on the condition of inclusion separation. The experiments to be reported below consist of tensile extensions to fracture in air at conventional extension rates of 0.05 and 0.5 min⁻¹ at temperatures of 450°C and 630°C which are 0.4 and 0.5 times the absolute melting temperature respectively.

The method of preparation of the spheroidized 1045 steel and the resulting equiaxed iron carbide inclusions were described earlier in Progress Report #2. The round bar specimens used in this investigation were prepared in the same manner. They were extended in an Instron machine, temperature was maintained by a resistance furnace.

The fractured specimens were sectioned along the axis, metallographically polished, lightly etched with Picral etch, and examined in the scanning electron microscope. In Fig. 1, curve 1 shows the cumulative distribution of inclusion sizes in the unstrained specimen, curve 2 shows the cumulative distribution of sizes of the separated inclusions in the center near the fracture surface in a specimen deformed at 630°C, while curve 3 shows the cumulative distribution of separated inclusions at a point along the axis a distance $3a$ (where a is the minimum radius of the neck) away from the fracture surface again at 630°C. Figure 1 is to be contrasted with Fig. 2 which shows the corresponding distribution of total numbers of inclusions and separated fraction for a specimen deformed at room temperature. Evidently at room temperature a much larger fraction of the inclusions have separated while this fraction at 630°C is at least a factor of 2 less. On the other hand examination of the holes in the specimen deformed at 630°C showed that they have grown to considerably larger size than those at room temperature. These observations confirm that the time dependent creep deformation and perhaps to a smaller extent the presence of vacancy currents have produced local stress relaxation and prevented the interfacial stresses from reaching the

high magnitudes necessary for separation. Generally it is known that large inclusions tend to separate before small ones do, especially when two large inclusions are near neighbors and the larger than average incompatibility displacements between them have to be accommodated in a smaller space. (see Progress Report #2). This effect is clearly visible in both Figures 1 and 2 in that the points of maximum slope in curves 2 and 3 are displaced toward the right of that of curve 1. The effect, however, is not as striking as the one observed by Palmer and Smith (1966) in copper with silica spheres.

Similar statistical evaluations will be performed in connection with experiments at much slower strain rates which are now in progress, to determine whether or not the expected trend toward increasing resistance to separation of inclusions with decreasing strain rate will continue.

C . Separation of Copper-Chromium Inclusions in Copper.

The room temperature experiments on inclusion separation are now being extended to copper with copper-chromium inclusions. Copper with (0.5)% chromium bars purchased from American Metal Climax Inc. have been aged at 700°C for a week to coarsen the equiaxed copper-chromium inclusions. After repeated trials the best conditions for coarsening quoted above produced inclusions with sizes in the submicron range. It has been found that such inclusions are very poorly stuck to the matrix and tend to be pulled out of the matrix during polishing. This problem was overcome by resorting to mechanical polishing under extremely light loads in a vibratory Syntron polisher. A family of specimens contoured to natural neck geometries and aged to obtain inclusion growth have now been obtained and are ready for testing and statistical evaluation.

From the difficulties with the polishing it is expected that in this material inclusions will separate readily after only very small amounts of plastic strain, making the total strain to fracture rather small.

D . Hole Nucleation from Plate-like Inclusions.

A few preliminary experiments were performed on 1045 steel with a coarse pearlitic microstructure. Examination showed that in such cases holes are often formed by fracturing of the inclusions. Further analysis and experiments are planned on pearlitic 1045 steel.

E. Evaluation of Inhomogeneous Strain Fields.

The relatively simple inhomogeneous plastic flow field in a neck of a bar extended in tension was used in the past to test the assumed critical interfacial stress condition for separation of inclusions from the matrix. (See progress report #2). For that purpose the available approximate solution of Bridgman had been extended to give the distribution of triaxial stress along the axis away from the surface of fracture (See Progress Report #2). Expecting that the level and range of the triaxial tensile stress in the center of the separated inclusions and the range of the cavitated material away from the surface of fracture, the triaxial tensile stress distribution along the axis obtained from the extended Bridgman solution was compared with the distribution of the density of separated inclusions along the axis in the necked and fractured specimens deformed at room temperature. It was observed that the actual density of separated inclusions falls off more sharply along the axis than the distribution of triaxial tensile stress obtained from the extension of the Bridgman solution. This

suggests that the Bridgman type solution overestimates the range of the triaxial stress leading to errors in the evaluation of the local conditions which are used as a test for the conditions of inclusion separation. To improve the analysis the solution of Needleman (1972) for the stresses in an extended and necked bar of a strain hardening material were examined. This solution was found to give very similar results to those of the modified Bridgman analysis for the cases of bars with initially uniform cross-section. If this solution was used to evaluate the triaxial tensile stress distribution in initially contoured bars stretched to fracture at a final axial contour the extent of the triaxial stress was found to be even larger than that in the modified Bridgman solution. Suggesting that in bars of plastically isotropic material with an initially machined axial neck contour the deformation is highly localized at the neck and that the correct distribution of stress can only be obtained by using the Needleman method of analysis on bars with initial neck contours but also starting with a state of plastic isotropy. Such solutions will now be obtained.

References

- A. Needleman, (1972), J. Mech. Phys. Sol., 20, 111.
- I. G. Palmer, and G. C. Smith, (1966), Proc. 2nd Bolton Landing Conf. on Oxide Dispersion Strengthening, Gordon and Breach, N.Y., pg. 253.

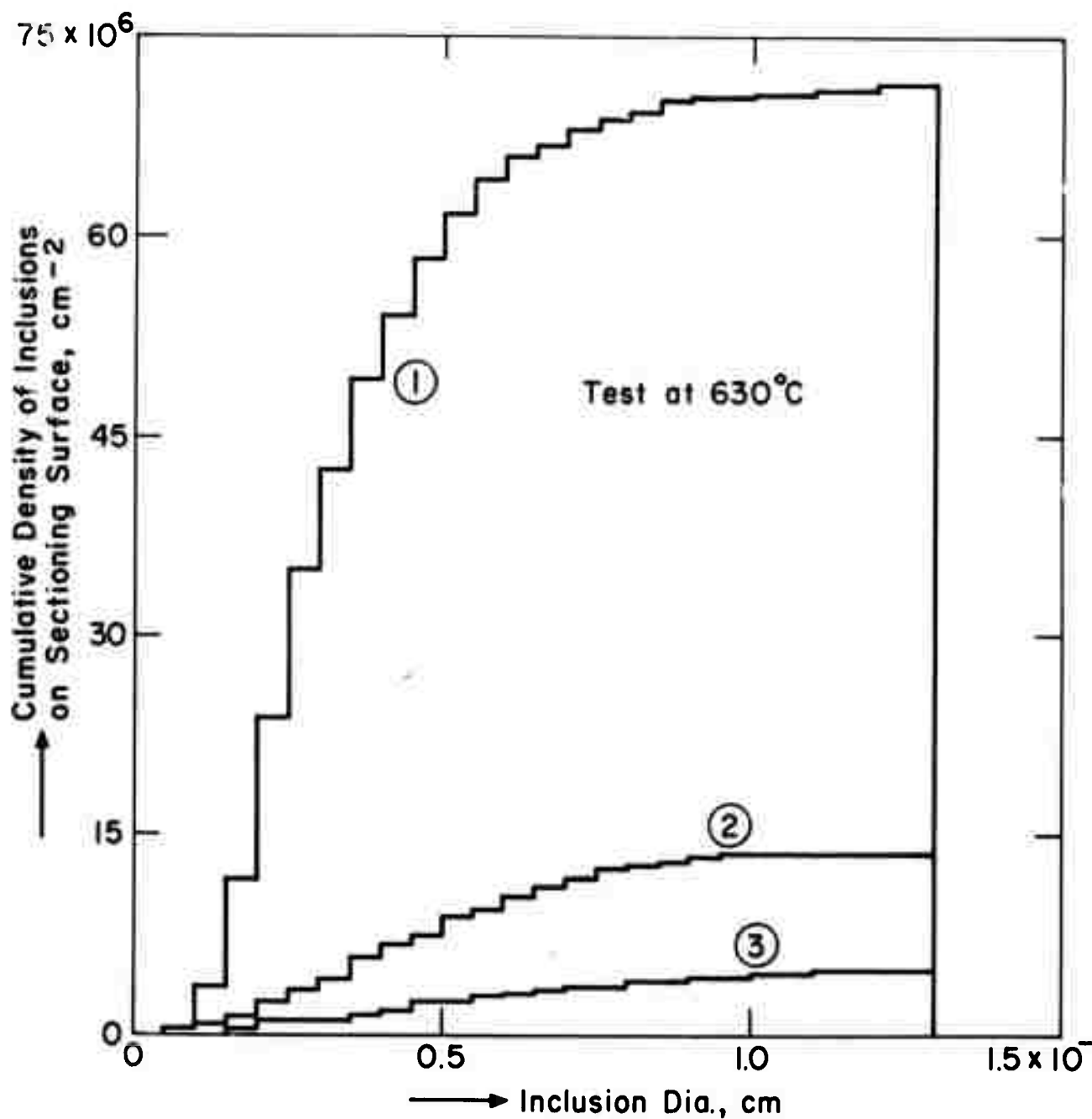


Fig. 1 Cumulative density of inclusions of all sizes (1), density of separated inclusions near the fracture surface (2), density of separated inclusions along the axis a distance of three neck radii away (3), in specimen fractured at 630°C.

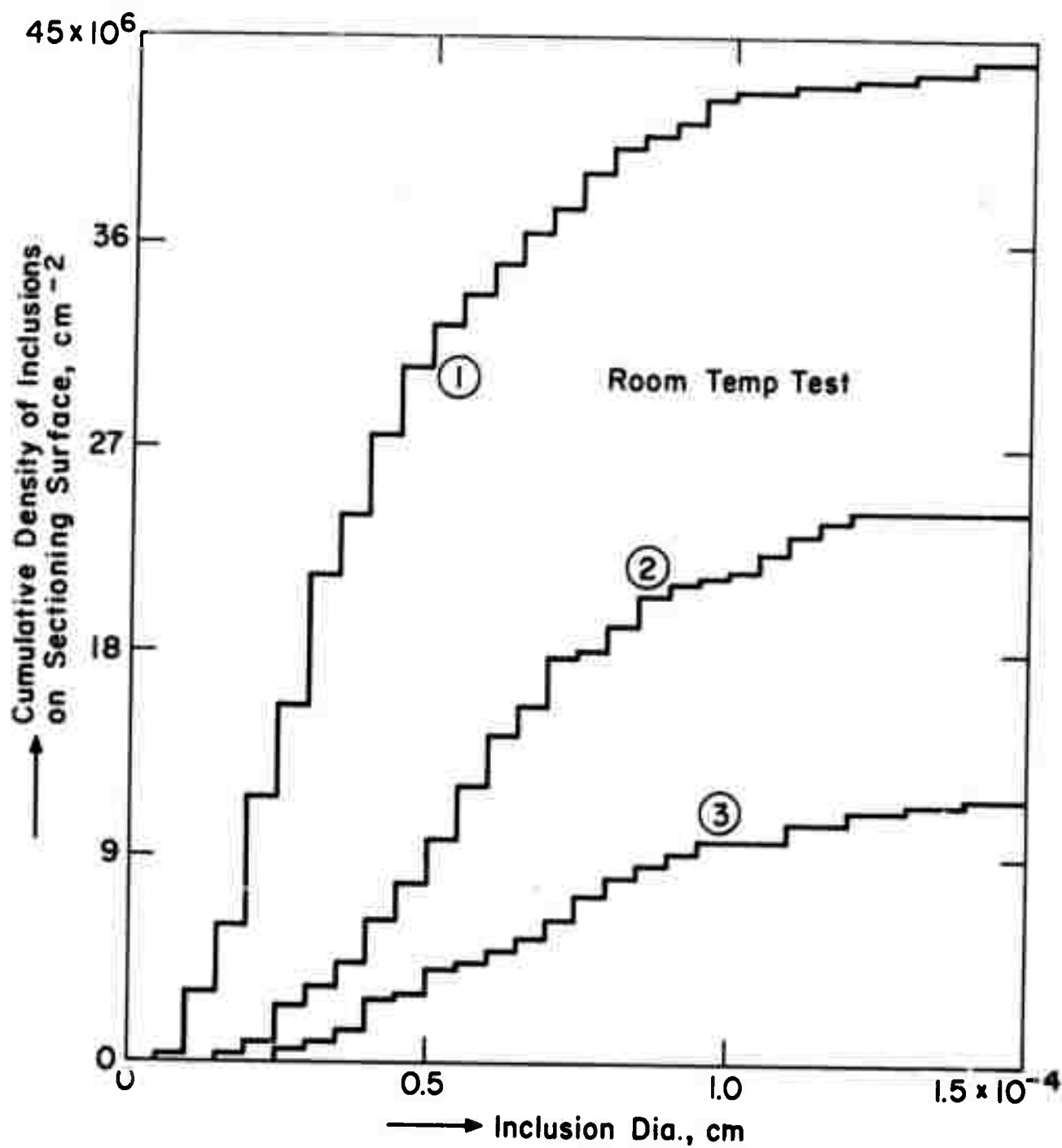


Fig. 2 Cumulative density of inclusions of all sizes (1), density of separated inclusions near the fracture surface (2), density of separated inclusions along the axis a distance of three neck radii away (3), in specimen fractured at room temperature.